AD-A086 964  CARNEGIE-MELLON UNIV  PITTSBURGH PA DEPT OF ELECTRICA--ETC  F/G 17/9
OPTICAL PROCESSORS FOR ADAPTIVE PHASED ARRAY RADARS.(U)
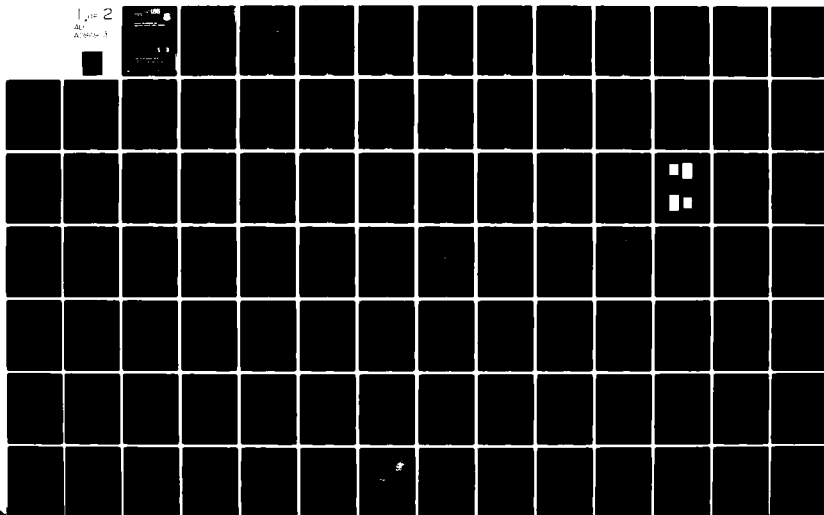MAR 80  D CASASENT                              F30602-78-C-0272
UNCLASSIFIED                           RADC-TR-80-53              NL

ADA086964

OPTICAL PROCESSORS FOR
ADAPTIVE PHASED ARRAY RADARS

Carnegie-Mellon University

David Casasent

DTIC
ELECTE
S
JUL 2 2 1980
D
B

**ROME AIR DEVELOPMENT CENTER**
**Air Force Systems Command**
**Griffiss Air Force Base, New York 13441**

80 7 21 010

APPROVED:

FRANK J. REDD
Technical Director
Surveillance Division

FOR THE COMMANDER:

JOHN P. HUSS
Acting Chief, Plans Office

If your address has changed or if you wish to be removed from the RADC
mailing list, or if the addressee is no longer employed by your organization,
please notify RADC (OCTS), Griffiss AFB NY 13441. This will assist us in
maintaining a current mailing list.

Do not return this copy. Retain or destroy.

UNCLASSIFIED

| REPORT DOCUMENTATION PAGE | | READ INSTRUCTIONS BEFORE COMPLETING FORM |
|---|---|---|
| 1. REPORT NUMBER<br>RADC-TR-80-53 | 2. GOVT ACCESSION NO. | 3. RECIPIENT'S CATALOG NUMBER |
| 4. TITLE (and Subtitle)<br>OPTICAL PROCESSORS FOR ADAPTIVE PHASED ARRAY RADARS | | 5. TYPE OF REPORT & PERIOD COVERED<br>Final Technical Report,<br>21 Aug 78 — 21 Aug 79 |
| | | 6. PERFORMING ORG. REPORT NUMBER<br>N/A |
| 7. AUTHOR(s)<br>David Casasent | | 8. CONTRACT OR GRANT NUMBER(s)<br>F30602-78-C-0272 |
| 9. PERFORMING ORGANIZATION NAME AND ADDRESS<br>Carnegie-Mellon University<br>Department of Electrical Engineering<br>Pittsburgh PA 15213 | | 10. PROGRAM ELEMENT, PROJECT, TASK AREA & WORK UNIT NUMBERS<br>61102F<br>2304J404 |
| 11. CONTROLLING OFFICE NAME AND ADDRESS<br>Rome Air Development Center (OCTS)<br>Griffiss AFB NY 13441 | | 12. REPORT DATE<br>Mar 80 |
| | | 13. NUMBER OF PAGES<br>123 |
| 14. MONITORING AGENCY NAME & ADDRESS(If different from Controlling Office)<br>Same | | 15. SECURITY CLASS. (of this report)<br>UNCLASSIFIED |
| | | 15a. DECLASSIFICATION/DOWNGRADING SCHEDULE<br>N/A |

16. DISTRIBUTION STATEMENT (of this Report)

Approved for public release; distribution unlimited.

17. DISTRIBUTION STATEMENT (of the abstract entered in Block 20, if different from Report)

Same

18. SUPPLEMENTARY NOTES

RADC Project Engineer: Vincent C. Vannicola (OCTS)

19. KEY WORDS (Continue on reverse side if necessary and identify by block number)

Adaptive phased array radar, correlation, iterative optical processor, optical correlation, optical data processing, optical signal processing, signal processing

20. ABSTRACT (Continue on reverse side if necessary and identify by block number)

Three new optical signal processing techniques and architectures have been considered for advanced adaptive phased array radar signal processing. The use of a residue arithmetic optical processor was studied. A new correlation approach to residue arithmetic operations was developed together with new optical decimal/residue and residue/decimal converters, a residue arithmetic adder and matrix processor. Format control of the data in such systems and the availability of the

DD FORM 1473 EDITION OF 1 NOV 65 IS OBSOLETE

UNCLASSIFIED

necessary components are two issues of concern in this type of optical processor. A multi-channel optical frequency plane correlator in which the received signals at the N array elements are correlated with a reference element was then studied. The output correlation plane pattern obtained is slit integrated in angles by a special detector to yield a map of the angular distribution of the noise field. From this output, an inverse DFT digital postprocessor was shown to yield the desired weights under restrictive cases. A time integrating acousto-optic correlator version of this system appears preferable, since it uses more available 1-D transducers and provides the high center frequency and large time bandwidth products necessary. An iterative optical processor was then considered. This system uses a linear LED input array, 2-D mask and 1-D photodetector array to perform a vector-matrix multiplication. With feedback, this system can solve the adaptive radar equation using a new iterative algorithm. This system is most promising, initial experiments have been quite successful, and available components make fabrication of such a system attractive.

## TABLE OF CONTENTS

i

iii

# LIST OF FIGURES

# LIST OF TABLES

# EVALUATION

Adaptive processing for radar systems becomes complex as the number of adaptive weights increase. Algorithms used to generate these weights are conventionally implemented through general purpose computers or dedicated hardware of which numerical operations are limited to discrete parameters and the instruction rate. Convergence time also becomes a problem as the number of weights becomes large.

In an effort to assess the parallel channel potential of optical processing, this effort was initiated. The number of parallel channels approaches a continuum mode where optical focusing replaces arithmetic operations. Results of the work demonstrate the feasibility of weight determination through direct methods and closed loop techniques.

Such approaches have the potential of leading to efficient and cost effective methods for realizing large scale adaptive radar systems.

VINCENT C. VANNICOLA
Project Engineer

CHAPTER 1

## 1.  INTRODUCTION

Adaptive phased array radars represent one of the most demanding signal processing problems that merits consideration of the use of advanced signal processing techniques such as optical processing.  In this report, we summarize the results of a one year research program in which three different optical techniques were considered for adaptive phased array radar processing.

The use of optical residue arithmetic systems is described in Chapter 2. A matrix multiplier using residue arithmetic is described as are decimal/residue and residue/decimal converters.  The speed and parallel processing possible with processors that operate in the residue number system are the main advantageous features of such systems.  An optical or similar analog processor using residue arithmetic is likewise attractive because of the increased accuracy that this type of arithmetic provides.  In Chapter 2, we present a new correlation approach that we developed for the formulation of problems and operations in residue arithmetic.  We also present the description of three new optical residue arithmetic systems that perform decimal/residue and residue/decimal conversion and a residue arithmetic adder.  We conclude with the design of a residue arithmetic matrix multiplier and our recommendations for future research in this area.

A modified coherent optical correlator (COC) system for adaptive phased array radar processing is described in Chapter 3.  In this system, the inputs to a multi-channel correlator are the heterodyne received array signals.  The correlation of the received signals with a reference array signal is formed in parallel.  When the output of this system is integrated along angular slits using  a  specially shaped solid-state detector, the output is a map of the angular distribution of the noise field.  As we show, a simple digital postprocessor that performs the inverse DFT can produce the desired adaptive weights from this

output in several restricted cases. A statistical analysis of this processor
is also provided.

An iterative optical processor (IOP) system using a linear input LED
array, 2-D mask and 1-D output detector with feedback is then described in
Chapter 4. This system performs a vector-matrix multiplication and with feed-
back results in an iterative processor that has the covariance matrix as an
input and that solves the vector-matrix adaptive phased array radar equation
for the desired weights using a new iterative algorithm.

For all three candidate optical processors, laboratory optical systems
were assembled, tests and demonstrations of each were conducted, and analysis
was conducted of the system's key features, a study of the availability of
components was made and recommendations for future work are advanced.

## 1.2 ADAPTIVE PHASED ARRAY RADAR PROCESSING REVIEW

A simplified block diagram of an adaptive phased array processor is shown
in Fig. 1.1. The basic concept is to multiply each of the received signals $v_n$
by an appropriate weight $w_n$ and to then sum these products to produce the output

$$E = \sum_{n}^{N} w_n v_n.$$ 

(1.1)

If the same weight is applied to all elements, the beam formed is normal to the
array and described by

$$E(\theta) = K \frac{\sin\left(\frac{\pi\, Nd\, \sin\theta}{\lambda}\right)}{\sin\left(\frac{\pi\, d\, \sin\theta}{\lambda}\right)},$$ 

(1.2)

where d is the element element spacing, $\theta$ is the steering vector of the array,
and N is the number of elements. By varying the phases of the weights $w_n$, the

beam can be steered to different directions. This is achieved by selecting the phases such that a signal incident from the desired scan angle adds in phase across the array.

By adjusting the amplitudes and phases of the $w_n$, the side lobe levels can be decreased and the effects of other noise sources in the antenna's field of view can be reduced. In such APAR systems, nulls are placed at angles and frequencies in the antenna pattern corresponding to different noise sources. This adaptive control is achieved by separate adaptive loops on each of the antenna elements as shown in Fig. 1.2. The steering signals $s_n^*$ indicate the direction in which the array is steered and hence the location of the antenna's main beam. The $u_n$ values are the correlation of the received array signals $v_n$ and the output $g = \sum w_n v_n$. When $w_n \circledast g$ is large, $u_n$ and hence $w_n$ change rapidly. The purpose of an adaptive array is to reduce the noise in $g$. When $u_n$ in a given channel is large, the corresponding weight $w_n$ has a larger effect on reducing the residue noise in $g$.

For receiver noise only, the same for all channels, the weights $w_n$ all approach the same value. If one $w_n$ is larger, the corresponding $w_n v_n$ term in $g$ is larger and this will cause larger $z_n$ and $u_n$ values for that channel, which will decrease $w_n$. Thus, an adaptive array achieves uniform illumination only for receiver noise alone. When the received signal energy is less than the interference and noise energy, the adaptive loops attempt to minimize the input power (subject to the steering vector constraint). If the noise in $g$ is approximately zero, the $z_n$ values will be small and the $w_n$ will be relatively constant.

The weights can be described by

$$w_n = G (s_n^* - u_n).$$  (1.3)
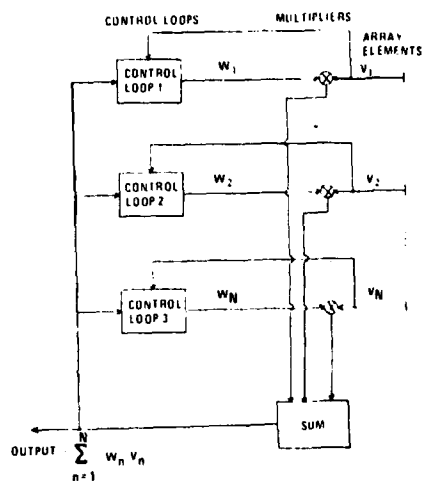
Fig. 1.1  Simplified block diagram of
an adaptive array



$$w_n = G(S_n^* u_n) \qquad \tau u_n + u_n = z_n \qquad z_n = v_n^* \left( \sum_{m=1}^{N} w_m v_m \right)$$
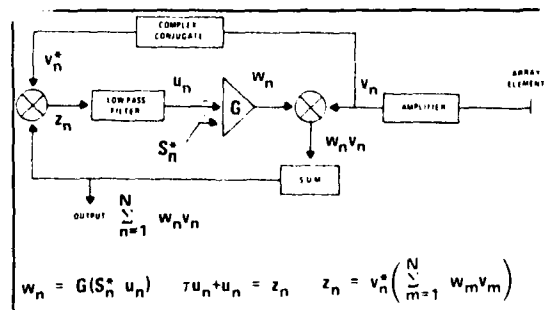
Fig.1.2    Diagram of one type of
adaptive control loop

The low pass filter with time constant $\tau$ can be described by

$$\tau \, \dot{u}_n + u_n = z_n, \tag{1.4}$$

and

$$z_n = v_n^* \, g = v_n^* \sum w_n \, v_n. \tag{1.5}$$

These equations describe the response of each of the N adaptive loops. The variation of $w_n$ depends on the inputs from all N channels and on the weights of the other $N - 1$ channels. In matrix form, we describe the loops by

$$W = G \, (S^* - U)$$

$$\tau \, \dot{U} + U = Z$$

$$Z = V^* \, (V - W), \tag{1.6}$$

where $V_T$ is a row vector and W etc. are column vectors. In terms of average values

$$Z = \overline{V^* V^T} \, W = MW, \tag{1.7}$$

where M is the covariant matrix

$$M_{ij} = Avg \, (V_i^* \, V_j). \tag{1.8}$$

If $S$ is a constant steering vector, $\dot{U} = \dot{W}/G$ and the loop is described by...

$$\tau\, \dot{W}/G + (M + I/G)\, W = S^*, \tag{1.9}$$

where I is the identity matrix. Equation (1.9) describes a set of N different equations that describe the average response of the array weights W. The values W depend upon the external noise (thru M) and the control loop parameters (S*, G and $\tau$). The conventional approach is to solve (1.9) for W and then apply these $W_n$ to the received array signals.

The covariance matrix M is fundamental to all APAR processing theory since it describes the noise environment. The diagonal terms in M are a measure of the power in each channel, whereas the off diagonal elements of M describe the direction of arrival of the noise. The rate of convergence of (1.9) depends upon the noise environment. The steady state solution to (1.9) is found with $\dot{W} = 0$ (assuming $G \gg 1$) to be

$$WM = S^*. \tag{1.10}$$

The desired weights W can then be found from S and $M^{-1}$ as

$$W = M^{-1} S^*. \tag{1.11}$$

Equation (1.11) can be obtained by inverting the matrix M, and forming the indicated vector/matrix product. Computation of M requires 2 N samples at the signal frequency to yield acceptable statistics.

Various correlation loop processors exist. The maximum SNR circuit is the most popular. It uses the Widrow least mean square circuit. It requires an

initial estimate for W, computation of the gradient at different surface points, etc. until the minimum concave surface is obtained. The system in Fig. 1.2 uses a typical Howells-Appelbaum loop in which the residue is fed back and correlated with each of the received signals. The filtered outputs are proportional to the gradient. When subtracted from the steering signal, they yield the adaptive weights. A modified random search technique with many variations also exists.

CHAPTER 2

A RESIDUE ARITHMETIC PROCESSOR FOR
ADAPTIVE PHASED ARRAY RADAR

2.1 INTRODUCTION

The data processing requirements for adaptive phased-array radar (APAR)
systems represent one of the largest challenges to present technology. For
this reason, new and fresh approaches to APAR processing are necessary
to handle the massive data processing requirements foreseen for the future,
The novel data processing approach considered in this chapter is the use of
residue arithmetic (RA).

Addition, subtraction and multiplication can be performed in RA with no
carries required. Because of this, RA is directly implementable in a parallel
processor and is thus one of the fastest computational methods available.
Since an optical system is inherently a parallel processor, a RA optical pro-
cessor implementation is most attractive. RA is also attractive because it
offers a solution to the problems of limited accuracy and limited dynamic range
present in many optical and analog data processors.

A brief review of residue arithmetic is included in Sect. 2.2. The rea-
sons for considering this novel processing approach (speed, parallel processing,
accuracy, high dynamic range, etc.) can then be seen more clearly (Sect. 2.3).
The first major issue to be decided upon in a residue processor is how to
realize the cyclic permutations required to represent numbers in moduli. In
Sect. 2.4, we discuss the various alternatives available and the reasons why
we chose pulse-position coding to represent numbers in RA.

The second issue to be addressed in a RA processor is the formulation of
the RA operations performed. One of the major original achievements of this
contract was the correlation formulation of RA operations. This is included

in Sect. 2.7. Specific RA system designs for decimal-to-residue and residue-to-decimal converters are provided in Sects. 2.5 and 2.6. As part of this program, we provided the first experimental demonstration of an optical RA system (Sect. 2.9). The design of a RA adder (Sect. 2.8) shows how the processing system's architecture directly follows from our correlation formulation approach. Another advantage of our correlation formulation of RA is the ease with which RA processors can be realized using many diverse technologies (LSI, CCDs, SAW, Acousto-Optics, Waveguides, Integrated Optics, etc.).

In Sect. 2.10, we quantify the dynamic range obtainable in a RA optical processor and suggest several added schemes to increase the system's dynamic range. A related aspect of a RA optical processor that emerges clearly and numerically in Sect. 2.10 is the utilization of the vast space bandwidth product available in an optical processor.

In Sect. 2.11, we briefly review another approach to the realization of residue operations (the use of maps). We also include system realizations of residue processors using technologies such as ROMs and integrated optics. The design of a multiplier in residue is then discussed in Sect. 2.12. With these basic building blocks (converters, adders and multipliers), we sketch the design of a parallel, pipelined matrix multiplier using residue arithmetic in Sect. 2.13. Conclusions are then advanced in Sect. 2.14.

## 2.2 RESIDUE ARITHMETIC

A brief review of residue arithmetic follows. In the residue number system, an integer is represented by the N-tuple set of residues $(R_{m_1}, R_{m_2}, \ldots R_{m_N})$ with respect to the N different relatively prime integer moduli $m_1, \ldots, m_N$. The residue $R_{m_1}$ is the least positive integer remainder of the quotient of X and $m_1$. The maximum integer value that can be represented by N moduli is M-1 where

$$M = \prod_{i=1}^{N} m_i.$$

An example will easily clarify this. To represent 13 in the residue system with moduli $(5,7,9,2)$, we divide 13 by the first modulus 5 and obtain 2 and a remainder of 3. Dividing 13 by the second modulus 7, we obtain 1 and a remainder of 6. Dividing 13 by $m_3 = 9$, the remainder is 4. For $m_4 = 2$, the remainder is 1. These four remainders are the representation of 13 in the residue number system with moduli $(5,7,9,2)$, i.e. $13 = (3,6,4,1)$.

To see the advantages of residue arithmetic, we consider how to realize the sum of 13 and 59 in residue with moduli $(5,7,9,2)$. Proceeding as before, we find $59 = (4,3,5,1)$. To sum two numbers in residue notation, we sum each separate pair of residue numbers in the same modulus $m_i$ and retain only the residue, i.e.

$$
\begin{array}{ll}
m_i & = (5,7,9,2) \\
\hline
13 & = (3,6,4,1) \\
+59 & = (4,3,5,1) \\
\hline
72 & = (2,2,0,0)
\end{array}
$$

where $3+4$ modulo 5 has a remainder 2, $1+1$ modulo 2 is 0, etc. Checking, we find that the decimal sum 72 is $(2,2,0,0)$ in moduli $(5,7,9,2)$.

To subtract two numbers in residue, e.g. $72-13$, we invert 13 in residue (by simply complementing each bit $i$ modulo $m_i$ in the residue representation) i.e.

$$
\begin{array}{ll}
m_i & = (5,7,9,2) \\
\hline
13 & = (3,6,4,1) \\
-13 & = (2,1,5,1)
\end{array}
$$

The bits $i$ of the residue numbers 72 and $-13$ are then added as before

$$
\begin{array}{ll}
72 & = (2,2,0,0) \\
-13 & = (2,1,5,1) \\
\hline
59 & = (4,3,5,1)
\end{array}
$$

To multiply two numbers in residue, we convert each number to its residue representation, multiply each bit pair, and retain the residue of each product modulo $m_i$. Consider forming the product of 19 and 12 in the same moduli.

$$m_i = (5,7,9,2)$$
$$\overline{19 = (4,5,1,1)}$$
$$12 = (2,5,3,0)$$
$$19 \times 12 = (3,4,3,0) = 228$$

where 1 times 0 is 0 in any modulo, 3 times 1 is 3 modulo 9, 5 times 5 is 25 but modulo 7 the remainder or residue is 4, and 4 times 2 is 8 which yields a residue of 3 in modulo 5. The product of 19 and 12 in decimal is 228. But 228/5 equals 45 and a residue of 3, etc. from which $228 = (3,4,3,0)$ with respective moduli $(5,7,9,2)$. From the above examples, the attractive features of residue arithmetic are apparent.

## 2.3  SPECIAL FEATURES

As shown in Sect. 2.2, no carries are required in a residue arithmetic computation. Thus this is inherently one of the fastest possible computing methods available [2.1 - 2.3] and thus of potential concern to the matrix inversion process. A second feature of residue arithmetic is that in residue processing a given computation is divided into subcomputations of reduced complexity. This allows these sub-operations to be performed in parallel with reduced dynamic range requirements. The accuracy of the resultant operations is high because the system's dynamic range is proportional to the product of the residue moduli used. Thus, residue arithmetic directly allows the use of multi-channel parallel computations that are the forte of optical computing and overcomes any potential dynamic range and accuracy limitations often associated with optical processors.

## 2.4  REALIZATIONS

Residue processing requires a cyclic permutation procedure.  This can be realized by:  polarization, phase, or pulse position coding.  The former two approaches are being pursued by Collins [2.4].  It appears unrealistic in practice since nearly ideal 2-D spatial light modulators are required.  Since such devices are space variant, we considered pulse position modulation.  Huang [2.5 - 2.6] was the first to suggest an optical residue arithmetic processor.  Recent work [2.7 - 2.8] has concentrated on similar pulse position coding.  We concur with such an approach because of the large overall error introduced into a residue processor when an error occurs in any bit.

## 2.5  DECIMAL-TO-RESIDUE CONVERSION [2.9]

We consider the conversion of a decimal number into the residue number $R_{m_i}$ modulo $m_i$ and the specific correlator topology in Fig. 2.1.  We define a unit decimal distance $\Delta x$ and thus represent the decimal number x by a delta function at $x_0 = X\Delta x$ in $P_0$.  The amplitude transmittance of $P_0$ is thus

$$g(x_0) = \delta(x_0 - X\Delta x).  \tag{2.1}$$

Lenses $L_1$ in Fig. 1 form the 1-D Fourier transform (FT) of g horizontally, while imaging vertically (i.e. a multi-channel 1-D FT).  We consider only one y channel for simplicity.  The FT of g incident on $P_1$ is

$$G(u) = \exp(j2\pi u X\Delta x).  \tag{2.2}$$

Spatial distance $x_1$ in $P_1$ is related to input spatial frequency u by

$$x_1 = \lambda f_L u,  \tag{2.3}$$

where $\lambda$ is the wavelength of the laser light used and $f_L = f_{Ls1}$ is the focal length of lens $L_{1s}$ in Fig. 2.2   Eq. 2.2)describes a planewave incident on $P_1$ at an angle that depends on $X\Delta x$ (the position of the input delta function and hence the value of the decimal input number X).

To realize the conversion of X to $R_{m_i}$ modulo $m_i$, we place at $P_1$ a square wave grating with transmittance

$$H_i(u) = \sum_{n = -\infty}^{\infty} \exp\,(j2\pi unm_i\Delta x), \qquad (2.4)$$

where the fundamental frequency $u_{gi}$ of the grating present on this channel i is chosen such that the separation between the dc and $\pm$ first order terms in the FT of (2.4) is

$$m_i\Delta x = u_{gi}\lambda f_L. \qquad (2.5)$$

For simplicity, the same unit distance $\Delta x$ is assumed for decimal units in $P_0$ and for residue units in $P_2$ (this is equivalent to assuming a 1:1 imaging system for $L_1$ and $L_2$).

In one version of a decimal/residue converter, the input $P_0$ data is a vertical slit (one decimal number) and the desired outputs at $P_2$ are the residue numbers $R_{m_i}$ for N moduli $m_i$ as shown in Fig. 2.1.   In such a case, the system will have N channels and at $P_1$ there will be N different square waves recorded on these N channels.   The frequency $u_{gi}$ of the grating on channel i will correspond to the modulus $m_i$ of that channel as in (2.5). Again, for simplicity, we restrict attention at present to one channel i.

The light amplitude distribution leaving channel i of plane $P_1$ is the product of (2.2) and (2.4) or

$$GH_i = \sum_{n = -\infty}^{\infty} \exp\,[j2\pi u(X-nm_i)\Delta x]. \qquad (2.6)$$

Lenses $L_2$ in Fig. 2.1 form the 1-D horizontal FT of (2.6) and at $P_2$ we find

$$f_2(x_2) = \sum_{n=-\infty}^{\infty} \delta[x_2-(X-nm_i)\Delta x], \tag{2.7}$$

where $x_2$ is the spatial coordinate of $P_2$. This $P_2$ pattern consists of delta functions with center-to-center spacings $m_i\Delta x$ proportional to the modulus $m_i$ and replicated at distances that are multiples of this modulus. These delta function outputs occur at

$$x_2 = (X-nm_i)\Delta x . \tag{2.8}$$

The pulse position coding of X in $P_0$ and the carrier modulation [multiplication of (2.2) by (2.4) and Fourier transforming the result] operations involved have now been explained. Before describing the last required operation (aperture control), we digress for the moment to a general description of decimal/residue conversion. Any decimal number X can be written as

$$X = nm_i + R_{m_i}, \tag{2.9}$$

where n is the number of times X is divisible by $m_i$ and where the remainder or residue $R_{m_i}$ must satisfy

$$0 \le R_{m_i} \le m_i - 1. \tag{2.10a}$$

Solving (2.9) for $R_{m_i}$, we find

$$R_{m_i} = X-nm_i. \tag{2.11a}$$

From(2.11a),we see that R is the remainder after $m_i$ has been subtracted n times from X. Multiplying (2.10a) and (2.11a) by $\Delta x$, we obtain

2.8
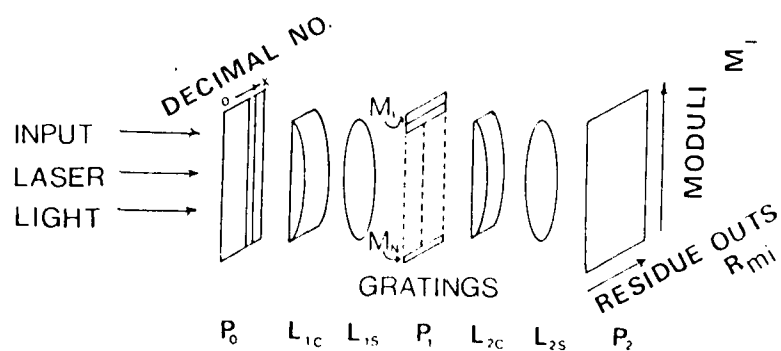


Fig. 2.1   Schematic diagram of a decimal-to-residue optical converter.
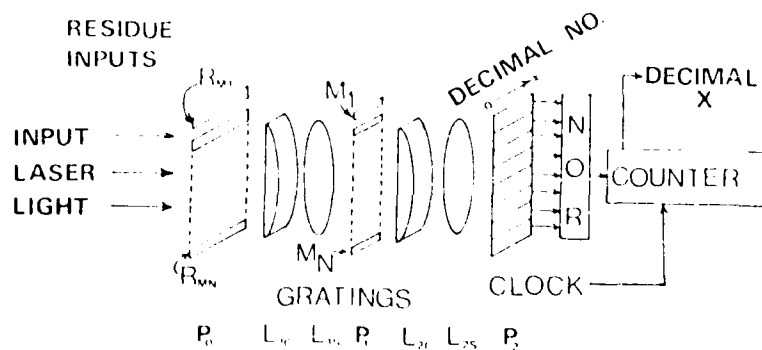


Fig. 2.2   Schematic diagram of a residue-to-decimal optical converter.

$$0 \leq R_{m_i} \Delta x \leq (m_i - 1)\Delta x \qquad (2.10b)$$

$$R_{m_i} \Delta x = (X - nm_i)\Delta x. \qquad (2.11b)$$

Now, returning to (2.7), we see that the locations of the n output delta functions in $P_2$ of Fig. 2.1 satisfy (2.8), which agrees with (2.11b). To insure that the subtraction of $m_i$ from X has been performed the proper number of times n so that (2.10a) and (2.10b) are satisfied, we examine only the $P_2$ region satisfying

$$0 \leq x_2 \leq (m_i - 1)\Delta x. \qquad (2.12)$$

This is obviously equivalent to satisfying (2.10a) and (2.10b). Only one of the delta function outputs in (2.8) satisfies (2.12).

If we place a rectangular aperture at $P_2$ of Fig. 2.1 of width $m_i \Delta x$ in $x_2$ centered at $P_2$ as defined by (2.12), there will be $m_i$ possible locations of the output spot of light withi this aperture. The location of the output peak of light within this aperture denotes the residue $R_{m_i}$ modulo $m_i$ of the decimal input X in terms of a unit residue distance $\Delta x$ (i.e. pulse-position coded). By aperture control we simply mean placing an aperture at $P_2$ to select the remainder or residue in the proper range.

The above analysis considered only one channel of the system of Fig. 2.1. If this system is to be used to convert the decimal number X into the N residues $R_{m_i}$ for the N moduli $m_i$, the input $P_0$ pattern is a slit as shown in Fig. 2.1. Its $x_0$ location $X\Delta x$ denotes the decimal input number X. At $P_1$, we now place N gratings of spatial frequencies $u_{gi}$ (corresponding to the N moduli $m_i$ to be used to represent X) on N separate lines or channels at $P_1$. Within the aperture placed at $P_2$ there will be N channels with an output spot of light at a different horizontal location on each channel. The horizontal location of the output on each channel i denotes the residue number $R_{m_i}$ for X

in the modulus $m_i$ for the particular channel. This particular arrangement of a decimal-to-residue converter may not be optimum from a system standpoint. We could also insert various decimal numbers on separate channels at $P_0$ in Fig. 2.1. By use of a single grating at $P_2$, the conversion of N decimal inputs into their equivalent residue representations with respect to one modulus results at $P_2$.

## 2.6 RESIDUE/DECIMAL CONVERSION

The schematic of a residue-to-decimal optical converter is shown in Fig. 2.2. The system is topologically the same as that of Fig. 2.1, however the inputs at $P_0$ are now N residue numbers in the N moduli $m_i$ chosen. These N input residue numbers $R_{m_i}$ are represented by a pulse of light whose horizontal distance $R\Delta x$, along channel n represents the residue number by pulse-position coding as before.

At $P_1$ of Fig. 2.2, N gratings are placed on the N different channels with the spatial frequency of each grating chosen to correspond to the modulus $m_i$ for that channel. The output along a given channel n at $P_2$ of Fig. 2.2 will be a set of delta functions as before. The horizontal positions of these delta functions now corresponds to all possible decimal numbers to which the input residue number could correspond (for the particular modulus of that channel). The horizontal position $X\Delta x$ in $P_2$ at which the delta functions on all N channels are aligned denotes the proper decimal output X corresponding to the N input residue numbers $R_{m_i}$ in the N moduli $m_i$. To detect the output, a set of horizontally-oriented linear photo diode or CCD self-scanned detector arrays can be placed at $P_2$. The output from an N input NOR or AND gate (depending on the polarity outputs desired) in synchronization

with a $\Delta x$ counter will denote the decimal output value $X'$ (or equivalently the horizontal $X\Delta x$ position in $P_2$ at which all delta functions on all channels are present).

The optical realization suggested in Fig. 2.2 is similar in principle to a scheme suggested earlier by Huang [2.6]. In the version in Ref. 2.6 (Fig. 6), input light was passed sequentially through gratings (corresponding to each $m_i$). However in this prior scheme the lateral positions of the gratings had to be adjusted to correspond to the $R_{m_i}$ inputs to achieve the proper superposition at the output. In our scheme suggested in Fig. 2.2 mechanical motion of the gratings is not required.

## 2.7 CORRELATION FORMULATION

The following general correlation formulation of residue operations will be more clear now that detailed descriptions of the two converters have been provided. The designs in Figs. 2.1 and 2.2 will also be clearer from the following formulation. In fact, an attractive feature of this correlation-based description is that the system architecture follows directly from the analytical formulation. Such a correlation formulation is most general, since it allows realization of residue operations using other technologies. We have selected a coherent optical realization because it is one of the easiest to demonstrate and because of the real-time and parallel-processing advantages of such processors.

We consider the decimal-to-residue conversion of $X$ to $R_{m_i}$ modulo $m_i$. Now that the pulse-position coding, carrier modulation and aperture control concepts have been described , the general description of the system as a correlator is straightforward. The input is a decimal number $X$ represented by $g(x_0) = \delta(x_0 - X\Delta x)$. The desired residue output $R_{m_i}$ is $f(x_2) = \delta[x_2 - (X - nm_i)\Delta x]$. The required system impulse response needed to convert $g$ into $f$ is

$$h(x_0) = \sum_n \delta(x_0 - nm_i \Delta x), \tag{2.13}$$

where $h$ is simply the FT of the grating at $P_1$ described by (2.4).

Since the system's impulse response is real and symmetric, the convolution and correlation operations are equivalent and the system's output at $P_2$ is the correlation of $g$ and $h$

$$g \odot h = \sum_n \int \delta(x_0 - X\Delta x) \; \delta(x_0 - nm_i \Delta x + x_2) dx_0$$

$$= \sum_n \int \delta(x_0 + x_2) \; \delta[x_0 - (X - nm_i)\Delta x] \; dx_0$$

$$= \sum_n \delta[x_2 - (X - nm_i)\Delta x], \tag{2.14}$$

The minimum positive location $x_2$ of the output delta function in the $P_2$ interval $0 \le x_2 \le (m_i - 1)\Delta x$ (where $x_2$ is now the shift parameter in the correlation or equivalently the output coordinate) is the desired residue output $R_{m_i}$. Residue-to-decimal conversion can be formulated similarly.

The general system block diagram for a residue converter is shown in Fig. 2.3. The input is pulse-position coded by a deflector or other component, the correlator can be realized using many technologies, the output window function is equivalent to looking only in the proper region of output correlation space. The approach allows one to more easily realize a residue arithmetic system in terms of the many technologies that use correlators (CCD, SAW, $I^2L$, Integrated optics, etc.). We consider only coherent optical techniques in the specific system designs to be described, thereby utilizing the space bandwidth, parallel processing and real time throughput of such systems. However, the correlation formulation presented is general enough to allow residue systems to be realized using other technologies. The specific optical system architectures presented
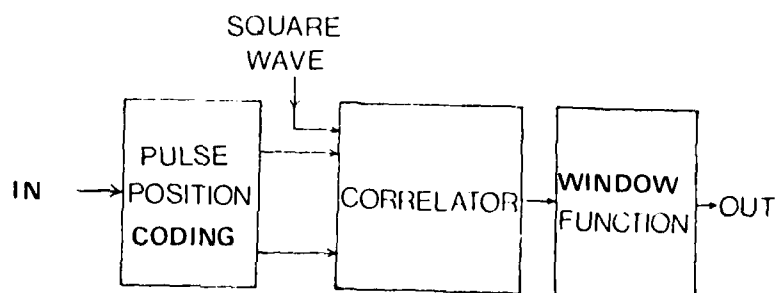
Fig. 2.3  General correlator schematic for a decimal/residue converter.
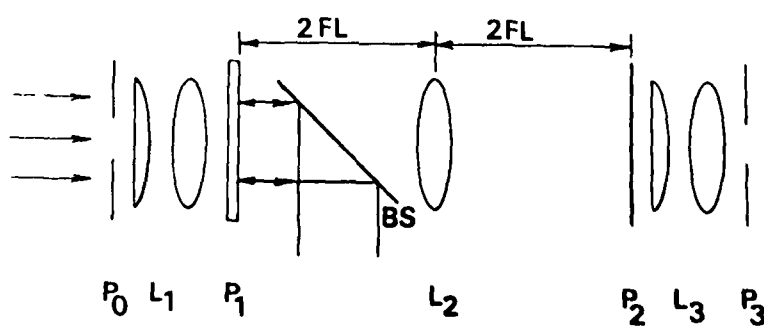


Fig. 2.4  Schematic diagram of a residue arithmetic optical adder.

and experimentally demonstrated have been included to better convey the
operations required and as examples of transitions from theory to system
architecture to experimental verifications.

## 2.8 RESIDUE ARITHMETIC OPTICAL ADDER

To demonstrate the utility of the correlation formulation of residue
arithmetic, we describe the addition of the two residue numbers $R_a$ and $R_b$
modulo $m_i$ as a correlation. We then sketch the design of a residue arithmetic
adder based on this formulation.

The two numbers to be added are represented in pulse-position coding by

$$a = \delta(x_0 - R_a \Delta x) \qquad (2.15a)$$

$$b = \delta(x_0 - R_b \Delta x) \qquad (2.15b)$$

The desired sum is

$$\left| R_a + R_b \right|_{m_i} \qquad (2.16)$$

where the subscript $m_i$ denotes that the output of the sum is the residue
modulo $m_i$. To produce the desired result, we form the correlation of a and
the mirror image of b,

$$a \circledast b = \int_{-\infty}^{\infty} \delta(x - R_a \Delta x)\delta(x + R_b \Delta x + x')dx$$

$$= \int_{-\infty}^{\infty} \delta[x - (R_a + R_b)\Delta x]\delta(x + x')dx$$

$$= \delta[x' - (R_a + R_b)\Delta x] \qquad (2.17)$$

From this, we see that the output of the above correlation is a delta
function located in correlation space at $x' = (R_a + R_b)\Delta x$ where $x'$ is the correla-
tion shift parameter. This corresponds to the **algebraic sum of the two residue**

numbers pulse-position coded. To convert this sum to the residue modulo $m_i$, we use a grating and output aperture as in Fig. 2.1 to produce the desired result in (2.16).

The schematic of an optical system to realize these operations is shown in Fig. 2.4. The two pulse-position coded input residue numbers to be added are placed side-by-side in the input plane $P_0$ of a joint transform correlator. We describe the transmittance of $P_0$ in more conventional optical notation (in 1-D for the case of one modulus only for simplicity) by

$$t_0(x_0) = \delta(x_0 - x_a) + \delta(x_0 + x_b),\tag{2.18}$$

where $x_a = R_a \Delta x$ and $x_b = R_b \Delta x$ denote the locations of the two delta functions (for $R_a$ and $R_b$) in $P_0$. Lens $L_1$ forms the 1-D Fourier transform at $P_1$ of $t_0$ in the x direction while imaging in the y direction.

The light distribution in 1-D incident on $P_1$ is thus

$$f_1(u) = \exp(j2\pi u x_a) + \exp(-j2\pi u x_b).\tag{2.19}$$

An optically addressed spatial light modulator [2.10] (SLM) is placed at $P_1$. The transmittance of $P_1$ after exposure is $|f_1|^2$ or

$$t_1 = \left| e^{j2\pi u x_a} + e^{-j2\pi u x_b} \right|^2$$

$$= 2 + 2 \cos [2\pi u(x_a + x_b)].\tag{2.20}$$

This SLM is read in reflection from the beam splitter BS in Fig. 2.4. Lens $L_2$ in Fig. 2.4 images $P_1$ onto $P_2$. At $P_2$, we place a grating whose transmittance in 1-D for the y channel of concern we represent by

$$t_2 = \sum_n e^{-j2\pi unm_i \Delta x} \tag{2.21}$$

The light distribution leaving $P_2$ is now

$$t_1 t_2 = \sum_n \exp\left[j2\pi u(x_a + x_b - nm_i \Delta x)\right]. \tag{2.22}$$

Lens $L_3$ in Fig. 2.4 forms the FT of (2.22) at $P_3$. This $P_3$ pattern is a set of delta functions,

$$f_3 = \sum_n \delta[x_3 - (x_a + x_b - nm_i \Delta x)] \tag{2.23}$$

$$= \sum_n \delta[x_3 - (R_a + R_b - nm_i)\Delta x].$$

The location of the delta function at $P_3$ of Fig. 2.4 in the range $0 \le x_3 \le (m_i - 1)\Delta x$ provides the desired residue of the sum of the two residue numbers modulo $m_i$.

In practice a and b are represented by N residue numbers (for the case of N moduli $m_i$). One way in which the contents of $P_0$ in Fig. 2.4 can be arranged to add two residue numbers with N moduli is to allot N channels in each half of plane $P_0$. The N pairs of residue numbers $R_{am_i}$ and $R_{bm_i}$ for the N moduli can be recorded on these N separate channels in pulse-position code. For this input data arrangement, we would use N gratings at N different spatial frequencies (corresponding to the N moduli) on N lines at $P_2$ of Fig. 2.4. At $P_3$ of Fig. 2.4, there will also be N channels with the position of the delta function on each vertical channel proportional to the residue of the sum of the corresponding residue numbers in the corresponding modulus of that channel. The adder element shown in Fig. 2.4 is one of the basic elemental building blocks of a residue arithmetic system (a multiplier can be realized by successive additions)

## 2.9 EXPERIMENTAL DEMONSTRATION

The system of Fig.2.1 was assembled to demonstrate and verify the decimal/ residue conversion method described **earlier**.

To keep the unit decimal distance $\Delta x_0$ in $P_0$ and the unit residue distance $\Delta x_2$ in $P_2$ equal to $\Delta x$, a 1:1 imaging system was used. The focal lengths of both cylindrical lenses were $f_{Lc}$ = 300 mm with $f_{Ls}$ = 762 mm focal lengths for both spherical lenses.

As noted several times earlier, the optimum decimal/residue converter need not always convert a decimal input number into its N residue numbers. To demonstrate an alternate scenario and to still demonstrate the basic principal of decimal/residue conversion as a correlation, the 21 decimal numbers 0 to 20 were used as the inputs on 21 channels in $P_0$ of Fig.2.1. We consider the conversion of these 21 decimal inputs to 21 residue numbers all in the same modulus. The input used (Fig. 2.5a) consists of an impulse on each of the 21 vertical channels in $P_0$. The horizontal position of each of these impulses denotes a different decimal input number. Since the spacings between impulses on successive channels are equal to $\Delta x$ = 0.7 mm (the unit input decimal distance), the decimal input on the bottom channel 0 is 0, the number on channel 1 is 1, etc., up to the top channel which represents the decimal number 20 in pulse-position code.

This input pattern was produced by superimposing a titled slit over a 1.4 cy/mm grating. The input pulses are then separated by $1/1.4 \simeq 0.7$ mm = $\Delta x$. Since the duty cycle of the 1.4 cy/mm grating was only 6%, the width of the input pulse is only 0.06 (0.7) mm $\simeq$ 40 μm or far less than the 0.7 mm decimal limit used. The capacity of the system is thus not even approached by the example shown.

At $P_1$ of Fig. 1, we place a grating of spatial frequency $u_g$ = 10 cy/mm. From (2.5), we see that $\Delta x$ and $u_g$ must satisfy

$$\Delta x = 0.7 \text{ mm} = u_g \lambda f_L / m_i \qquad (2.24)$$

from which the modulus corresponding to the grating frequency used is found to be $m_i$ = 7. Thus the system of Fig. 1, as designed above, will convert the 21 pulse-position coded decimal numbers (Fig. 2.5a) into residue numbers modulo $m_i$ = 7.

The next step is to properly position the output plane $P_2$ aperture. To do this, we must calibrate the system. Since the residues modulo 7 of the decimal numbers 0, 7 and 14 are all 0, we chose input channel 7 for calibration purposes. With only the input impulse on channel 7 present, the $P_2$ pattern in Fig. 2.1 consists of a dc, $\pm$ 1 order, etc. spots of light. We position a rectangular aperture of width $7\Delta x$ in $P_2$ such that the dc spot appears just inside the left edge of the aperture (when viewed from the detector plane). The -1 order spot is cut off and lies just outside the edge of this aperture. The system is now aligned.

With the full input plane $P_0$ pattern (Fig. 2.5a) illuminated, the output plane $P_2$ pattern of Fig. 2.5b results. It contains 21 vertical channels (corresponding to the decimal numbers 0 to 20 on the 21 input channels). On each vertical channel, the horizontal position of the output spot (within the rectangular aperture at $P_2$) lies in one of seven possible locations. These locations correspond to the seven possible residue numbers 0 to 6.

The residues modulo 7 of the decimal numbers 0 to 6 are just 0 to 6 respectively. In these cases the dc spot simply shifts across the $P_2$ aperture from left to right. For the decimal input 7, the dc spot now shifts out the right-hand side of the $P_2$ aperture and the first-order spot enters the

left-hand side of the $P_2$ aperture. Thus the correct residue number 0 results. Use of a high threshold SLM (or a thresholded TV monitor) at $P_2$ can restore the intensity of all spots of light to the same level.

To demonstrate residue-to-decimal conversion, the system of Fig. 2.2 was assembled with the same lenses used in the above experiment. The conversion performed was of the residue number (1,1,3) with moduli (3,4,5) into its decimal equivalent 13. Only three input channels are required for this case. The unit distance $\Delta x$ for $P_0$ and $P_2$ of Fig.2.2 was now 0.48 mm. The three gratings used on the three channels at $P_1$ were at 3,4, and 5 cy/mm (corresponding to the three moduli $m_1 = 3$, $m_2 = 4$, and $m_3 = 5$).

The three input residue numbers were pulse-position coded on three channels at $P_0$ of Fig.2.2 with $\Delta x = 0.48$ mm as shown in Fig. 2.6a. The resultant output plane $P_2$ pattern in Fig.2.2 is shown in Fig.2.6b. The horizontal locations of the impulses on each output channel correspond to all of the possible decimal numbers that could be represented by the corresponding residue input in the specific modulus chosen. As seen in Fig.2.6b, impulses from all three channels occur only at the horizontal location 13. Thus the decimal equivalent of the residue input (1,1,3) is found to be 13 and residue-to-decimal conversion has been demonstrated.

CHANNEL 1
R=3, $M_i$=5

CHANNEL 2
R=1, $M_i$=4

CHANNEL 3
R=1, $M_i$=3

RESIDUE NUMBER

DECIMAL OUTPUTS

CHANNEL NUMBER
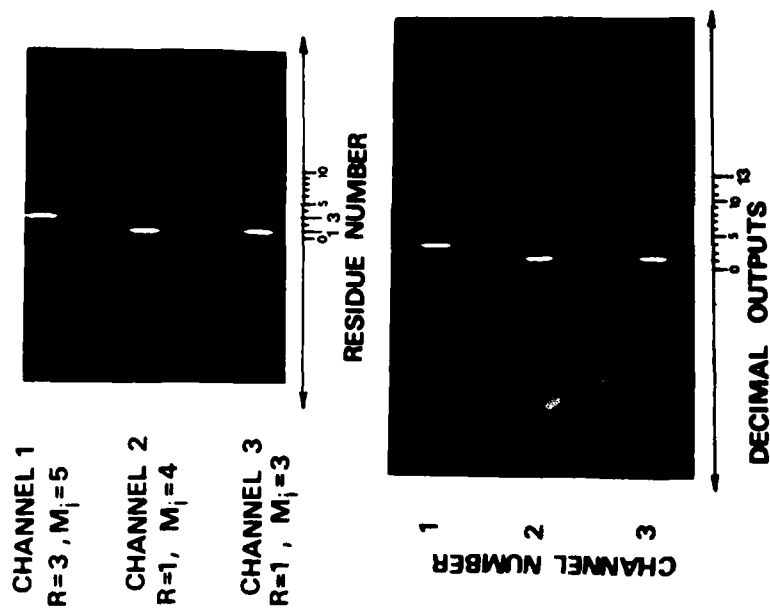
Fig. 2.6 Experimental demonstration of the conversion of the residue number (1,1,3) with moduli (3,4,5) into the decimal number 13 using the optical system of Fig. 2. (a) Input $P_0$ pattern, (b) Output $P_2$ pattern.



DECIMAL NUMBER

CHANNEL NUMBER

RESIDUE NUMBER, R,

CHANNEL NUMBER
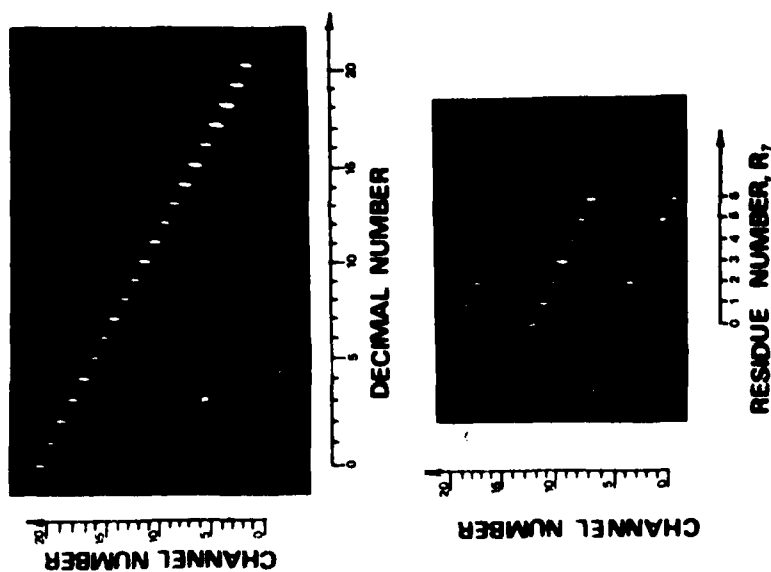
Fig. 2.5 Experimental demonstration of the conversion of the 21 decimal input numbers 0 to 20 into residue numbers modulo 7 using the optical system in Fig. 1. (a) Input $P_0$ pattern, (b) Output $P_2$ pattern.

## 2.10 DISCUSSION

The dynamic range of an optical residue arithmetic processor is the product of the moduli used, this is also the largest number M that can be represented in residue. As the number of moduli increases, each required subcalculation (recall that all calculations in all moduli are performed in parallel) needs only a dynamic range equal to the modulus chosen. In the pulse-position coding scheme used, M resolution elements are needed in the input plane $P_0$ of Fig. 1 and the output plane $P_2$ of Fig. 2 to represent the full range of decimal numbers possible. Thus the system's most severe bandwidth and dynamic range requirements occur during the input and output conversions, since the full dynamic range of the decimal number must be realized in these stages.

The resolution $\Delta x$ possible and needed in $P_0$ of Fig. 2.1 is related to M and the input aperture $\Lambda$ by

$$M = \Lambda/\Lambda x \qquad (2.25)$$

To increase M, we must increase $\Lambda$ and decrease $\Delta x$. The upper limit on $\Lambda$ is set by the lens system following $P_0$. The lower limit for $\Delta x$ is determined by the minimum resolvable spot size and geometrical accuracy with which the input can be recorded. We investigated the positional accuracy of a FT lens [2.11] and found it to be better than 0.06%. In general the accuracy and fidelity with which input data can be recorded limits the performance of an optical processor. Thus, we expect $\Delta x$ and positional inaccuracies in recording the input data to limit the dynamic range of an optical residue arithmetic system.

The motivation for considering an optical implementation of a residue arithmetic processor was to increase the dynamic range and accuracy obtainable in an optical system. However, the approximately 1000 point linear SBWP presently obtainable with scanners and spatial light modulators [2.10] still does not permit more than 10-bit dynamic range (if the pulse-position coding scheme and optical systems described earlier are used). Two approaches by which increased input space-bandwidth and hence system dynamic range can be obtained are now discussed.

The first is the use of input numbers in binary rather than decimal notation. For an input dynamic range of 64,000 we require 16 bits to represent the input data in binary notation (compared to a linear input SBWP of 64,000 for the pulse-position coded decimal representation of the largest input number). However, a binary/residue converter is now required. Such an optical system can be realized using the joint transform correlator adder of Fig. 2.4 for B (equal to the number of bits) cycles. To visualize such a system, recall that N in decimal notation is related to its binary representation $(a_0, a_1, a_2 \ldots a_B)$ by

$$N = \sum_{n=0}^{B} a_b 2^b$$

where each $a_b$ is 0 or 1. In residue notation N modulo $m_i$ is

$$|N|_{m_i} = [a_0 |2^0|_{m_i} + a_1 |2^1|_{m_i} + a_2 |2^2|_{m_i} + \ldots]_{m_i} \qquad (2.26)$$

From this, we realize that N can be represented modulo $m_i$ as the residue sum of B numbers $2^b$ in residue, and that these $2^b$ modulo $m_i$ values are known in advance. In essence, we can realize (2.26) by adding 0 or $2^b$ to a running residue sum depending on whether the corresponding binary bit of N is 0 or 1.

The resultant output after the addition of the most significant bit is then $|N|_{m_i}$ in residue modulo $m_i$. Realization of this conversion by the cyclic operation of one adder of the type shown in Fig. 2.4 may be preferable to a cascade of B-1 such adders.

However, an alternate method exists whereby the dynamic range of N can be increased, without exceeding the assumed input linear SBWP of 1000. This approach involves raster recording the input data with zero-retrace time and use of the folded spectrum optical spectrum analyzer [2.12]. In the optical residue arithmetic version of such a high dynamic range raster recorded decimal/residue converter, pulse position coding of N is still employed. However K lines at $P_0$ of Fig. 2.1 are used to represent N as

$$Nx_0 - KN_L x_0 = (N - KN_L)x_0. \qquad (2.27)$$

In other words, for a maximum N = 10,000 and a linear positional or resolutional $N_L$ = 1000, we use K = 10 lines at $P_0$ to represent N. If $0 \le N \le 1000$, a delta function of light appears on line K = 1. If $1000 \le N \le 2000$, the delta function appears on line K = 2 at $P_0$, etc. If we use $N = nm_i + R_{m_i}$ and assume $KN_L = rm_i + R'_{m_i}$, then

$$N - KN_L = (n-r)m_i + R_{m_i} - R'_{m_i}, \qquad (2.28)$$

which reduces to

$$R_{m_i} = (N - KN_L) - (n-r)m_i \qquad (2.29)$$

when $N_L$ is a multiple of $m_i$, since then $R'_{m_i} = 0$.

As a numerical example, consider the conversion of N = 168 to residue modulo 5 assuming a maximum $N_L$ = 50. In our raster recorded version of the input $P_0$ pattern in Fig.2.1, the delta function corresponding to N = 168 occurs 18 spaces ($18\Delta x$) from the left edge of the k = 4 line in $P_0$. Since $N_L$ = 50 is an integer multiple of $m_i$ = 5, N = 0 to 49 appear on line k = 1, N = 49 to

99 appear on line 2, etc. Then,

$$18_5 = (168-150)_5 = 168_5 - 150_5 = 168_5.$$ (2.30)

The schematic diagram for such a system is shown in Fig. 2.7. With K lines required at $P_0$ to represent N, the $m_i$ grating at $P_1$ is also replicated for K lines (assuming 1:1 imaging optics for $L_1$). A second grating at a spatial frequency corresponding to the second $m_i$ is recorded on the next K lines at $P_1$ (or alternatively a grating at one $u_{gi}$ is present at $P_1$ depending upon the system scenario). In all cases only one spot appears within the first K lines of the $P_2$ aperture, etc. and thus as before the horizontal locations of the peaks of light at $P_2$ correspond to the desired $R_{mi}$. The vertical $P_2$ axis is now partitioned into sets of K lines with each set corresponding to one $R_{m_i}$. Since the two-dimensional SBWP of available spatial light modulators [ .10] is so large, this utilization of available real estate at $P_0$ is warranted if the desired system dynamic range is to be realized. One shortcoming of the system of Fig. 2.7 is the low usable input light level.

This can be improved if the decimal input number is used to control an oscillator to raster record the input as a signal at frequency $f_N$ proportional to N on K lines. The 2-D Fourier transform of such a raster-recorded input pattern contains coarse and fine frequency axes. The location of the output peak along the fine frequency axis is the desired residue modulo the input horizontal line scan rate [2.12]. The modulus is thus set by the input line scan rate and a set of gratings is not required.

At the output plane $P_2$ of Figs. 2.1 or 2.7, another accuracy issue arises. Positional accuracy represents no major problem since only $m_i$ resolution points per channel are needed. Rather, the diffraction efficiency of the grating used at $P_1$ must be sufficient to produce enough detectable light in the $M/m_i$-th order of the grating. The problem can be relieved by use of larger $m_i$ values, by use of blazed or bleached gratings, etc. The accuracy of the spatial frequency

of this grating will also affect performance but this is not expected to be a major error source since the grating need be produced only once.

Since the aperture of the grating at $P_1$ determines the spot size in the output plane $P_2$, we must insure that this aperture remains above some minimum value for all beams emerging from different locations in $P_0$ that strike $P_1$ at different angles.

For simplicity in the analyses used, we assumed equal unit distances $\Delta x_0 = \Delta x_2 = \Delta x$ in $P_0$ and $P_2$. In Fig. 2.1 the $P_0$ resolution must be superb, however there is no reason to retain fine resolution in $P_2$ since only $m_i$ points per line are needed in $P_2$. Thus, in practice choosing $m_i$ large and $\Delta x_2 > \Delta x_0$ should improve performance. However, utilization of the available space bandwidth (SBW) and a full system design will determine the optimum values.

We demonstrate by example this latter point and why the architecture of the converters and adder shown may be altered. Consider the input SBW requirements for a residue adder to add in parallel 100 pairs of numbers each of which is described in residue by $N = 11$ moduli (with the largest modulus equal to 31). Since $\max(m_i) = 31$ and $N = 11$, we require a SBW = 343 to fully represent one number in residue. To represent 100 numbers, we require a SBW = 34,300. Thus to add two such pairs of 100 decimal numbers, we require an input SBW = 68,600.

This value may seem quite formidable and in fact it is for many systems. However, the input SBW achievable in real time on a spatial light modulator[2.10] in a coherent optical processor easily exceeds $10^3 \times 10^3 = 10^6$. Thus the input SBW required for the above example leaves 931,400 of the $10^6$ possible input pixels unused. As this numerical example rather vividly demonstrates, the increased SBW requirements of a residue arithmetic system represent no problem
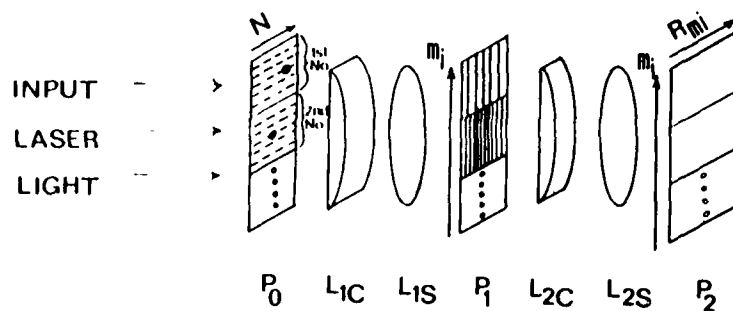
Fig. 2.7  Schematic diagram of a high dynamic range
decimal to residue converter using raster
recorded input data.
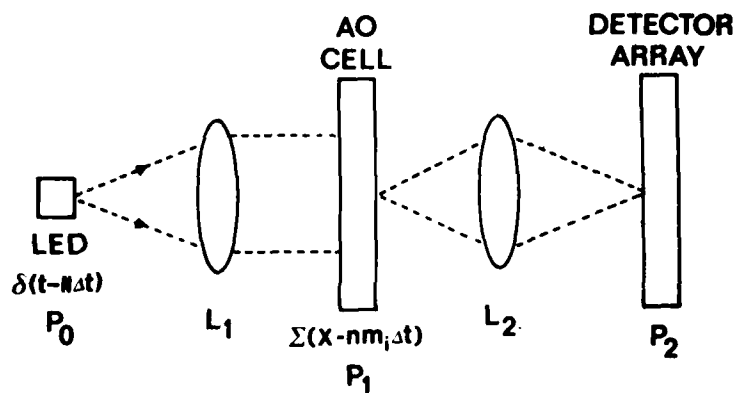


Fig. 2.8  Large time bandwidth decimal-to-residue converter.

in an optical residue arithmetic system. Thus, utilization of the large available input SBW of an optical processor will definitely require far more elaborate input formats than those described earlier.

In the numerical example presented above in which $N = 11$ moduli with $\max(m_i) = 21$, the largest input number that can be represented is about $2^{42}$. Thus, this system with eleven moduli has the equivalent accuracy and dynamic range of a 42-bit digital computer.

The most promising design we have found for a high dynamic range decimal-to-residue converter is shown in Fig. 2.8. In this system, the output from an LED source is expanded by lens $L_1$ and passed through an acousto-optic (AO) cell at $P_1$. The wavefront leaving $P_1$ is then imaged onto a detector array at $P_2$ by lens $L_2$.

To utilize this system topology as a decimal-to-residue converter, we temporally modulate the LED (in time) with a pulse of width $\Delta t$ occuring at time $N\Delta t$, where N is the input decimal number. The light output from the LED and hence the signal incident on the AO cell is thus

$$u_0(t) = \delta(t-N\Delta t) \ . \tag{2.31}$$

We choose the acoustic time length of the AO cell to be $m_1 \Delta t$ and describe the signal in the AO cell (as a function of time t and distance x across the $P_1$ aperture) by

$$u_1(t) = \sum_n \delta(x-n \ M_1 \Delta t + t) \ . \tag{2.32}$$

This represents a pulse of width $\Delta t$ and period $M_1 \Delta t$ traveling in time t and distance x across $P_1$.

The light distribution leaving $P_1$ and incident on $P_2$ is thus the product of (2.31) and (2.32). The detector array at $P_2$ integrates this signal for a time $M_1 \Delta t$. The output at $P_2$ is thus

$$u_2(x) = \sum_n \int_{n M_i \Delta t}^{[(n+1)M_i-1]\Delta t} \delta(t-N\Delta t) \; \delta(x-n \, M_i \Delta t+t) \; dt = \delta[x-(N-n \, M_i)\Delta t] \qquad (2.33)$$

Only one pulse will be present somewhere in the AO line when the LED pulses

on. Thus, only one of the $M_i$ detectors at $P_2$ detects energy. Its location x

is proportional to N is residue modulo $M_i$ as shown in (2.33). The integration

time of the photodetectors is $M_i\Delta t$ (not $N\Delta t$). The photodetector outputs are

threshold detected and cleared each $M_i\Delta t$ seconds. Thus detector noise which

will limit the system's dynamic range normally in $\alpha$ time integrating correlator,

does not affect this system. The pulse itself present on the detector is only

of duration $\Delta t$, but the position of the pulse within the AO cell is not known

(hence the $M_i\Delta t$ integration time at the detector). The time aperture length

of the AO cell need be only $M_i\Delta t$. Thus the system is most conducive to direct

realization.

## 2.11 ALTERNATE APPROACHES TO RESIDUE ARITHMETIC PROCESSORS

The prior correlation-based approach to residue arithmetic processors are

original and advantageous compared to others. However, for completeness, we

summarize the residue work of other (most notably A. Huang, et al., [2.7,2.8])

and an alternate mapping approach to residue computations. When two residue

numbers are operated on (added, subtracted, multiplied, or converted), a fixed

map or look up table can be constructed that automatically "looks up" the out-

put value given the inputs and the operation to be performed. This look-up-

table approach is possible in residue arithmetic because of the limited dynamic

range of all operations (in any modulus, the accuracy required equals the

modulus). Mapping approaches are directly realizable using ROM (read-only

memory) digital integrated circuits as shown in Fig. 2.9. The approach to a

larger system of this type is easily pipelined to produce high speed computa-

tions in parallel.

The most difficult computations in any residue system are the conversions from decimal to residue at the input and from residue to decimal notation at the output. In the mapping approach, the output conversion is of paramount concern since it cannot easily be pipelined. This occurs because the results of one computation are needed for the next calculation.

One optical residue arithmetic system using maps is shown [2.7,2.8] in Fig. 2.10. In this system, the positions of the horizontal and vertical slits at $P_0$ and $P_1$ select one element of the look up table at $P_2$ that is imaged onto the output at $P_3$. This 2-D map scheme is of limited use. Alterable 1-D maps (Fig. 2.11) are preferable. In these systems in Fig. 2.11, we assume the two numbers are to be added. In such schemes [2.7,2.8], one of the residue numbers (in one modulus) to be added is used to alter the mapping topology as shown in the two examples in Fig. 2.11 (adding 1 and 2 to $\alpha_n$ input residue number modulo 5).

One of the most attractive methods of realizing an alterable map as in Fig. 2.11 is by integrated optical switches. An example of such a map to add +3 and +4 to an input residue number modulo 5 is shown in Fig. 2.12. In these devices, each input is a focused laser beam at an input position proportional to the input residue number. The diagonal lines in Fig. 2.12 represent reflecting surfaces that cause the location of the output beam to occur at a position proportional to the appropriate output residue number (pulse position coded). The system shown adds 4 to the residue input number modulo 6. For example, an input at 0 exits at 4 (the sum of 0 and 4 is 4). An input at 4 exits at 2 (the sum of 4 and 4 is 8 or 2 modulo 6).

Tsai at Carnegie-Mellon University [2.13] has studied such integrated optical switches. However, considerable research remains before such systems appear realizable. Issues, such as the cascading of such switches and a large

OUTPUTS
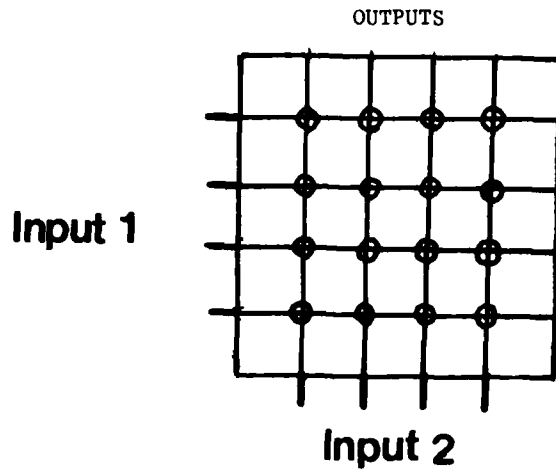
Input 1

Input 2

Fig. 2.9 Simplified concept of a map using a ROM
(Read only memory) or similar element.

$P_0$        $P_1$        $P_2$        $P_3$

| HORIZ. | IMAGING | VERT. | IMAGING | LOOK-UP | INTEGR. | OUTPUT |
| SLIT | LENS | SLIT | LENS | TABLE | LENS | PLANE |
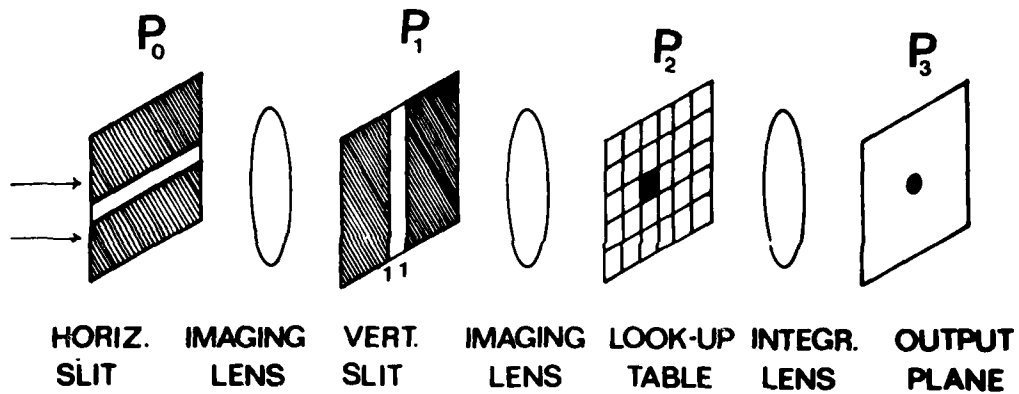
Fig. 2.10  Optical system to realize a fixed map.

(a)                    (b)
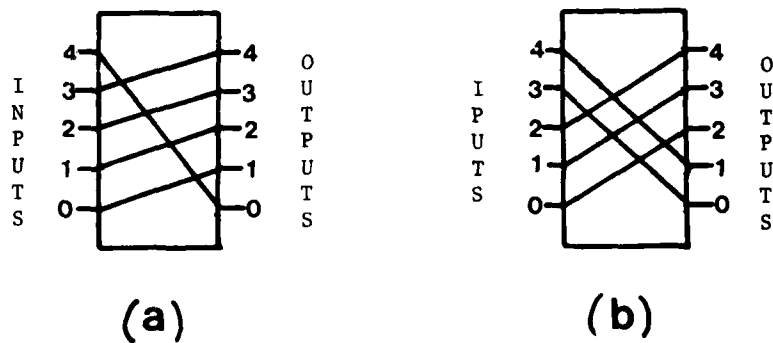
Fig. 2.11 Simple alterable maps to add 1 (Fig. a) or 2 (Fig. b)
to an input residue number modulo 5.

reduction in their cost remain to be solved, before the components for such an approach are available and before a final design can be produced. Similar remarks can be advanced on other alterable map conceptual designs [2.7,2.8] using other technologies.

## 2.12 RESIDUE MULTIPLICATION

Addition and conversion are cyclic in a residue arithmetic computer (using maps as well as our correlation approach). However, multiplication is not cyclic (incrementing the input by 1 does not increment the output cyclically by 1). For example, in Fig. 2.13a we show the map for multiplication of an input residue number by 2 modulo 4. Residue multiplication can be made cyclic as shown in Fig. 2.13b by performing an input (map 1) and output (map 2) permutation leaving the multiplication map cyclic. The general approach to be used for the permutations (maps 1 and 2 in Fig. 2.13b) that yield a cyclic multiplication remains to be fully analyzed. Residue multiplication can thus be performed as in Fig. 2.13b or by cascading $M_i-1$ adders. Such a cascading approach is feasible in a residue system because the moduli $M_i$ are small numbers. It can also be realized on a single SLM using feedback or integrated optics.

## 2.13 RESIDUE ARITHMETIC MATRIX MULTIPLIER

The basic residue arithmetic element in a phased array radar processor is a matrix multiplier. In prior sections, we have described several implementations of the basic building blocks of a residue arithmetic processor (converters, adders, and multipliers) and experimental demonstrations of several of these operations. From these components the block diagram of a residue arithmetic matrix multiplier in Fig. 2.14 follows directly. The pipelined system design shown in Fig. 2.14 requires parallel computations in real

INPUT                           INPUT



(a)   Add 3 to input          (b)   Add 4 to input
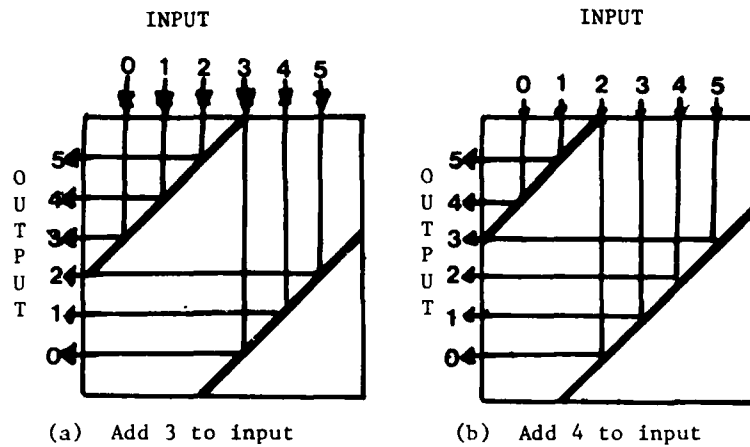
Fig. 2.12   Integrated optical alterable map to add 3 and 4
            to an input residue number modulo 6.

Tsai at CMU [2.13] has been studying such integrated optical
switches.   However, considerable research remains before such systems
appear realizable.   Issues such as the cascading of such switches and
a large reduction in their cost remains (among other efforts) before
the components for such an approach are available and before a final
design can be produced.   Similar remarks can be advanced on other
alterable map conceptual designs [2.7,2.8] using other technologies.



(a)                           (b)
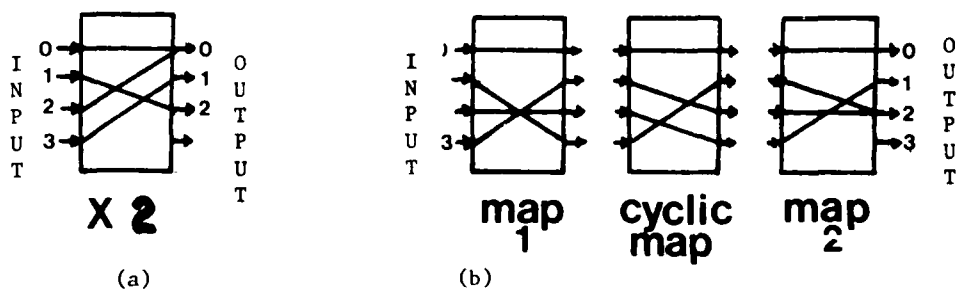
Fig. 2.13   Multiplication (Fig. a) as a noncyclic operation and how
            it can be made cyclic (Fig. b) by input and output
            permutations (maps 1 and 2).
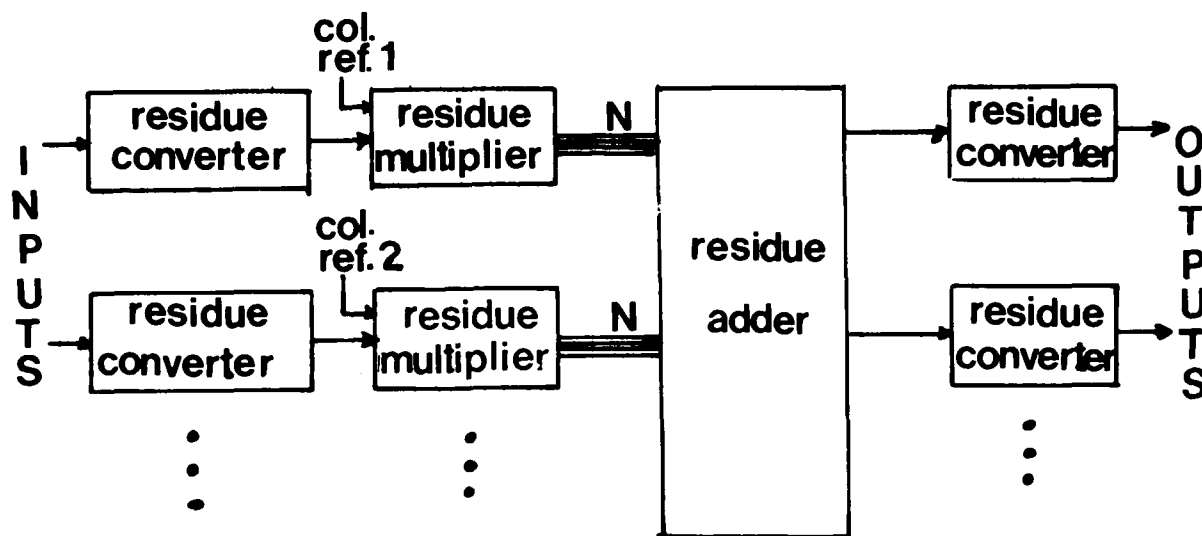
Fig. 2.14 Block diagram of a residue arithmetic matrix multiplier for adaptive phased array radar.
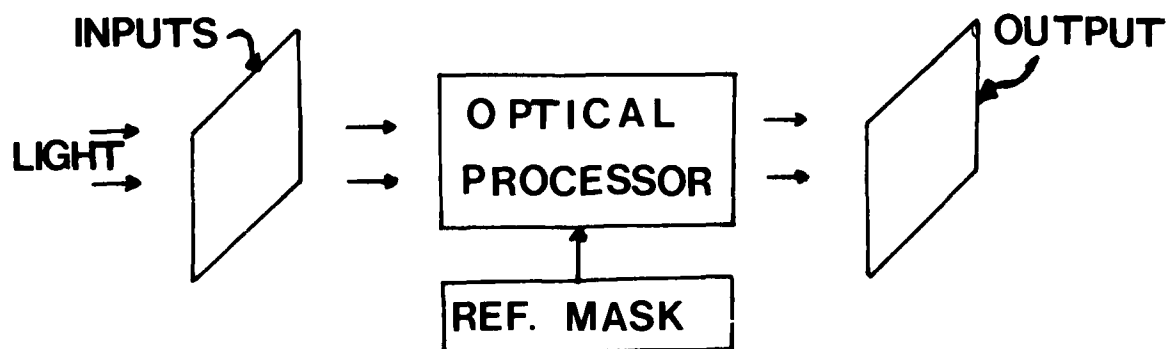


Fig. 2.15 Simplified diagram of a residue arithmetic optical matrix multiplier.

time.  Integration of the component subsystems using LSI, CCD, Integrated Optics, etc. is the key to such an approach, with the hope that interconnection problems do not arise.  Only added research can answer such questions.

A second approach (Fig. 2.15) that we advocate utilizes the vast space bandwidth SBW available in an 2-D optical processor and the parallel nature of such systems.  In this case, the major problem becomes one of how to arrange and format the input SLM data to adequately use the available SBW product to perform the required matrix multiplication with minimum complexity (without feedback and using a single SLM).

## 2.14  SUMMARY AND CONCLUSIONS

The need for a novel and fresh processing approach to the adaptive phased array problem merits the use of a new number system such as residue arithmetic. As we have shown, residue arithmetic offers the advantages of:  parallel processing, format control,pipelining, high speed, and increased accuracy and dynamic range.  Thus, it has great potential for use, in situations where a high computational load is required, such as adaptive phased array radars.  The major problem areas in such a processor are the conversions from analog or digital input data into residue and back.  We thus emphasized these problem areas in our experimental work.  We formulated a novel correlation approach that is directly implementable in many available technologies.  We have likewise reviewed other approaches using maps, integrated optics, etc.

From this phase of our program we conclude:  (1) that residue arithmetic offers the fast parallel and accurate processing required for adaptive array radar; (2) that pulse position modulation should be used; (3) that a correlation-based formulation is more easily implementable than alternate techniques (for practical reasons); (4) that added research is needed on the light losses present in certain approaches and on the input format needed to utilize the

vast SBWP and parallel processing of an optical processor and the associated optical system to realize a simple processor; and (5) that the state-of-the-art and expected time frame at which cascaded integrated optics switches will be available appears to be far too long for such an approach to be considered at present.

We thus recommend that RADC remain abreast of advances in related technologies such as SAW, AO, CCD, ROM, Integrated Optics, etc. and uses the expected time frame within which these component technologies will have matured to be of use in the fabrication of a residue arithmetic and to allow proper architectural designs for such a system dedicated to the adaptive phased array problem. We strongly advocate that an all optical approach be pursued (as opposed to one in which 1-D devices are paralleled and pipelined) in which the input format and SBWP issues advanced in point (4) above are specifically addressed.

2.36

REFERENCES

2.1 H. L. Garner, "The residue number system," IRE Trans. Electron. Comput. Vol. EC-8, pp. 140-147, June 1959.

2.2 N. S. Szabo and R. I. Tanaka, Residue Arithmetic and its Applications to Computer Technology, New York, McGraw-Hill, 1967.

2.3 D. E. Knuth, Seminumerical Algorithms, Vol. 2, pp. 248-256, Addison-Wesley Reading, MA 1969.

2.4 S. Collins, Proc. SPIE, 128, pp. 313-319, September 1977.

2.5 A. Huang, Proc. IOCC Conf., pp. 14-18, Washington, D.C., April 1975.

2.6 A. Huang, Proc. EOSD Conf., pp. 208-212, Anaheim, October 1977.

2.7 A. Huang, Y. Tsunoda, and J. W. Goodman, Appl. Opt., to appear 1978.

2.8 A. Huang, Y. Tsunoda, and J. W. Goodman, Stanford Electronics Lab Report, 6422-1, March (1978).

2.9 D. Psaltis and D. Casasent, Appl. Opt., 15 January (1979).

2.10 D. Casasent, Proc. IEEE, 65, 143 (1977).

2.11 D. Casasent and T. Luu, Appl. Opt., 17, 1701 (1978).

2.12 C. Thomas, Appl. Opt., 5, 1782 (1966).

2.13 S. K. Sheem and C. S. Tsai, CLEA, 2.7, 7 (1977).

2.14 W. Stoner (private communications).

CHAPTER 3

## COHERENT OPTICAL CORRELATOR (COC) FOR ADAPTIVE PROCESSING

### 3.1 INTRODUCTION

An adaptive array is intended to cancel the effect of noise background and thus enhance target detection etc. This process involves two steps: estimation of the ambient noise field and determining the weighting coefficients that minimize the effects of the noise field. In this chapter, we consider use of a coherent optical correlator (COC) processor to estimate the noise field. We then discuss the methods by which the desired weights for the array elements can be obtained from this output noise field distribution.

In Sect. 3.2, we discuss the basic operation of the COC system and its use in estimating the noise distribution. In Sect. 3.3, we introduce two different COC architectures and describe the system assembled. Different models for the noise sources, the method used to simulate them and the noise estimates obtained from simulations are then presented in Sect. 3.4. In Sect. 3.5, we consider the COC system from a statistical view point and provide analytical expressions for the accuaracy of the noise estimate obtained and the available resolution of such a system. In Sect. 3.6, several important post processing issues involving the estimation of the weights are addressed. Experimental results are included in Sect. 3.7 and our conclusions are advanced in Sect. 3.8.

### 3.2 BASIC OPERATION

The COC system which we designed and fabricated computes the angular distribution of the noise field as its output. In this section, we consider the basic operation of such a COC system.

We consider an antenna system with N elements that receive noise signals. We assume the noise distribution to be far from the antenna and thus assume plane noise wave fronts incident on the array. As a result, the signals received at different array elements differ only by time delays. Since the noise field originating at different angular positions in the far field results in different element-to-element time delays at the antenna, the desired N ($\theta$) angular noise field distribution can be estimated by determining these delays present in the received signals.

Let us consider the situation where the far field noise consist of M discrete noise sources, each at a different angle $\theta_m$ and with a different power $N_m$. The notation used is shown in Table 3.1. We consider the signal received at the central element of the array as the reference $f_R$ (t). The COC system forms the correlation of $f_R$ with all other received array signals $f_n$. Using the notation of Table 3.1, the signal received at the n th element can be related to the reference signal by

$$f_n(t) = \sum_{m=1}^{M} f_{Rm} (t-\tau_{mn}) \qquad (3.1a)$$

$$f_R(t) = \sum_{m=1}^{M} f_{Rm} (t), \qquad (3.1b)$$

where

$$\tau_{mn} = k(R-n)d \sin \theta_m, \qquad (3.1c)$$

and k = 2 $\pi/\lambda$. When the reference signal is correlated with the signal received at the n th array element, we obtain

$$f_R(t) \circledast f_n(t) = [\sum_{m}^{M} f_{Rm} (t-\tau_{mn})] \circledast [\sum_{m}^{M} f_{Rm} (t)]$$

$$= \sum_{mj}^{MM} [f_{Rm} (t) \circledast f_{Rj} (t-\tau_{jn})]. \qquad (3.2)$$

## Table 3.1 Phased Array Radar Notation

| | | | |
|---|---|---|---|
| N | Number of phased array elements | k | Wave number, $k = 2\pi/\lambda$ |
| n | A given phased array element | M | Number of noise sources |
| $f_n$ | Received signal at element n | m | A given noise source |
| $f_{nm}$ | $f_n$ due to a source at angle $\theta_m$ | $\theta_m$ | Angle of noise source m |
| d | Center-to-center separation of array elements | $s_m$ | Noise source m at angle $\theta_m$ |
| $\lambda$ | Wavelength of radiation | | |

We assume that the statistical characteristics of the noise sources at different angular locations are independent. The cross correlation of $f_{Rm}(t)$ and $f_{Rj}(t)$ is thus zero unless m = j and (3.2) simplifies to

$$f_R(t) \circledast f_n(t) = \sum_m^M [f_{Rm}(t) \circledast f_{Rm}(t-\tau_{mn})]$$

$$= \sum_m^M C_m(t-\tau_{mn}). \tag{3.3}$$

From (3.3), we see that the correlation of $f_R(t)$ and $f_n(t)$ is the summation of M noise signal auto correlations, each shifted by an amount $\tau_{mn}$ given by (3.1). When these N correlations are performed in a multichannel optical correlator, the output plane light pattern of Fig. 3.1 results. The vertical axis in Fig. 3.1 represents array elements number n, whereas the horizontal axis represents the time delay.
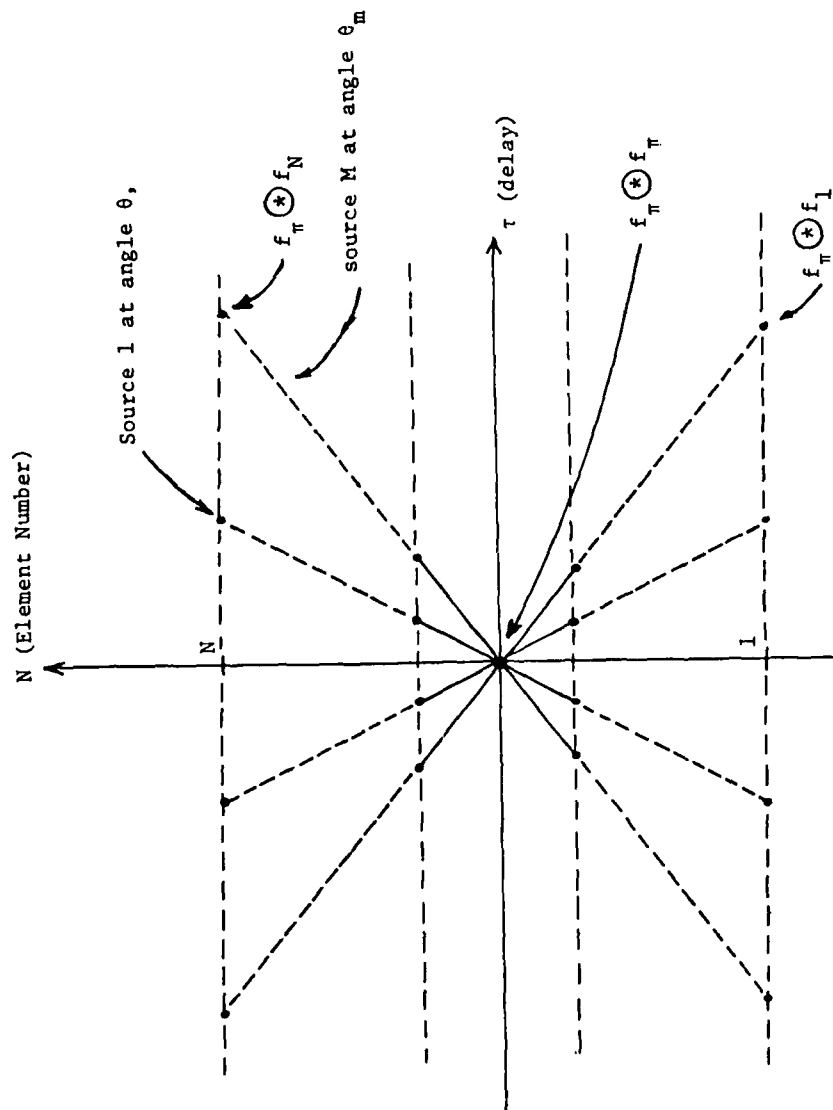
Fig. 3.1  Output plane pattern of multichannel correlator.

If the correlation peak due to each noise source is sharp and if the array elements are uniformly placed along a line, the correlation peaks corresponding to noise source m form a line at an angle proportional to $\theta_m$. To see this we evaluate (3.3) at a fixed point $\tau_{pn}$ in the output plane along the n th channel and obtain

$$f_R(t) \circledast f_n(t) \Big|_{t = \tau_{pn}} = \sum_m^M C_m (\tau_{pn} - \tau_{mn}) = C_p (o) \qquad (3.4)$$

where the contribution of terms other than $C_p(o)$ in the summation are ignored because of the sharp correlations.

Thus, integrating along these correlation peaks, we obtain an estimate of the noise power as a function of angle. It should be noted that a multi-channel correlator followed by an integration along $\theta$ provides information only about the noise power and not the noise bandwidth. Although $N(\theta)$ does not yield complete noise field information, we often can assume that the noise bandwidth is identical to that of the antenna and thus obtain all of the desired information.

To provide the integration along different $\theta$ lines in the output plane of Fig. 3.1, three candidate methods are suggested. The first involves the use of a rotating slit whose light output is integrated onto a detector using a 2-D Fourier transform lens. The disadvantages of this system are the slit width (which causes loss of resolution) and the mechanical motion required (which reduces the processor's throughput speed). In the demonstration stages of this project, a slit is still useful.

The second method uses a detector with wedged shaped elements with parallel electrical outputs mounted in the output plane of the optical correlator. The

outputs from this detector array are estimates of the light in each sector and hence of the noise verses θ. This system eliminates the mechanical motion disadvantage of the rotating slit system, but the number of angles that can be isolated is still limited by detector technology.

The third method uses a polar camera. In this system, the output plane light distribution is sampled at fine intervals along the two cartesian coordinates and the camera's supportive electronic processor then coverts this input light distribution into $(\rho, \theta)$ coordinates. By integrating along $\rho$, we can then obtain the output noise estimate as a function of θ as before. This method may be suitable for the final stage of the COC system, but it requires too extensive support electronics to be included at this point. Thus, for the initial experiments, a mechanical rotating slit was used and for the final system a specially fabricated wedge-shape detector appears to be the best choice.

A block diagram of the COC system is shown in Fig. 3.2. It is described in more detail in Sect. 3.3.

### 3.3 OPTICAL SYSTEM

In this section, we consider two of the COC optical systems considered and explain their operation. We then describe the system assembled and the reasons for it as well as the components used.

### 3.3.1 JOINT TRANSFORM CORRELATOR (JTC)

The JTC is shown in Fig. 3.3. In this system, the same reference signal $s_R$ is recorded on all channels in one half of plane $P_1$ and the other received signals $s_1-s_N$ are written in the other half of plane $P_1$ with a center-to-center
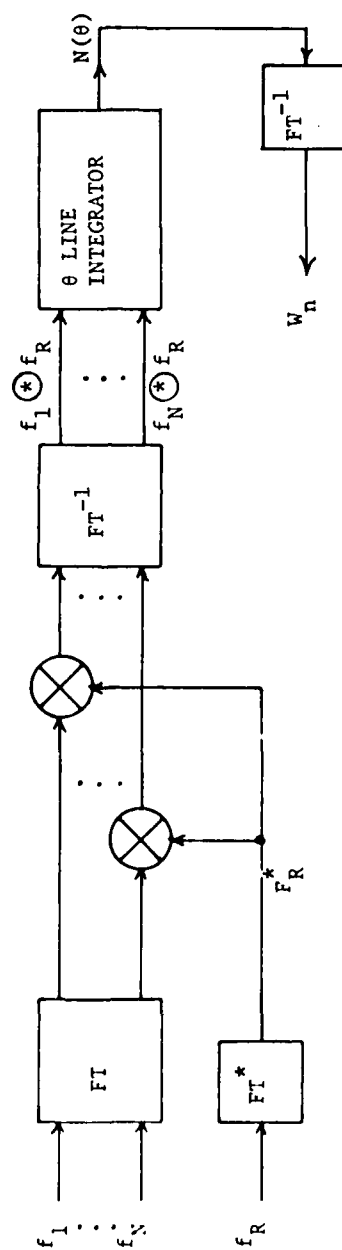
Fig. 3.2   Block diagram of the COC adaptive processor.

separation of "2a". Since the system uses 1-D operations, we can consider what occurs to each line separately. The light transmittance along the n th line in $P_1$ is

$$P_{1n}(x) = s_n(x-a) + s_R(x + a). \tag{3.5}$$

Lens system $L_1$ forms the 1-D Fourier transform of $P_{1n}(x)$ in plane $P_2$. When this pattern is recorded at $P_2$, the subsequent transmittance of $P_2$ is

$$P_{2n}(f) = \left| S_n(f)e^{j2\pi fa} + S_R(f)e^{-j2\pi fa} \right|^2, \tag{3.6}$$

where $S(f)$ is the Fourier transform of the signal $s(x)$. This recording is placed in plane $P_2$ and its 1-D Fourier transform (FT) in x is produced at $P_3$ by $L_2$. At the output plane $P_3$, we obtain

$$P_{3n}(f) = \mathfrak{F}\{|S_n(f)|^2 + |S_R(f)|^2\} \qquad \text{at } x = 0$$

$$+ \mathfrak{F}\{S_n(f)\ S_R^*(f)\} \qquad \text{at } x = -2a$$

$$+ \mathfrak{F}\{S_n^*(f)\ S_R(f)\}. \qquad \text{at } x = +2a \tag{3.7}$$

From (3.7), we see that the desired correlation is located at $x = +2a$. The three terms (3.7) can be separated in the output plane if "a" is chosen larger than 2b, where b is the width of each signal recording in $P_1$. The disadvantage of this system is that the full space bandwidth product (SBW) possible in $P_1$ is not utilized. Similarly the SBW and aperture requirements of the input spatial light modulator required at $P_1$ and of the lens system are much more stringent for this joint transform correlator topology. We thus reject this system in favor of the FPC system of Sect. 3.3.2.

IN          IDFT        BS        JTP        IDFT        OUT

$S_R$

$S_1$

$S_N$

$P_1$      $L_1$      Read Laser      $P_2$      $L_2$      $P_3$
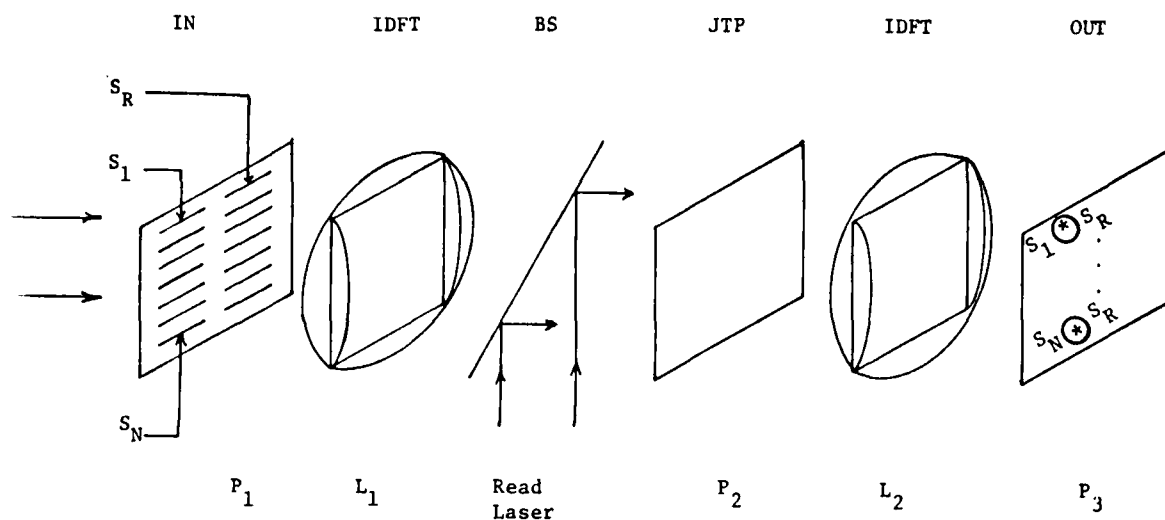
Fig. 3.3   Joint transform optical correlator for adaptive radar processing.

IN              MSF             OUT

$S_1$

$S_N$

$S_1 \circledast S_R$

$S_1 \circledast S_N$

$S_R^*$

$P_1$      $L_1$      $P_2$      $L_2$      $P_3$
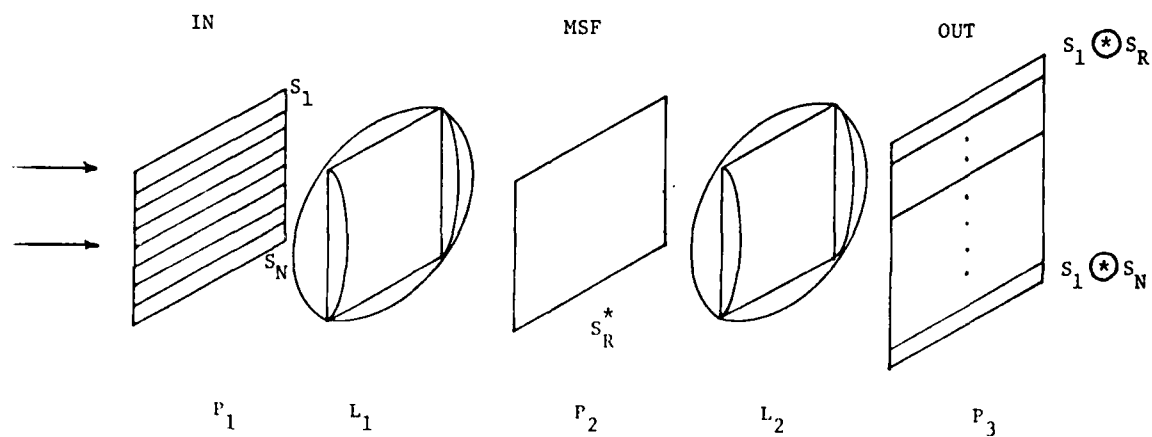
Fig. 3.4   Frequency plane optical correlator for adaptive radar processing.

### 3.3.2  FREQUENCY PLANE CORRELATOR (FPC)

The FPC system is shown schematically in Fig. 3.4.  The lens system $L_1$ and $L_2$ are 1-D FT systems.  At $P_2$, we record $S_R^*$ on all lines using holographic techniques.  When the different received signals $s_1$-$s_N$ are written on different channels in plane $P_1$, the light leaving $P_2$ is

$$P_2(f) = S_R^*(f) \; S_n(f). \tag{3.8}$$

Lens system $L_2$ performs a 1-D FT of (3.8) along the f axis.  This results in the desired multi-channel correlations in the output plane $P_3$.  The output will contain other undesired terms, but these can easily be separated from the correlation by proper choice of the signal to reference beam angle used when forming the $P_2$ pattern.  In this system, the SBW of the $P_1$ plane material can be much better utilized than in the JTC system.  This FPC system also has less stringent lens requirements then does the JTC one.  Because of these reasons, *the FPC system was chosen for the COC adaptive processor.*

### 3.3.3  SYSTEM DESIGN

The lay out of the FPC system that we assembled is shown in Fig. 3.5.  A 50m W helium-neon laser ($\lambda$ = 633nm) was used as the coherent light source.  This light output was divided into reference and signal beam paths by the beam splitter (BS) and mirrors (M) shown.  The lenses used are described in Table 3.2.  The angle of the reference plane wave illumination was chosen to be $15^o$.

M1, M2 -- Mirrors
O1, O2 -- Objective
PH1, PH2 -- Pinhole Spatial Filters
CL1, CL2 -- Collimating Lenses
BS -- Beam Splitter

LG -- Liquid Gate
CYL1, CYL2 -- Cylindrical Lenses
HPH -- Hologram Plate Holder
SL1, SL2 -- Spherical Lenses
IS -- Integrating Slit
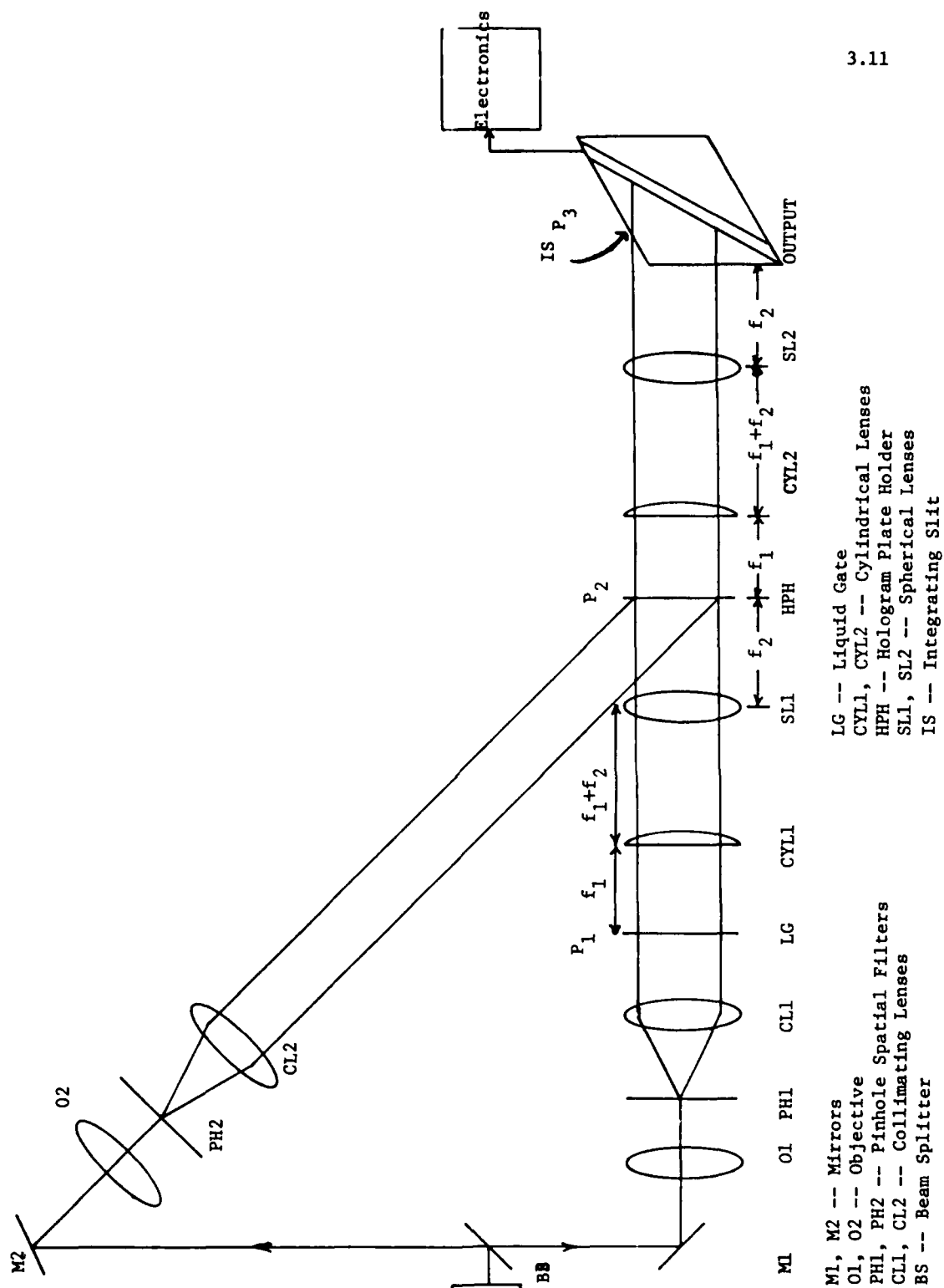
Fig. 3.5   Layout of the frequency plane correlator.

Table 3.2

Component Specification

| Component | Specification |
|-----------|---------------|
| 01, 02 | Magnification 5x |
| PH 1, PH 2 | 10μ Pinhole |
| CL 1 | Focal Length 495 mm |
| CL 2 | Focal Length 762 mm |
| CYL 1, CYL 2 | Focal Length $f_1$ = 200 mm |
| SL 1, SL 2 | Focal Lengths $f_2$ = 762 mm |
| Integrating Slit | 2.5 x Objective, 50μ x 1250μ Slit Probe |

The $P_2$ pattern in Fig. 3.4 is a matched spatial filter (MSF). It is formed with $s_R$ recorded on all lines in $P_1$ by recording the interference of the FT $S_R$ of $s_R$ and the reference beam. For all experiments, the inputs at $P_1$ were placed in a liquid gate (LG) and the MSF at $P_2$ was recorded on a holographic plate. The BS was orientated so that the ratio of the reference power to signal power at the dominant carrier spatial frequency was close to unity. This yields the maximum modulation or fringe constrast in the MSF. A wedge/ring detector was placed at $P_2$ and the BS was adjusted during MSF synthesis to achieve equal beam balance and modulation of the MSF. The exposure time was chosen to produce a bias exposure with a bias transmittance of 0.5.

The MSF recording was then developed in D-19 solution for five minutes at $70^\circ$ F. After the emulsion was dried, the holographic plate was placed in a

hologram plate holder (HPH) and the reference beam was blocked. The signals $s_1$-$s_N$ are recorded on different lines in $P_1$ (on film during initial experiments) which was then placed in the LG. The resulting multichannel correlation pattern in n (3.3) appears in the output plane $P_3$ where it is integrated in $\theta$ by a slit. This integrated intensity is then recorded versus $\theta$ by the support electronics.

## 3.4 NOISE MODELS

In this section, we describe the computer simulation used to model the COC system and to model the different noise sources and noise conditions considered for the array antenna. The FORTRAN routine that performs the multi-channel correlation is included in the Appendix.

### 3.4.1 SOFTWARE

The optical COC multi-channel correlator was digitally simulated in FORTRAN. The MAIN program generates single frequency jammer signals of the desired amplitude and frequency. The subroutine CORREL performs the desired correlation and PLOT2D is used to produce a 2-D display of the output. The routine NOISAN plots the noise distribution as a function of angle. It utilizes the subroutine PLOT1D to produce the 1-D output displays. The subroutine CORREL produces the correlation of the two sequences by forming the FFT of each, the product of these FTTs, and the inverse FFT of the result using a circular correlation. By appending a sufficient number of zeros to both sequences, the desired linear correlation results.

### 3.4.2 SIMULATION NOISE MODEL

As our first noise model, we consider the received signals from one noise source at a single frequency and an angle of $60^\circ$ to be present at the received

elements of an N = 39 element array. A total of 128 samples of each of the received signals were calculated with the sampling rate chosen so that these 128 samples covered 20 cycles of the sinusoidal noise signal. From (3.3), the output along each channel is

$$f_R \circledast f_n = C(t-\tau_n) \qquad (3.9)$$

$$= \mathrm{Sin}\{2\pi f(t-n\tau)\}$$

where N = -50...0...50 and τ is the delay from element – to – element and f is the frequency of the narrowband noise source. For this example, the output correlation consists of very diffusely spread light alternating at the frequency f. The resultant simulated output correlation surface is shown in Fig. 3.6 from which the sinewave as an envelope over a bias level is apparent. This bias level is used to simulate the fact that such biasing is necessary when recording any signal on film. Integration of the output pattern in Fig. 3.6 along different angles results in the noise estimate N (θ). The results of this are shown in Fig. 3.7, from which we notice a single peak at the angle θ = 60° of the noise source as expected.

### 3.4.3 NARROWBAND TWO NOISE SOURCE MODEL

As our second noise model, we choose 2 single frequency noise sources at angles $\theta_1 = -45°$ and $\theta_2 = +45°$. We choose the two frequencies so that they do not cross correlate. We also modulated these two single frequencies by a small amount of narrowband noise so that they would produce sharper correlation peaks in the output than would pure single frequency noise sources. This noise model also better approximates the expected situation than does the first model.

The resultant output correlation plane pattern is shown in Fig. 3.8. It contains two lines of correlation peaks at angles ± 45°. It is obvious from Fig. 3.8 that the slit angular integration of this output plane pattern will result in two large peaks at θ = + 45°. This noise estimate, obtained from
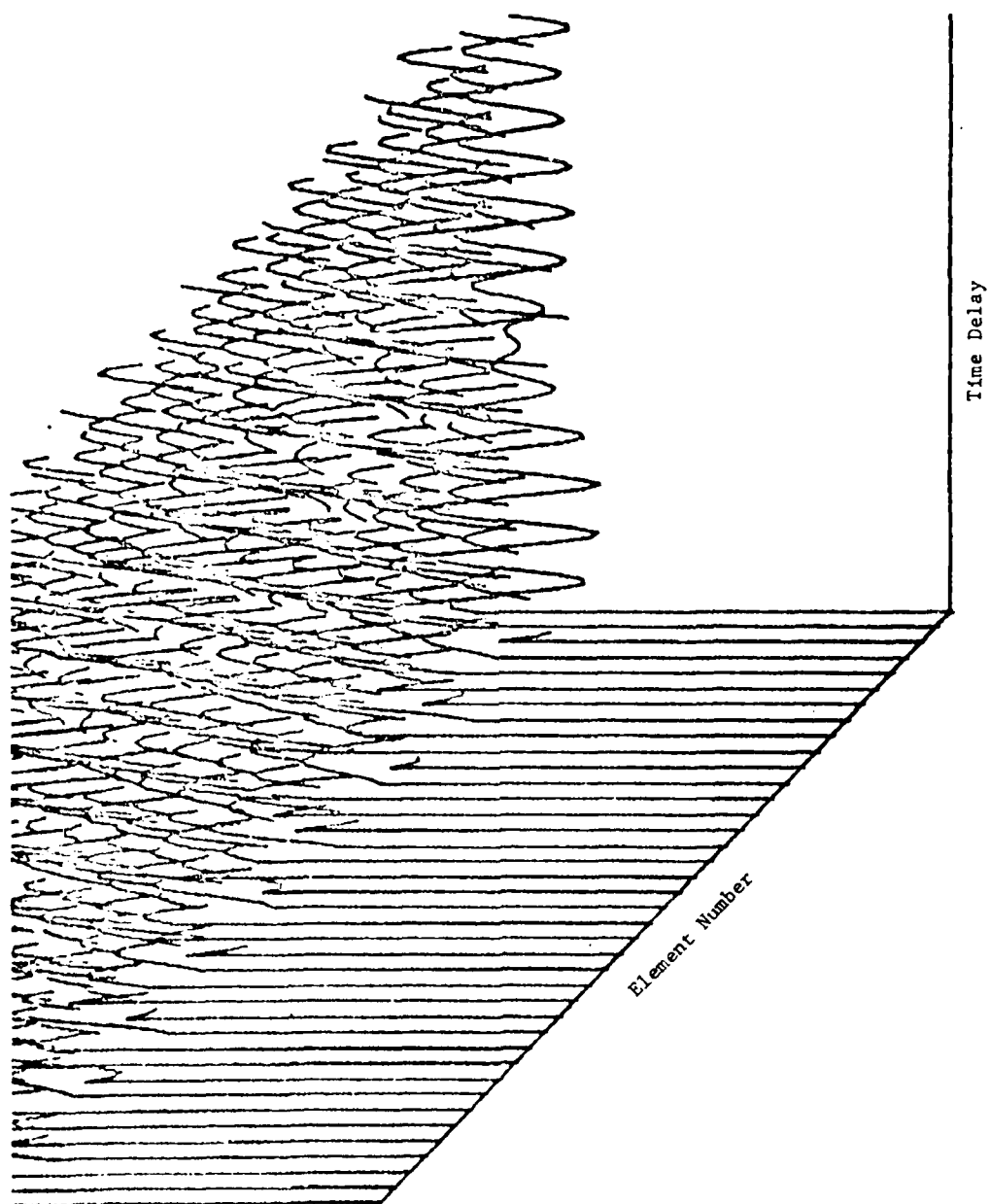
Fig. 3.6    Output correlation plane pattern for a Sinewave input.
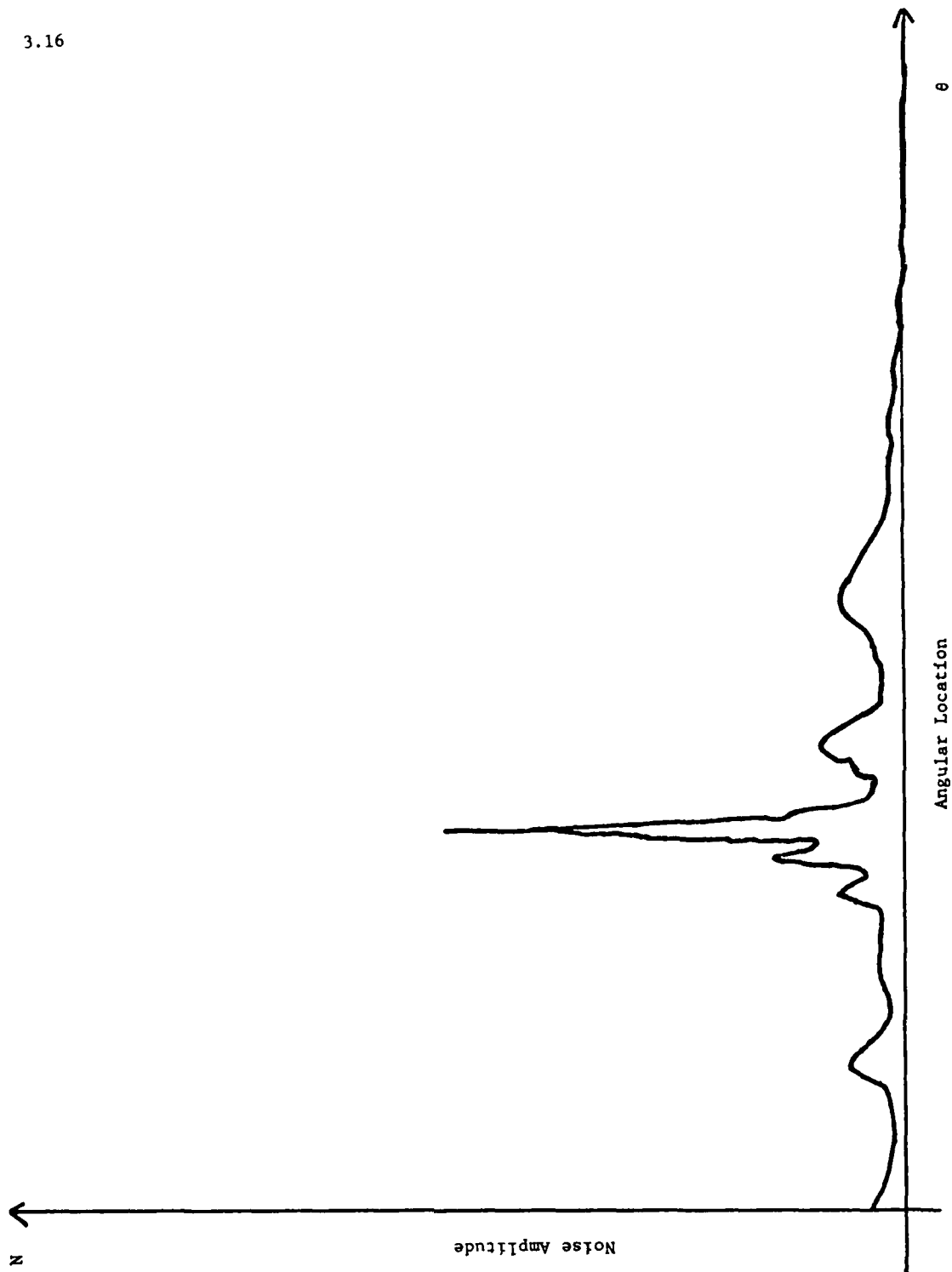
Fig. 3.7   Output of Fig. 3.6 after scanning with a slit.
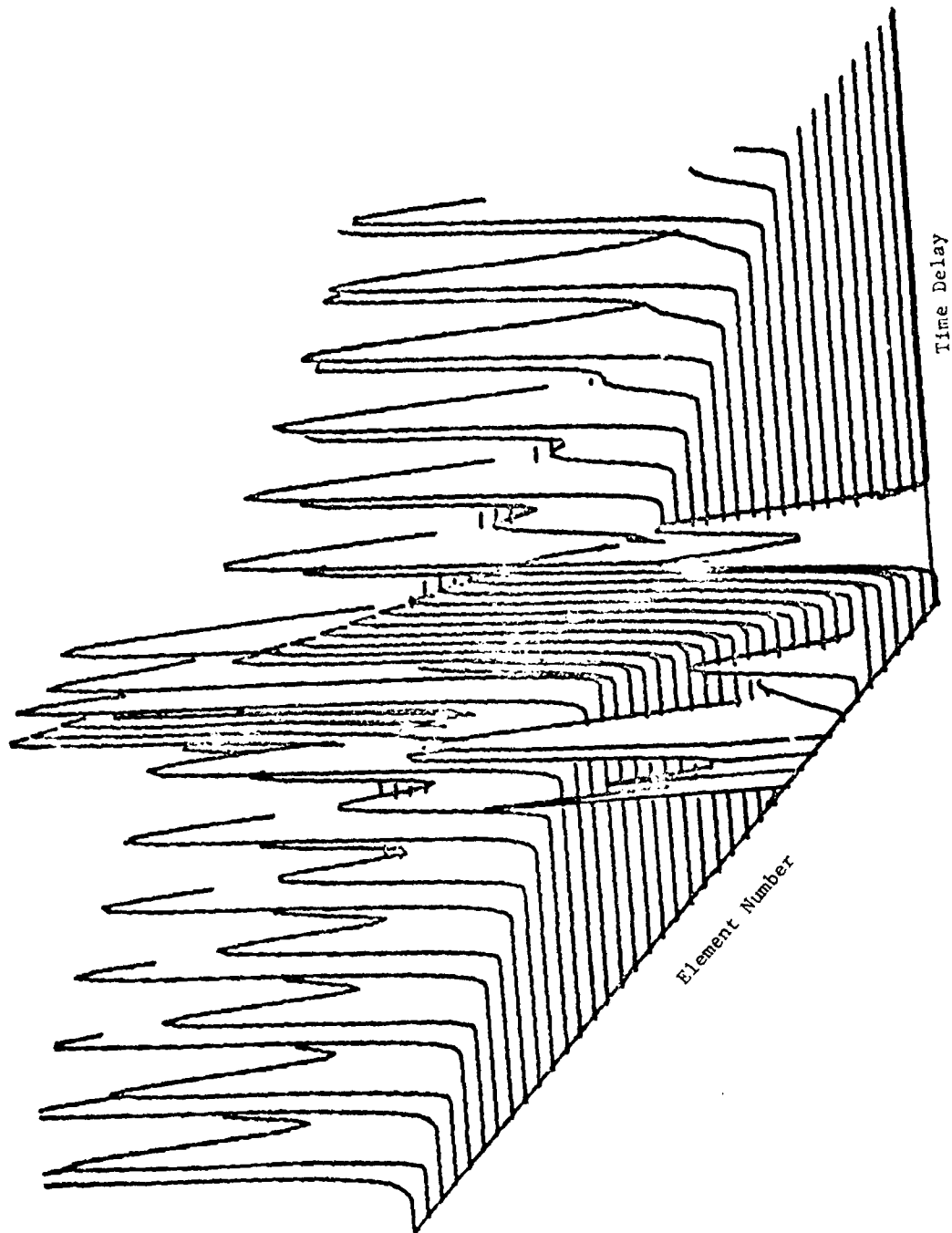
Fig. 3.8    Correlation output in the presence of two noise sources.

3.18
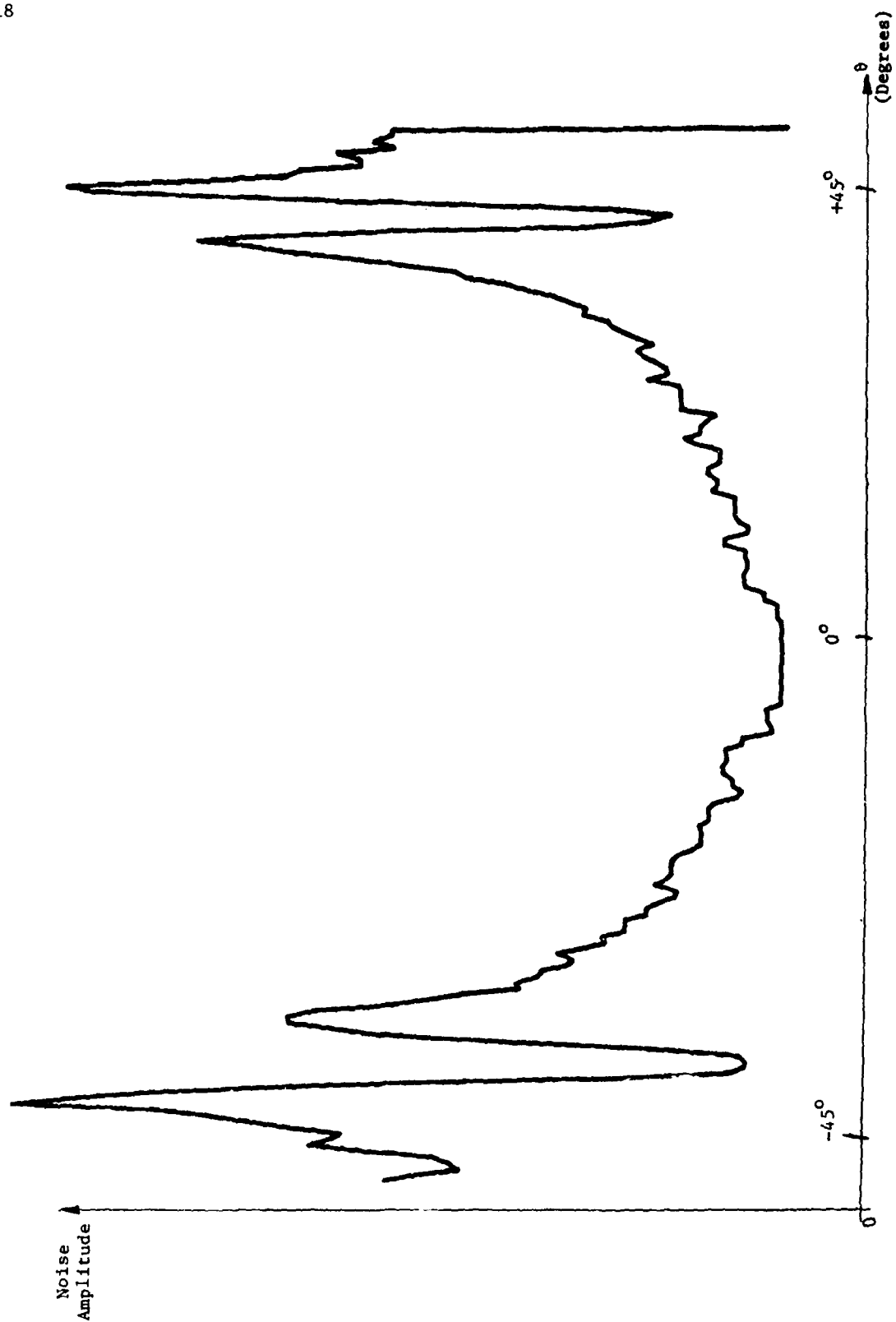


Fig. 3.9    Noise estimate from Fig. 3.8 for two noise sources at ± 45.

Fig. 3.8, is shown in Fig. 3.9. Its pattern is as expected and displays two prominent peaks at the correct locations.

### 3.4.4 STOCHASTIC NOISE MODEL

The signals we have considered thusfar are deterministic and do not fully reflect the random nature of the actual signals expected. In our third simulation, we model each of the two noise sources by random sequences to better simulate the presence of two uncorrelated noise sources. To produce such signals, a long random sequence of 5000 points was generated using the RAN function in Fortran. The first 2000 points were chosen as one sequence and the last 2000 points as the other sequence. The resultant two signals are the two uncorrelated sequences desired.

The two digital random sequences obtained have white spectra. This was confirmed by calculation. The desired received radar signals are band limited noise patterns. Since in the optical experiments, we will record these signals on film using a film recorder with constant modulation out to 15 cy/mm spatial frequency, we chose to model the bandpass noise signals with a spatial frequency spectrum between 5-15 cy/mm. Since the film recorder spots are spaced at intervals of 10 μm, the corresponding Nyquist frequency is $1/20$ μ = 50 cy/mm and any attempt to record higher frequencies will result in aliasing. We let the digital radial frequency of $\pm$ 1.0 π correspond to $\pm$ 50 cy/mm spatial frequency. To produce the desired noise spectrum with flat response over the 5-15 cy/mm band and 0 elsewhere, we used a digital filter described below.

The uniformly distributed white noise sequences were passed throug! a low-pass digital filter with extent from -5 cy/mm (-0.1 π) to +5 cy/mm (+ 0.1 π). The low pass filtered output was then multiplied by a sinusoidal frequency 10 cy/mm (0.2 π) to shift the bandpass spectrum to the desired center spatial frequency. The design of the digital filter is discussed below.

### 3.4.5 DESIGN OF THE DIGITAL LOW-PASS FILTER

Following Oppenheim and Schafer, we use a technique of bilinear transformation and a Butterworth filter to realize the digital low-pass filter. Since the cutoff frequency desired is 0.1 $\pi$, we introduce the condition that ripple in the passband be less than 1 dB, while in the stop band we require attenuation of more than 20 dB, i.e.

$$20 \log_{10} |H_a(e^{j0.1\pi})| \geq -1 \qquad (3.10a)$$

and

$$20 \log_{10} |H_a(e^{j0.15\pi})| \leq -20 \qquad (3.10b)$$

The Butterworth filter is described by

$$|H_a(j\Omega)|^2 = \frac{1}{1 + (\Omega/\Omega_c)^{2N}} \qquad (3.11)$$

where N is the order of the filter. Solving (3.10) using (3.11), we obtain N = 8 and $\Omega_c$ = 0.3446824. For this value of $\Omega_c$, all specifications are met. The poles of the digital filter are found by choosing 8 left half plane poles in the s-plane that are uniformly spaced on a circle of radius $\Omega_c$.

To obtain H (z), we first find its digital transfer function in terms of the z-transform using the bilinear transformation

$$s = \frac{2(1-z^{-1})}{(1+z^{-1})} \qquad . \qquad (3.12)$$

The resultant transfer function is very complex, but it can be separated into the product of 4 cascaded functions, which are easier to implement both from software and from hardware viewpoints. We thus write H(z) as

$$H(z) = H_1(z) \cdot H_2(z) \cdot H_3(z) \cdot H_4(z) \tag{3.13}$$

where

$$H_1(z) = 0.023615(1+z^{-1})^2/[1-1.769z+0.8774z^{-2}]$$

$$H_2(z) = 0.023615(1+z^{-1})^2/[1-1.589z^{-1}+0.6864z^{-2}]$$

$$H_3(z) = 0.023615(1+z^{-1})^2/[1-1.4744z^{-1}+0.5647z^{-2}]$$

$$H_4(z) = 0.023615(1+z^{-1})^2/[1-1.4189z^{-1}+0.5057z^{-2}] \tag{3.14}$$

Digital filtering is usually performed in a computer, thus the white noise sequence $x(n)$ is passed through $H_1$ to produce an output

$$y(n) = 1.769\, y(n-1)-0.8779\, y(n-2)+0.023615[x(n)+2x(n-1)+x(n-2)] \tag{3.15}$$

We then pass $y(n)$ through $H_2$, $H_3$ and multiply the result by $\cos(0.2\,\pi n)$ to obtain the desired bandpass noise sequence. This was done. To verify the nature of the resultant noise sequences obtained, we performed a 2048 point FFT on the noise sequence. The magnitude spectrum obtained is shown in Fig. 3.10. A noisy spectrum rather than a smooth one was obtained because of the finite precision of the FFT. However, we notice that the spectrum is limited to the desired frequency band and has above 20 dB rejection in the stop band and a fairly uniform response in the passband.

The noise sequence as described above was recorded on film using our film recorder and used in the optical experiments described in Section 3.7. We defer further discussion of these results until Section 3.7.

### 3.5 ACCURACY OF THE COC NOISE ESTIMATE

In this section, we analyze the COC noise estimation method from a statistical viewpoint. We define the estimation SNR when one noise source is present and

Fig. 3.10 Digital spectrum of stochastic noise model.
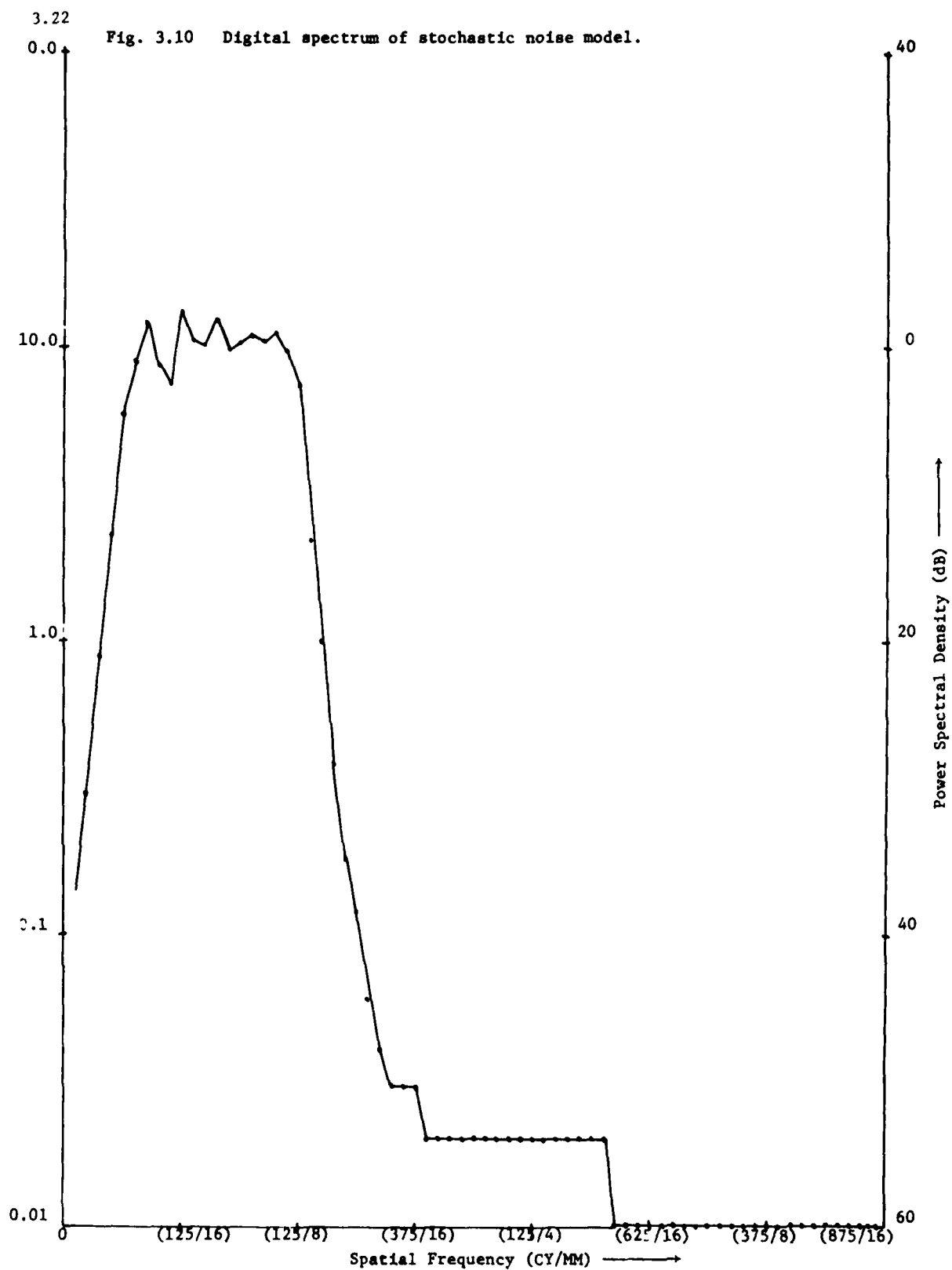
obtain the resolution performance when two noise sources are present.

Let the receiving array consist of N (odd number) antenna elements and let the noise source be at an angle $\theta$. If s (t) is the signal received at the central element, the signal received at the i th element is

$$s_i(t) = s(t-\tau_i),\qquad(3.16)$$

where $i = - (N-1)/2...0...(N-1)/2$ and

$$\tau_i = i \ (d \cos \theta)/c.\qquad(3.17)$$

When the array elements are spaced on a line at uniform intervals d, the N optical correlations yield

$$C_i(\tau) = \int_{-T/2}^{T/2} s \ (t) \ s_i \ (t + \tau)dt$$

$$= \int_{-T/2}^{T/2} s \ (t) \ s \ (t + \tau - \tau_i)dt,\qquad(3.18)$$

where T is the integrating aperture or the time interval over which the signal is obtained (whichever is smaller). As an estimate of the noise distribution, we integrate the output along radial lines and obtain the estimate

$$\hat{N}(\beta) = \sum_{i=-N^1}^{N^1} C_i \ (\beta i)$$

$$= \sum_{n=-N^1}^{N^1} \int_{-T/2}^{T/2} s(t) \ s(t + \beta i - \beta^* i)dt,\qquad(3.19)$$

where $(N - 1)/2 = N^1$ and $\beta^* = (d \cos \theta)/c$ is proportional to the correct angle.

An ideal estimate $\hat{N}(\beta)$ will be zero for $\beta \neq \beta^*$ and will peak at $\beta = \beta^*$. Let us assume that $s(t)$ is a sample realization from a zero mean, stationary, stochastic process. Then the average noise estimate is

$$\overline{\hat{N}(\beta)} = E[\sum_{i=-N^1}^{N^1} \int_{-T/2}^{T/2} s(t) \, s(t + i\beta - i\beta^*)dt]$$

$$= \sum_{i=-N^1}^{N^1} \int_{-T/2}^{T/2} R_s(i\beta - i\beta^*)dt$$

$$= T \sum_{i=-N^1}^{N^1} R_s[i(\beta-\beta^*)], \tag{3.20}$$

where $R_s(\tau)$ is the auto correlation function of the signal process. Since $R_s(0)$ is always greater than $R_s(\tau)$ for $\tau \neq 0$, we see that $\overline{\hat{N}(\beta)}$ is maximum at $\beta = \beta^*$ as is desired. The sharpness of this correlation peak can be characterized by the SNR with a larger value of SNR resulting in a sharper correlation peak and hence a better estimate of the location of the noise source. For SNR, we write

$$SNR = \frac{|E\{\hat{N}(\beta^*)\}|^2}{Var\{\hat{N}(\beta)\}|_{\beta >> \beta^*}}. \tag{3.21}$$

From (3.19), we can write

$$E\{\hat{N}(\beta^*)\} = T \sum_{i=-N^1}^{N^1} R_s(0) = TNR_s(0). \tag{3.22}$$

The variance can be estimated as below

$$Var[\hat{N}(\beta)]_{\beta >> \beta^*} = \sum_i\sum_j \iint_{-T/2}^{T/2} \{R_s(t-u)R_s[t-u+(\beta^*-\beta)(j-i)]+R_s[t-u-j(\beta-\beta^*)]$$

$$R_s[t-u+i(\beta-\beta^*)]\}dtdu$$

$$= \sum_i \iint_{-T/2}^{T/2} R_s^2(t-u)dtdu$$

$$= NT \int_{-T}^{T} (1-|\tau|/T)R_s^2(\tau)d\tau, \tag{3.23}$$

where we use the assumption that $R_s(\tau)$ is essentially zero for large values of $\tau$. The SNR can then be expressed as

$$\text{SNR} \simeq NT[\int_{-T}^{T} (1-|\tau|/T)[R_s^2(\tau)/R_s^2(0)]d\tau]^{-1}. \qquad (3.24)$$

To better understand the behavior of    SNR with the various parameters, we assume that the signal has the exponential  auto correlaton function

$$R_s(\tau) = \exp(-a|\tau|), \qquad (3.25)$$

where "a" is a measure of the signal bandwidth.  Substituting (3.25) into (3.24), we obtain

$$\text{SNR} = \frac{NT}{2} \left[\frac{2aT-1+\exp(-2aT)}{4a^2T}\right]^{-1}. \qquad (3.26)$$

For   large time bandwidth products, aT >> 1, we can approximate (3.26) by

$$\text{SNR} \simeq NaT = (\text{No. Ant. Elem.}) (\text{Noise BW})(\text{Observ. Time}). \qquad (3.27)$$

From (3.27), we find that the noise angle estimate can be improved by either increasing the number of antenna elements N or by increasing the space bandwidth product (aT).

For purposes of resolution analysis, we postulate the presence of two noise sources at angles $\theta_1$ and $\theta_2$.  We also assume that these noise signals belong to uncorrelated random processes with zero means and with auto correlation functions $R_1(\tau)$ and $R_2(\tau)$.  The average noise estimate is then given by

$$\overline{\hat{N}(\beta)} = T \sum_{i=-N}^{N} \{R_1[i(\beta-\beta_1^*)]+R_2[i(\beta-\beta_2^*)]\} \qquad (3.28)$$

where

$$\beta_1^* = (d \sin \theta_1)/c \qquad (3.29)$$

and

$$\beta_2^* = (d \sin \theta_2)/c. \qquad (3.30)$$

If the auto correlation function of both noise sources are sharp, the average noise estimate will appear as shown in Fig. 3.11. The Rayleigh criteria can then be used to judge whether the two noise sources are resolvable. For the sake of simplicity, we assume $\beta_1^* = \beta^* = -\beta_2^*$ and $R_1(\tau) = R_2(\tau)$. Then, the two noise sources at angular locations $\theta$ and $-\theta$ will be resolvable if

$$\sum_{\substack{i = -N^1 \\ i \neq 0}}^{N^1} \{R(-i\beta^*)+R(i\beta^*)\} \leqslant 1/2 \sum_{\substack{i = -N^1 \\ i \neq 0}}^{N^1} \{R(0)+R(2i\beta^*)\}, \tag{3.31}$$

where $i = 0$ is deleted from the summation because $C_0(\tau)$ does not provide any information on the location of the noise source. Here we assumed that the two peaks in the noise estimate were resolvable if $\overline{\hat{N}(0)}$ was less than 1/2 (3dB) of $\overline{\hat{N}(\beta^*)}$.
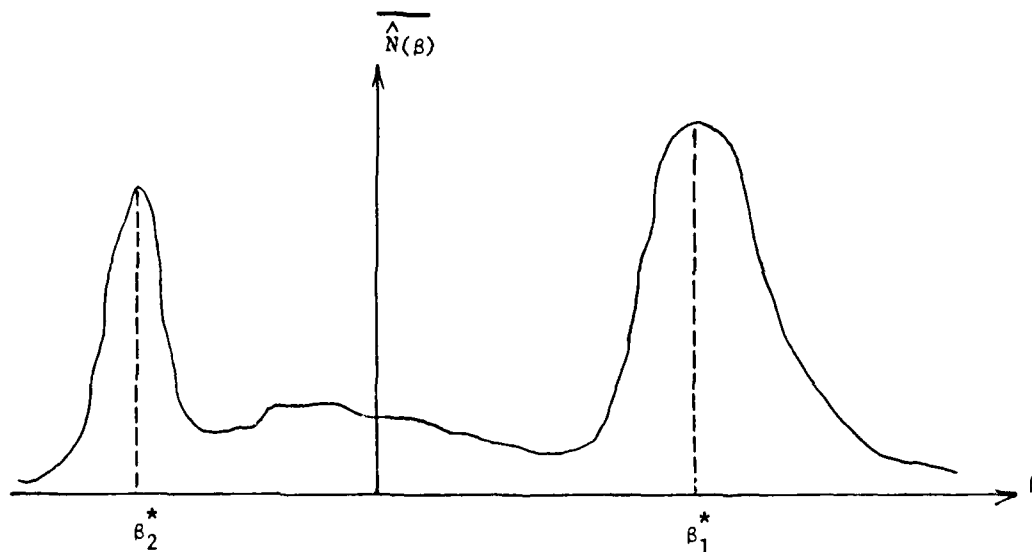


Fig. 3.11   Average noise estimate for two noise sources.

If we assume that $R(\tau)$ is sharply peaked, we can approximate (3.31) by

$$R(\beta^*)/R(0) \leq N/8. \qquad (3.32)$$

From (3.32), the following observations can be made:

(i) since $R(\tau)$ usually decreases as $\tau$ increases, increasing the value of N allows smaller $\beta^*$ values to satisfy (3.32). Thus as N increases, the sources can be more closely spaced and yet still be resolvable.

(ii) The aperture of integration T does not effect (3.32) and as a result a larger time of integration will not improve the available system resolution.

(iii) Larger signal bandwidths imply faster decay of $R(\beta)$, thus allowing smaller values of $\beta^*$ to satisfy the condition in (3.32).

## 3.6 POST PROCESSING

Thus far, we have been concerned with estimating the angular distribution of the far field noise. We now consider an equally relevant aspect of adaptive array processing: the determination of the accompanying weights to be applied to the elements of the phased array. In this section, we consider two methods to accomplish this and the difficulties associated with each.

We assume a scenario in which there are M noise sources $s_m(t)$ and a target return $s(t)$ and we assume that the desired target is at boresight. The signal received at the n th antenna element is thus

$$f_n(t) = s(t) + \sum_{m=1}^{M} s_m(t-\tau_{mn}). \qquad (3.33)$$

When the adaptive array has weights $w_n$, the array output is

$$f(t) = \sum_{n=-N}^{N^1} w_n f_n(t) = s(t) \sum_n w_n + \sum_{nm} w_n s_m(t-\tau_{mn})$$

$$= 0_s(t) + 0_n(t), \qquad (3.34)$$

where the index n varies from $-N^1$ to $N^1$, while the index m varies from 1 to M. The array output f(t) is divided into a deterministic part $0_s(t)$ and a random part $0_n(t)$ as shown in (3.34).

We now consider two approaches to determining the weights: (i) maximizing the SNR and (ii) minimizing the noise variance.

Case (i):  Maximize SNR:

The output SNR is defined as

$$SNR = \frac{\left| E[f(t)] \right|^2}{Var[f(t)]} .$$

(3.35)

We assume that the M noise sources belong to uncorrelated, gaussian processes with zero mean and stationary statistics.  With this assumption and (3.34),

$$E[f(t)] = s(t) \sum_n w_n$$

(3.36a)

$$Var[f(t)] = \sum_{nj} w_n w_j C_{nj}$$

(3.36b)

where

$$C_{nj} = \sum_m R_m(\tau_{mn} - \tau_{mj}) .$$

(3.36c)

To determine the weights $w_n$ necessary to maximize SNR, we must satisfy

$$\frac{\partial}{\partial w_k} \left[ \frac{\sum_{me} w_m w_e}{\sum_{nj} w_n w_j C_{nj}} \right] = 0,$$

(3.37)

for $k = -N^1 \cdots 0 \cdots N^1$.  This results in the condition

$$2[\sum_{nj} w_n w_j C_{nj}] - [\sum_n w_n][\sum_j w_j (C_{kj} + C_{jk})] = 0.$$

(3.38)

Using vector notation, the above condition can be written as

$$[\underline{W}^T \underline{C} \underline{W}] \underline{U} - [\underline{W}^T \underline{U}] [\underline{C} \underline{W}] = \underline{0}, \tag{3.39}$$

where $\underline{W}$ is a column vector $[W_{-N}1, \ldots W_N1]^T$, $\underline{C}$ is the NxN matrix (symmetric) with elements $C_{ij}$ and $\underline{U}$ is the unit column vector $[1 \ldots 1]^T$ of size N. The optimal weight vector is then

$$\underline{W} = [\frac{\underline{W}^T \underline{C} \underline{W}}{\underline{W}^T \underline{U}}] \underline{C}^{-1} \underline{U} = K' \underline{C}^{-1} \underline{U}, \tag{3.40}$$

where the term inside the brackets does not affect the SNR as can be seen from (3.35). From (3.40), we see that determination of the optimum weights $\underline{W}$ requires knowledge of the covariance matrix $\underline{C}$ and the operation of inverting $\underline{C}$.

Case (ii): Minimizing Noise:

Another view point which reduces the computational requirements is to minimize the variance of $O_n(t)$ given in (3.34). This is different from maximizing the SNR as discussed above. In this case, we assume that the contribution $O_s(t)$ due to the signal remains constant, i.e.

$$\Sigma \, w_n = 1. \tag{3.41}$$

The noise variance is then

$$Var[f(t)] = \sum_{nj} C_{nj} w_n w_j,$$

where

$$C_{nj} = \sum_m R_m (\tau_{mn} - \tau_{mj}). \tag{3.36}$$

To minimize (3.36), we differentiate (3.36) with respect to each weight and set the derivatives equal to zero. This results in the set of equations:

$$\Sigma \, w_n = 1 \qquad\qquad (3.42a)$$

$$\underset{n}{\Sigma} \, w_n C_{nj} = 0 \qquad\qquad (3.42b)$$

for $j = -N^1, \cdots 0 \cdots N^1$.

Considering the $(N-1)$ equations in (3.42b) and (3.42a), we find the optimal weight vector to be

$$\underline{W} = \underline{C}_1^{-1} \underline{U}_1, \qquad\qquad (3.43)$$

where $\underline{C}_1$ is a modified matrix and $\underline{U}_1 = [1,00 \cdots 0]^T$. From (3.43) we notice that we need to compute only the first column of the inverse matrix rather than the complete matrix as in case (i) in (3.40). Since the inversion of this matrix involves far more computational load than estimating it, we chose to reduce the computational time by following such a method. As suggested earlier, this method will not yield the best possible output SNR, but it is more easily implemented optically.

We now proceed with an approximate solution to (3.40). The optimal weights given by (3.40) are first rewritten as

$$\underset{n}{\Sigma} \, C_{nj} w_n = k, \text{ for all } j. \qquad\qquad (3.44)$$

In the case of a linear array with uniform spacing d and single frequency noise sources, we find

$$\tau_{mn} - \tau_{mj} = (2\pi/\lambda)(j-n)d \cos \theta_m \qquad\qquad (3.45a)$$

$$R_m(\tau) = \exp(j2\pi \, \tau \nu) \qquad\qquad (3.45b)$$

where $\nu = c/\lambda$ and c is the velocity of the radiation. In this case, (3.44) becomes

$$\underset{n}{\Sigma} \, w_n \underset{m}{\Sigma} \exp[j2\pi\nu(2\pi/\lambda)(k-n)d \cos \theta_m] = \text{constant for all } k. \qquad (3.46)$$

For the case of a single noise source, (3.46) becomes

$$\sum_n w_n \exp[j4\pi^2(\nu d/\lambda)(k-n) \cos \theta_m] = \text{constant.} \qquad (3.47)$$

Ignoring the phase factors in (3.47), we obtain

$$\sum_n w_n \exp(-j2\pi bn) = \exp(j2\pi bk), \qquad (3.48)$$

where

$$b = 2\pi\nu d(\cos \theta)/\lambda. \qquad (3.49)$$

From (3.48) we see that the weights must be chosen so that the Fourier transform (DFT) of $w_n$ results in $\exp(j2\pi bk)$ for different values of k. Once the noise distribution is estimated, $\hat{\theta}$ is known and can be used to estimate $\hat{b}$ from (3.49). Then, computing the weight vector involves only an inverse DFT of the right hand side of (3.48). This can easily be performed in a digital FFT post processor.

We should reiterate the above conclusion that a simple FFT post processor is of use in the COC system only for the case of single frequency signals and for uniformly spaced linear array antennas.

## 3.7 EXPERIMENTAL RESULTS

In this section, we consider the optical experimental computations of the noise estimation. The data used at $P_1$ and $P_2$ in the system of Fig. 3.5 were recorded on film using our film recorder. The recorded data is described and the expected estimates are compared to the outputs obtained experimentally.

We simulated the presence of two band pass noise sources as described in Sects. 3.4.4 and 3.4.5 and recorded these signals on film in the format described

in Sect. 3.3. The two noise signals are uncorrelated and have a spectrum that is limited to the spatial frequencies (5-15 cy/mm). These signals were recorded in the format shown in Fig. 3.12.

The shaded part of Fig. 3.12 represents the opaque region of the recorded film. The line-to-line spacing used was 10 μm and the recording spot size was 10 μm. The composite reference signal $f_1(n,x)$ was recorded on 1000 lines in the top half of the film. If the two uncorrelated noise signals are $s_1(x)$ and $s_2(x)$, then $f_1$ is described by

$$f_1(n,x) = s_1(x) + s_2(x) \text{ for all n.} \tag{3.50}$$

The received signals at the other antenna elements are similarly described by

$$f_2(n,x) = s_1(x+n \cdot 10 \text{ μm}) + s_2(x-n \cdot 20 \text{ μm}). \tag{3.51}$$

The horizontal locations of $s_1$ and $s_2$ where chosen to correspond to a delay of 10 μm in one direction for $s_1$ and a delay of 20 μm in the other direction for $s_2$. The top half of the film is used during preparation of the MSF at $P_2$ and the bottom half during the correlation process itself.

When $f_2$ is placed at $P_1$ of Fig. 3.5 and an MSF of $f_1$ at $P_2$, the expected multichannel optical output correlation plane pattern should consist of narrow correlation peaks at angles corresponding to the $\pm 45^\circ$ angles of the noise sources in the model as shown in Fig. 3.13. The central channel in both films was left blank since it does not contain any useful information and since the dark line present there serves us well for alignment purposes.

The observed correlation peaks from the experiment appear to form into two lines as in Fig. 3.13 at angles $\theta_1$ and $\theta_2$ corresponding to the correct angles
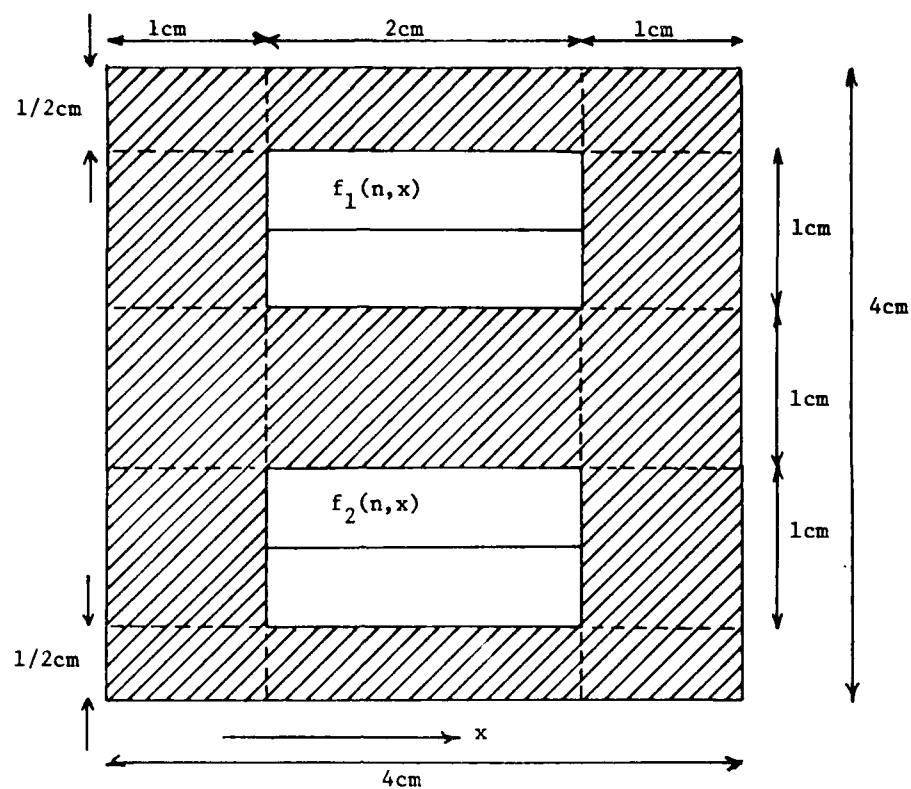
Fig. 3.12    Format of recording on the film.
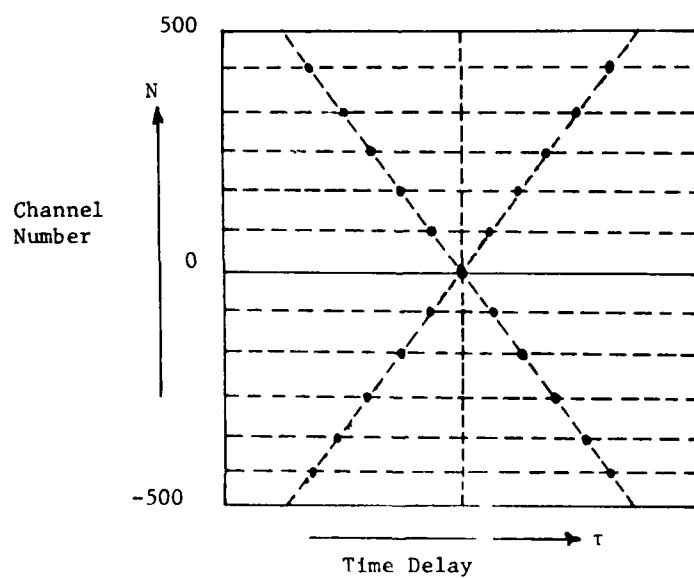


Fig. 3.13    Expected correlation output pattern.

of the noise sources. An isometric view of the output obtained is shown in Fig. 3.14. It clearly exhibits the two angular lines of correlation peaks predicted by theory. The results of an angular slit integration of the pattern in Fig. 3.14 along radial lines provides the $N(\theta)$ noise estimate shown in Fig. 3.15. As shown, the output is as expected. Various other cases yielded similar excellent agreement between theory and experiment.

## 3.8 CONCLUSIONS

The theoretical analysis of a frequency plane correlator COC system for adaptive processing has been performed, an optical system has been fabricated, a digital simulation of the system has been completed and various noise source models have been produced and analyzed. The results of our initial experiments using the optical FPC version of the COC system to compute the angular noise field distribution and noise estimates were successful and agreed well with theory as shown.

A detailed analysis of the statistics of the noise estimate obtained from the COC system, the postprocessing requirements, and the number of samples necessary to obtain an adequate estimate of the noise statistics were conducted and provided the valuable information on further direction for an alternate COC processor for adaptive radar.

From a statistical analysis of the method of estimating the angular noise distributions, we found that the SNR of the estimate was directly proportional to the number of antenna elements and the space bandwidth product of the noise signal. We also observe that the resolution of the estimate was independent of the integrating aperture and improved with an increase in the noise band-width or an increase in the number of antenna elements.

We have also determined that the postprocessing to calculate the adaptive weights from the output of the COC system can be approached either by maximizing SNR (this requires knowledge of the complete covariance matrix and its complete
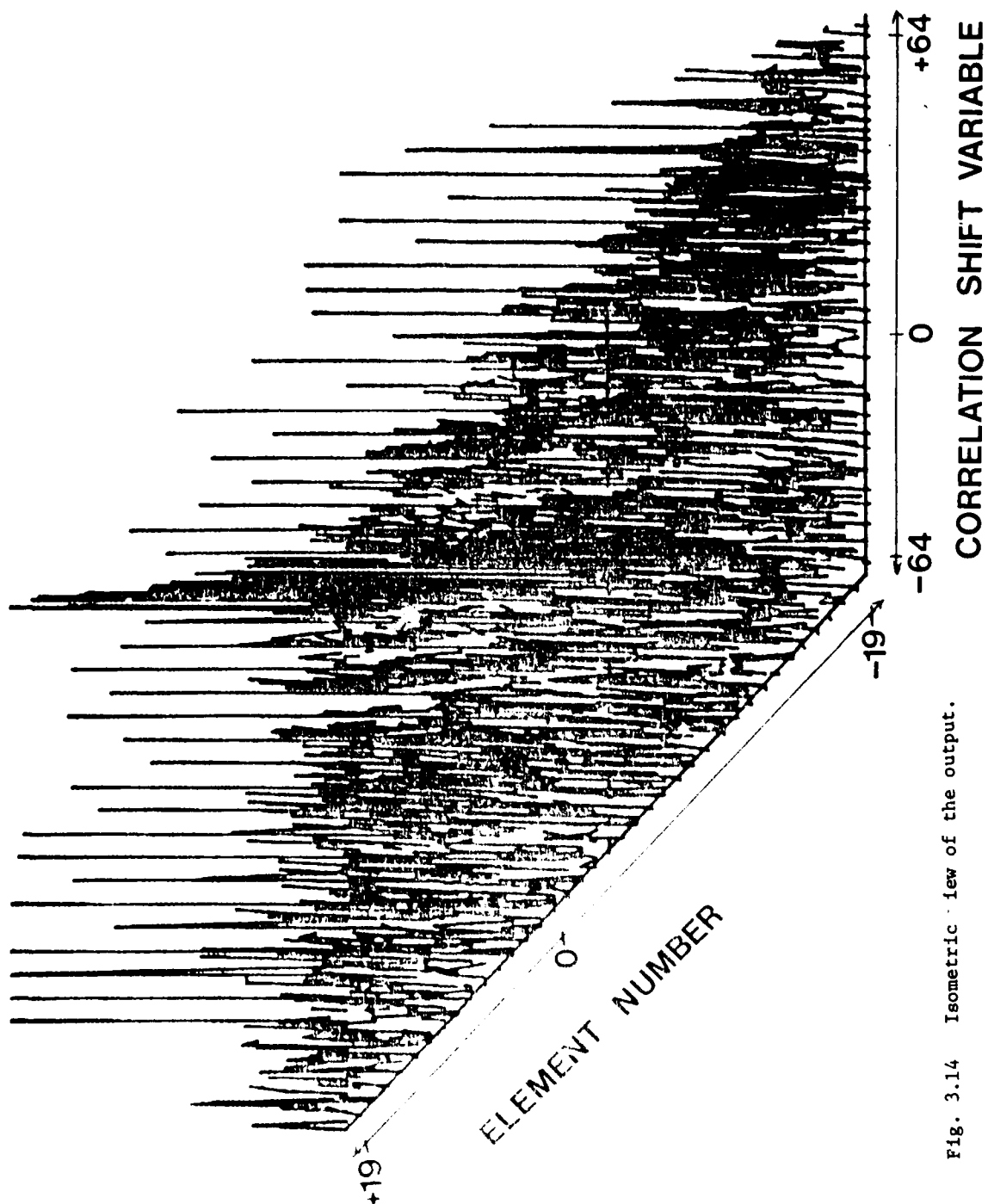
Fig. 3.14  Isometric view of the output.

SLOPE IN OUTPUT PLANE m, ANGLE OF NOISE SOURCE θ
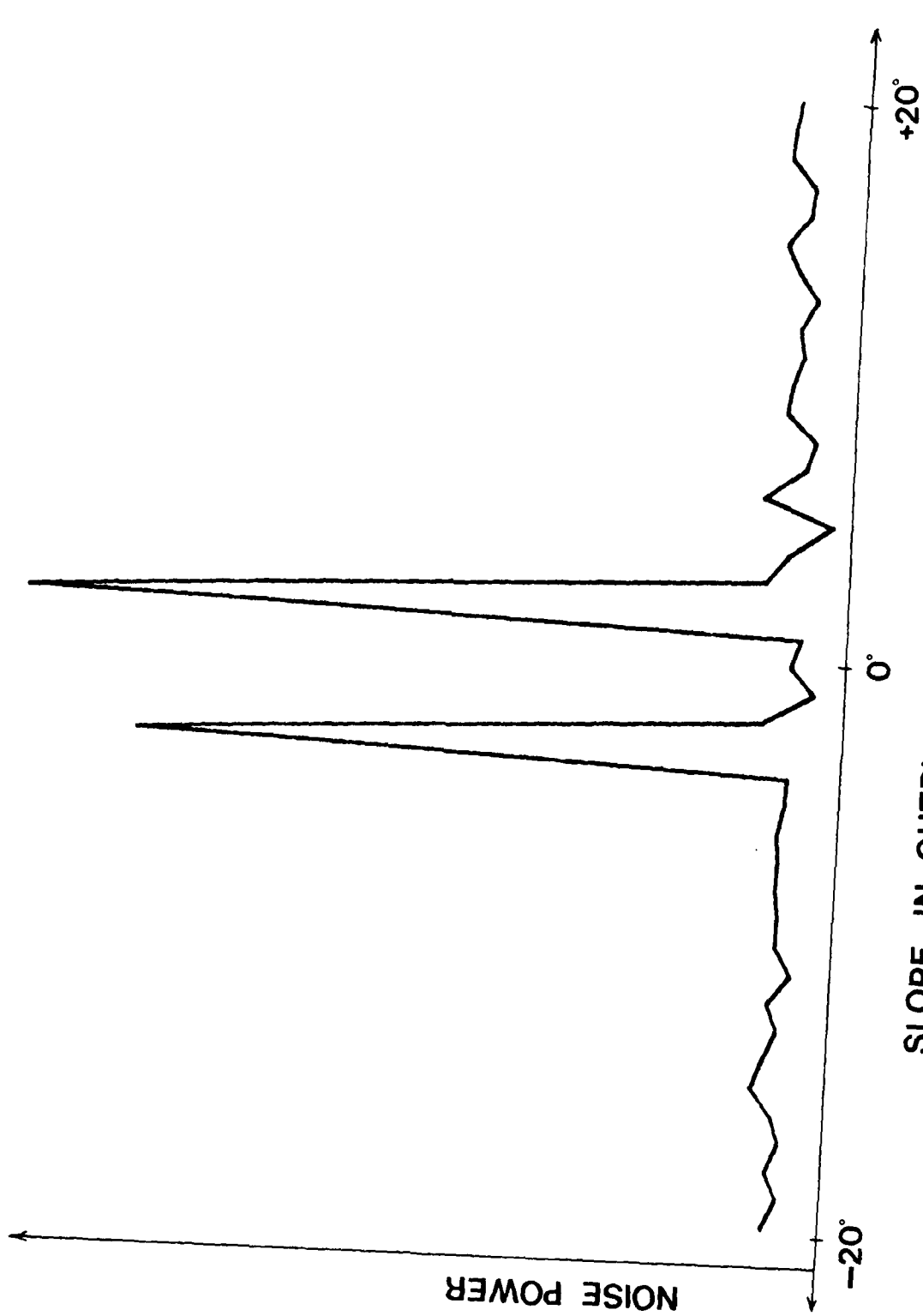
Fig. 3.15  $\hat{N}(\theta)$ after scanning along the slit in Fig. 3.14

NOISE POWER

+20°

0°

−20°

inverse) or by minimizing the noise variance (this requires knowledge of the full covariance matrix but only the first column of its inverse). This latter solution results in a considerably simpler COC electronic postprocessor.

Moreso, our analysis demonstrated that the postprocessor that computes the weights from the angular noise distribution outputs of the COC system is a simple inverse FFT system only for the case of a linear array and for mono-frequency noise sources. These conclusions are less disturbing when time and frequency diversity are considered, since in this case, we can simply bandpass the data into narrow enough frequency bands to allow use of a simple inverse Fourier transform digital postprocessing operation for each adaptive frequency.

A more major concern with the frequency plane correlator version of the COC adaptive processor is its limited input time bandwidth product and the failure for 2-D spatial light modulators to mature signigicantly in the past year. Since 2 N samples at the noise bandwidth are necessary per antenna element to accurately estimate the noise statistics for an N element adaptive array and since we must record the heterodyne carrier to obtain the necessary angular resolution, a very large input time bandwidth product is necessary for an optical COC adaptive radar processor. We thus propose to utilize a COC system with 1-D acoustic-optic transducers of high center frequency and with more reliability and availability than the 2-D spatial light modulators initially contemplated and required in the FPC version of the COC system. This will solve our component availability problem. To obtain the large time bandwidth product necessary, we will employ a time integrating correlator structure. We plan to pursue these new COC system design considerations in the next phase of this program. The basic conceptual idea of this new COC system is the same as the one described here. The modifications noted are made to allow adequate noise statistics to be obtained and sufficient angular resolution to be retained. A version of this time integrating acousto-optic system with both angle (space) and frequency diversity also appears possible.

BIBLIOGRAPHY

1.  C. Cook and M. Bernfeld, Radar Signal, Academic Press, New York (1969).

2.  M. Skolnik, Radar Handbook, McGraw-Hill, New York (1970).

3.  D. Vakman, Sophisticated Signals and the Uncertainty Principle in Radar, Springer-Verlag, Berlin (1968).

4.  A. W. Rihaczek, Principles of High Resolution Radar, McGraw-Hill, New York (1969).

5.  L. J. Cutrona, E. N. Porcello and W. E. Vivian, Proceedings IEEE, 54, 1026-32 (1966).

6.  H. L. Van Trees, Detection, Estimation and Modulation Theory - Part I, Wiley, New York (1968).

7.  A. Papoulis, Probability, Random Variables and Stochastic Processes, McGraw-Hill, New York (1965).

8.  W. Hoefer, IRE Military Electronics, 6, 174, (1962).

9.  A. Vander Lugt, IEEE Trans. on Inform. Theory, 10, 139-145 (1964).

10. J. E. Rau, Journal of Optical Society of America, 57, 798-802 (1967).

11. D. Casasent and A. Furman, Applied Optics, 16, 1662 (1977).

12. A. V. Oppenheim and R. W. Schafer, Digital Signal Processing, Prentice-Hall, New York (1975).

CHAPTER 4

ITERATIVE OPTICAL PROCESSOR FOR ADAPTIVE PHASED ARRAY RADAR

4.1  INTRODUCTION

The most immediately realizable electro-optical processor for APAR that
we have investigated is described in this chapter.  It is basically a non-
coherent, feedback, iterative, vector-matrix multiplier using a linear LED
input source array, a fixed covariance matrix and an orthogonal linear output
photodetector array with appropriate intermediate optics.  The APAR loop
equation is reformulated in Section 4.2 as a vector-matrix equation.  The basic
iterative optical processor (IOP) system is then described in Section 4.3.  The
system we fabricated to test the components and to demonstrate use of this novel
system design are described in Section 4.4.  Since the data to be processed are
complex numbers, the various methods to accommodate such operations in this
system are summarized in Section 4.5.

Our experimental demonstration of the use of the IOP system in an APAR
application on complex data are then described in Section 4.6.  A new electro-
optical color-multiplexed IOP technique for accommodating complex data in a
vector-matrix processor is presented in Section 4.7 together with our experi-
mental demonstration of this system.  Several general system application issues
are then addressed in Section 4.8.

4.2  MATHEMATICAL FORMULATION

The N intermediate differential equations that describe the average weights
W are given by

$$\tau \dot{\vec{W}}/G + (M + I/G)\vec{W} = \vec{S}^*.$$

(4.1)

The steady state solution of (4.1) for $\vec{W}$ is obtained by setting $\dot{\vec{W}} = 0$ and assuming $G \gg 1$ to be

$$M\vec{W} = \vec{S}\star.$$
(4.2)

The desired weights $\vec{W}$ can be obtained from $\vec{S}\star$ and M by

$$\vec{W} = M^{-1}\vec{S}\star.$$
(4.3)

The electro-optical system described in this chapter solves (4.2) for the weights $\vec{W}$ using the iterative algorithm

$$\vec{W}_{i+1} = \vec{S}^{\star} + (1-M)\,\vec{W}_i \quad.$$
(4.4)

where $\vec{W}_i$ is the ith estimate of $\vec{W}$ (after iteration i), $\vec{W}_{i+1}$ is the i+1st estimate, etc. When $\vec{W}_i = \vec{W}_{i+1}$, (4.4) reduces to $0 = S^{\star} - MW_i$ or $S^{\star} = MW_i$ and the corresponding W value is the solution of (4.2) as desired.

## 4.3  IOP SYSTEM DESCRIPTION

Refer to the upper portion of the electro-optical system in Fig. 4.1.  The inputs to the system at plane $P_1$ are the elements $W_n$ of the vector $\vec{W}$.  The transmittance of the mask at $P_2$ is assumed for now to be $M_{mn}$, the elements of the covariance matrix M.  The system in Fig. 4.1 is drawn to demonstrate the system's operation rather than its detailed fabrication.  Specifically, the input light source at $P_1$ is an array of LEDs.  Their outputs are $W_n$.  The input LED array is imaged vertically onto $P_2$ and the output of each LED is expanded horizontally to uniformly illuminate the corresponding horizontal line of the $P_2$ mask.  The light distribution leaving $P_2$ is described in 2-D by $W_n M_{mn}$.  The optical system between $P_2$ and $P_3$ then images $P_2$ horizontally onto a linear horizontal photodetector array at $P_3$.  Each column of $P_2$ is focused onto a single photodetector at $P_3$.  The resultant light distribution at $P_3$ is thus

$$\sum_n W_n \cdot M_{mn}.$$
(4.5)

or the vector-matrix product of $\vec{W}$ and M.

IF $W_i = W_{i+1}$ , THEN $S = MW$
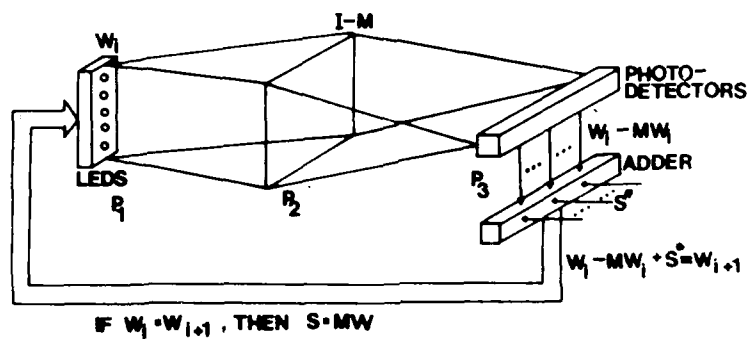
Fig. 4.1 Schematic diagram of an iterative optical
processor for adaptive phased array radar processing.



$F_{L1 L2 L3 L4} = 100 mm$

$d_1 = d_4$ to satisfy horizontal and

vertical imaging conditions between P2 and P3
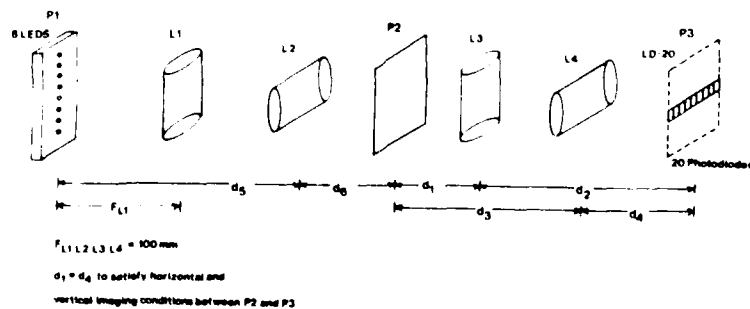
Fig. 4.2 Schematic diagram of the IOP system fabricated.

We have modified this basic electro-optical vector-matrix system first described in [4.1] for use in adaptive phased array radar processing and in the solution of vector-matrix equations by: (a) modifying the transmittance of $P_2$ to be [I-M], where I is the identity matrix, (b) addition of $S^*$ to the output at $P_3$ and (c) returning this output back to the LED input at $P_1$ [4.2,4.3]. The output at $P_3$ is now $W_n$ [I-$M_{mn}$]. After addition of $S^*$, the output is $W_n$[I-$M_{mn}$] + $S_m^*$. The corresponding $\overrightarrow{W}$ input that produced this output is denoted by $\overrightarrow{W}_i$. The output from the parallel adder is fed back to become the new $\overrightarrow{W}$ input estimate, which we denote by $\overrightarrow{W}_{i+1}$. The system shown in Fig. 4.1 is thus described by

$$\overrightarrow{W}_{i+1} = \overrightarrow{W}_i \ [I-M] + \overrightarrow{S}^* \ , \qquad (4.6)$$

where $W_i$ denotes the LED system input and hence the estimate of $\overrightarrow{W}$ at iteration i, whereas $W_{i+1}$ denotes the output of the system after iteration i and the new estimate of $\overrightarrow{W}$ for iteration i+1. As seen, (4.6) agrees with (4.4) and hence the output of the system when $\overrightarrow{W}_i = \overrightarrow{W}_{i+1} \pm \varepsilon$ is the desired adaptive weights solution in (4.3) to the steady state equation (4.2) version of the adaptive loop described by (4.1).

## 4.4 IOP SYSTEM DESCRIPTION

The IOP system fabricated used eight Hewlett-Packard LED inputs (model #5082-4101) in a 20.2 x 2.54 mm$^2$ assembly fabricated in-house. The M mask used at $P_2$ for this system had 8 x 8 elements in an 4 x 4 mm$^2$ area. The width of each individual cell in the mask was 0.5 x 0.5 mm$^2$. The IOP system fabricated is shown schematically in Fig. 4.2. A photograph of this system is included in Fig. 4.3. Pulse width modulation was used for each mask element, with the transparent mask area varied to produce different desired gray levels. The design of the integration optics $L_3 - L_4$ is chosen to demagnify $P_2$ vertically

Fig. 4.3  Photograph of the IOP system fabricated.

LED CURRENT DRIVE CIRCUITRY



Fig. 4.4 Schematic diagram of the source drive circuitry used.

by $1/M_{34}$ = 1.88 and magnification of $P_2$ horizontally by $M_{12}$ = 1.88. These values were set by the 7.55 x 4 $mm^2$ size of eight of the output detector elements.

Referring to Fig. 4.2, $d_1 + d_2 = d_3 + d_4$, $M_{12} = d_2/d_1$ and $M_{34} = d_4/d_3$. The focal length of all cylindrical lenses used was 100 mm. The imaging conditions $1/d_1 + 1/d_2 = 1/d_3 + 1/d_4 = 1/100$ require $d_3 d_4/d_5 d_6 = 1$. If $d_1 = d_4$ and $d_2 = d_3$ and $M_{12} = 1/M_{34}$, the values $d_1 = d_4 = 153$ mm and $d_2 = d_3 = 288$ mm resulted.

The amplitude driver used to amplitude modulate all eight LEDs in parallel is shown in Fig. 4.4. Since the output light intensity from the Hewlett-Packard LEDs used is nearly linearly related to the input current and is relatively independent of temperature, the above circuit suffices for the present experiments. The output detector circuitry used is shown in Fig. 4.5. The uniformity with which each row of the $P_2$ mask is illuminated was improved to several percent by defocusing $L_1$ slightly. Use of LEDs with narrower cone angles can likewise improve uniformity of illumination. The fiber optic connections we plan between $P_1$ and $P_2$ in the next version of this system will greatly decrease this problem. Use of a fixed mask in front of $P_2$ can adequately improve the uniformity of illumination problem. Cross talk between rows of the mask at $P_2$ was measured to be as much as 40%. This can be decreased by use of guard rings on the LEDs and mask, use of smaller LEDs and moreso by the planned fiber optic system.

## 4.5  COMPLEX DATA HANDLING

In practice, for the APAR problem, the vector and matrix masks used at $P_1$ and $P_2$ will contain complex elements. There are several ways by which complex data can be handled in such a non-coherent system. One of the most attractive techniques appears to be the representation of a complex quantity by its three projections [4.4,4.5] (at $0^o$, $120^o$ and $240^o$) in complex space, i.e., we represent a complex vector element $A_n$ by

$$\vec{A} = \vec{A_0} + \vec{A_1} + \vec{A_2}$$

$$= A_0 \exp 0) + A_1 \exp (j2\pi/3) + A_2 \exp (j4\pi/3). \qquad (4.7)$$

4.8



Fig. 4.5  Schematic diagram of the detector electronics fabricated.
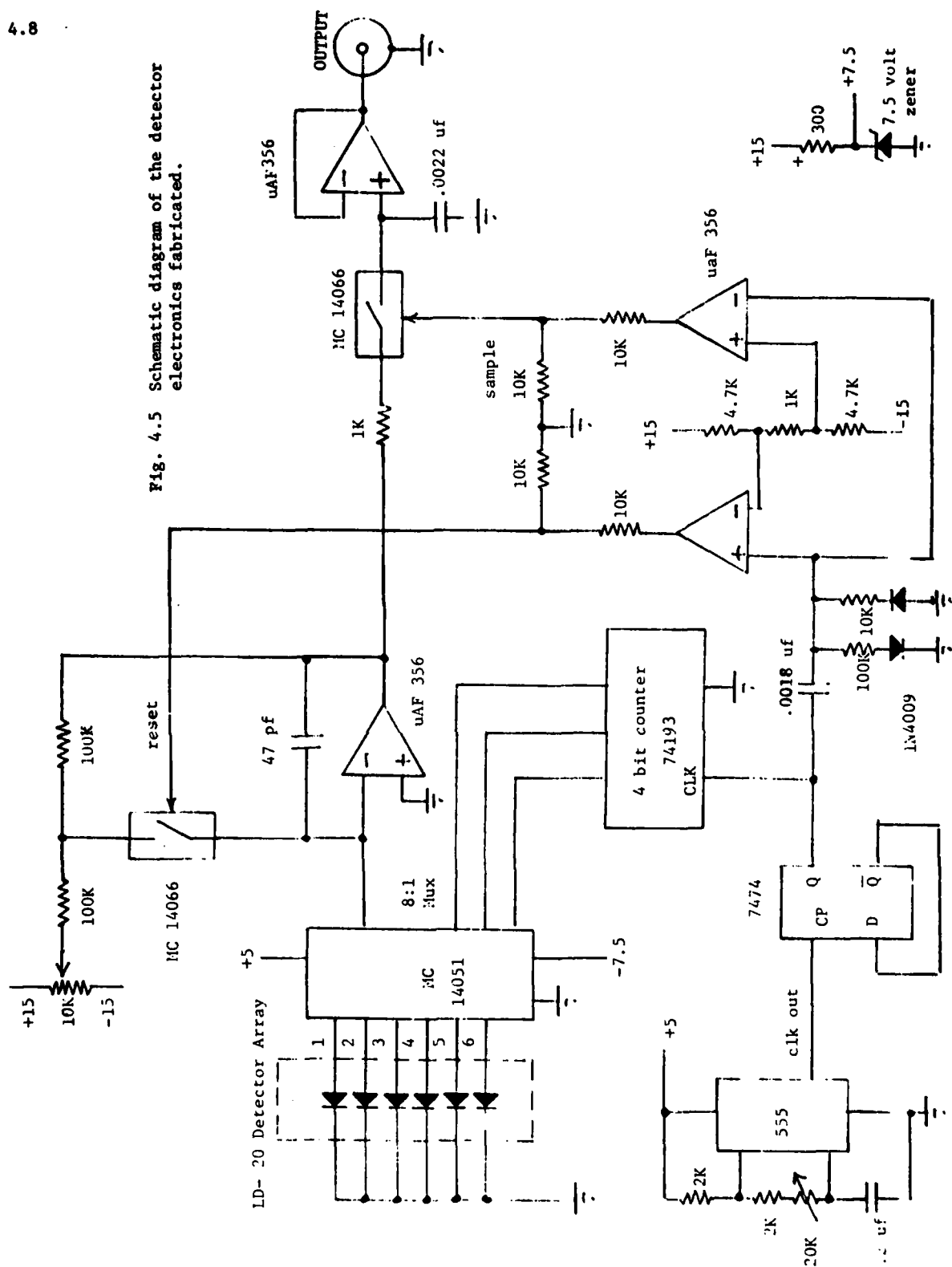
In this notation, the complex vector-matrix product is then described by

$$\vec{C} = \overline{B}[A]$$

$$= [\vec{A_{\hat{0}}} + \vec{A_{\hat{1}}} + \vec{A_{\hat{2}}}] \, [B_{\hat{0}} + B_{\hat{1}} + B_{\hat{2}}] \tag{4.8a}$$

$$= [\vec{A_{\hat{0}}B_{\hat{0}}} + \vec{A_{2}B_{\hat{1}}} + \vec{A_{\hat{1}}B_{\hat{2}}}]_{\hat{0}}$$

$$+ [\vec{A_{\hat{0}}B_{\hat{1}}} + \vec{A_{\hat{2}}B_{\hat{2}}} + \vec{A_{\hat{1}}B_{\hat{0}}}]_{\hat{1}}$$

$$+ [\vec{A_{\hat{0}}B_{\hat{2}}} + \vec{A_{\hat{1}}B_{\hat{1}}} + \vec{A_{\hat{2}}B_{\hat{0}}}]_{\hat{2}} \tag{4.8b}$$

Realization of a vector-matrix multiplier and IOP system with complex vector and matrix elements requires an input array at $P_1$ of length 3M and a mask at $P_2$ of size 3 N x 3 M.  We describe such an IOP system operating on complex data for an APAR application in Section 4.6.  An alternate technique for handling complex data is described in Section 4.7.

## 4.6  DEMONSTRATION OF THE IOP SYSTEM

To demonstrate the use of the IOP system described in Section 4.3 on complex data for the APAR problem, a simple two element linear array with one external noise source at an angle $\theta_i$ with respect to the normal to the array is considered with the addition of additive noise also present [4.2].  The signals  received at the two array elements are

$$v_1 = x_1 + y_1 \tag{4.9a}$$

$$v_2 = x_2 + y_2. \tag{4.9b}$$

In (4.9), $x_1$ is the interference voltage in channel i and $y_i$ is the noise voltage in channel i.  The voltage $x_2$  lags $x_1$ by a phase angle

$$\gamma = (2\pi d/\lambda) \sin \theta_i, \tag{4.10}$$

i.e., $x_2 = x_1 \exp(-j\gamma)$ and the noise voltages $y_1$ and $y_2$ will be independent of each other and of the interference signals.

We denote the noise power in each element channel due to this external noise source by P and the receiver power in each channel by N. In this case, the covariance matrix becomes

$$M = \begin{bmatrix} P+N & P \exp(-j\gamma) \\ P \exp(j\gamma) & P+N \end{bmatrix}. \qquad (4.11)$$

In the specific APAR problem considered to demonstrate the use of this processor, we chose a noise source emitting $P = 0.1$ watts at an angle $\theta_1$ such that

$$(2\pi d/\lambda) \sin \theta_1 = \pi/3. \qquad (4.12)$$

We assume a receiver noise power $N = 0.5$ (5 times larger than the received power P due to the noise source itself). Thus, $N/P = 5$ results in a fast convergence rate for the iterative processor. The actual mask used at $P_2$ of Fig. 4.1 is

$$[I-M] = \begin{bmatrix} 1-P-N & P \exp(-j4\pi/3) \\ P \exp(j4\pi/3) & 1-P-N \end{bmatrix}. \qquad (4.13)$$

The form used for this mask is shown in Fig. 4.6. The matrix elements $m_0'$, $m_1'$, $m_2'$ are all real and positive as shown in Section 4.5 and Fig. 4.6 and below.

$$M_0' = [I-M]_{\hat{0}} = \begin{bmatrix} 1-P-N & 0 \\ 0 & 1-P-N \end{bmatrix} \qquad (4.14a)$$

$$M_1' = [I-M]_{\hat{1}} = \begin{bmatrix} 0 & P \\ P & 0 \end{bmatrix} \qquad (4.14b)$$

$$M_2' = [I-M]_{\hat{2}} = \begin{bmatrix} 0 & 0 \\ P & 0 \end{bmatrix} \qquad (4.14c)$$

The general form for the mask is shown in Fig. 4.6a, the specific form for our example is shown in Fig. 4.6b.

To demonstrate the use of the electro-optical IOP system of Fig. 4.1 for this application, six of the eight input LEDs were used and the mask [I - M] was arranged as shown in Fig. 4.6. The six LED outputs at iteration I are described by

$$\begin{bmatrix} m'_0 & m'_2 & m'_1 \\ m'_1 & m'_0 & m'_2 \\ m'_2 & m'_1 & m'_0 \end{bmatrix}$$

(a)

$$\begin{bmatrix}
0.4 & 0 & 0 & 0 & 0.1 & 0 \\
0 & 0.4 & 0.1 & 0 & 0 & 0 \\
0.1 & 0 & 0.4 & 0 & 0 & 0 \\
0 & 0 & 0 & 0.4 & 0 & 0.1 \\
0 & 0 & 0 & 0 & 0.4 & 0 \\
0.1 & 0 & 0 & 0 & 0 & 0.4
\end{bmatrix}$$

(b)

Fig. 4.6  The mask [I-M] for complex matrix multiplication.
(a) general form  (b) specific form for our scenario.

$$\vec{W}_i = (W_{i,\hat{0}}(1), W_{i,\hat{0}}(2), W_{i,\hat{1}}(1), W_{i,\hat{1}}(2), W_{i,\hat{2}}(1), W_{i,\hat{2}}(2)). \quad (4.15)$$

For our example, the output from the six photodetector elements (after addition of S) are described by

$$(4.16)$$

$$\vec{W}_{i+1} = (W_{i+1,\hat{0}}(1), W_{i+1,\hat{0}}(2), W_{i+1,\hat{1}}(1), W_{i+1,\hat{1}}(2), W_{i+1,\hat{2}}(1), W_{i+1,\hat{2}}(2)).$$

This simple APAR processor was simulated. The theoretical results expected after the first six iterations in the steady state (infinite iterations) are shown in Table 4.1. The resultant experimental results obtained (after the first, second and fifth iterations) are shown in the A scope displays in Fig. 4.7.

Solving for the adaptive weights, we obtain

$$\begin{bmatrix} W \end{bmatrix} = \frac{C}{(P+N)^2 - p^2} \begin{bmatrix} P+N-P \ \exp(-j\gamma) \\ P+N-P \ \exp(+j\gamma) \end{bmatrix}. \quad (4.17)$$

We chose $C = 0.3$, where the steering vector is

$$[S^*] = \begin{bmatrix} C \\ C \end{bmatrix} \quad (4.18)$$

This choice of C simplifies the multiplicative factor in (4.17) to be approximately unity. Evaluation of the six components of $\vec{W}_{i+1}$ in (4.17) for the first six iterations are given in Table 4.1. The evaluation of (4.17) for this case yields

$$[W] = \frac{0.3}{0.35} \begin{bmatrix} 0.6-0.1 \ \exp(-j\pi/3) \\ 0.6-0.1 \ \exp(+j\pi/3) \end{bmatrix}. \quad (4.19)$$

The results shown in Fig. 4.7 are quite close to the predicted values in Table 4.1 as seen. As demonstrated, the results of this initial IOP system demonstration are most promising.

(a)

(b)

(c)
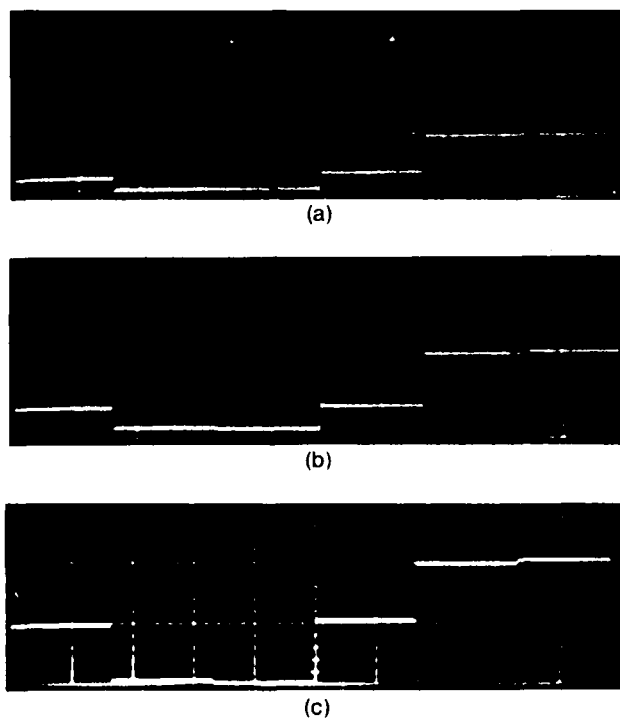
Fig. 4.7   Outputs obtained from the six photodetector elements
in the IOP system after iteration 0, 1, and 5.

TABLE 4.1 Theoretical $W_{i+1}$ Outputs from the IOP of Fig. 2 at Iteration 1

| | $W_{i+1,\hat{0}}(1)$ | $W_{i+1,\hat{0}}(2)$ | $W_{i+1,\hat{1}}(1)$ | $W_{i+1,\hat{1}}(2)$ | $W_{i+1,\hat{2}}(1)$ | $W_{i+1,\hat{2}}(2)$ |
|---|---|---|---|---|---|---|
| 0 | 0.3 | 0.3 | 0 | 0 | 0 | 0 |
| 1 | 0.42 | 0.42 | 0.03 | 0 | 0 | 0.03 |
| 2 | 0.471 | 0.471 | 0.054 | 0 | 0 | 0.054 |
| 3 | 0.4938 | 0.4938 | 0.0687 | 0 | 0 | 0.0687 |
| 4 | 0.5043 | 0.5043 | 0.0768 | 0 | 0 | 0.0768 |
| 5 | 0.5094 | 0.5094 | 0.0811 | 0 | 0 | 0.0811 |
| 6 | 0.5118 | 0.5118 | 0.0834 | 0 | 0 | 0.0834 |
| 8 | 0.5142 | 0.5142 | 0.0857 | 0 | 0 | 0.0857 |

## 4.7 COMPLEX DATA REPRESENTATION BY COLOR MULTIPLEXING

The complex data representation scheme noted in Section 4.5 and experimentally demonstrated in Section 4.6 requires three times the space bandwidth product for the input LED array and the output photodetector array and nine times the space bandwidth for the matrix mask at $P_2$. These input and output plane requirements can be reduced by use of a novel color multiplexing technique shown in Fig. 4.8. In this method, three linear input LED arrays (each of a different color or wavelength) are used and three linear output photodetector arrays are required. Each of the three components $\vec{W_0}$, $\vec{W_1}$, $\vec{W_2}$ of $\vec{W}$ are represented by a separate linear LED input array. A grating inserted between $P_2$ and $P_3$ enable separation of the three output products on the three linear photodetector arrays. Summation of the proper photodiode outputs at $P_3$ yields the correct vector-matrix product which can then be fed back to $P_1$ in the IOP system [4.3].

The results of our initial experiments to demonstrate [4.3] the use of this color multiplexed IOP system of Fig. 4.8 are shown in Fig. 4.9. In this experiment, an arc lamp source was used with three spectral lines ($\lambda_1$ violet, $\lambda_2$ green, and $\lambda_3$ orange). A two element input vector with components

$$a_{\lambda 1} = (1,0), \quad a_{\lambda 2} = (1,1), \quad a_{\lambda 3} = (0,1) \tag{4.20}$$

was used as the 2 x 3 input (Fig. 4.9a). We consider the multiplication of $\vec{A}$ by B. The output from the 2 x 6 mask B used is shown in Fig. 4.9b. The three rows of the matrix B are read out with $\lambda_1 + \lambda_2$, $\lambda_2$, and $\lambda_3$ light, respectively, because of the input pattern chosen in (4.20). The mask $P_2$ output shown are as expected. The $P_3$ output consists of three rows of six detector elements per row (Fig. 4.9c). These correspond to the eighteen possible cross products. All are of the proper form as indicated. These initial experiments using this novel complex data representation method were most promising. Their future use requires the need for several parallel arrays of laser diodes, which we hope to have and
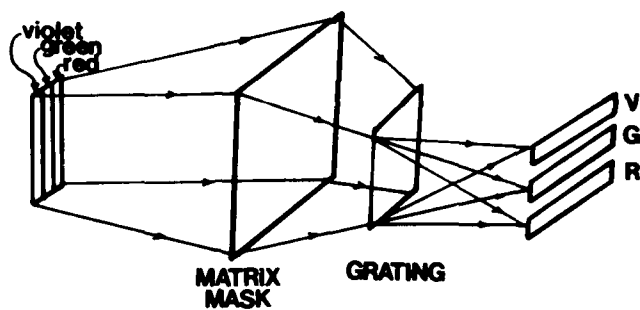
Fig. 4.8 Schematic diagram of a color-multiplexed optical processor.
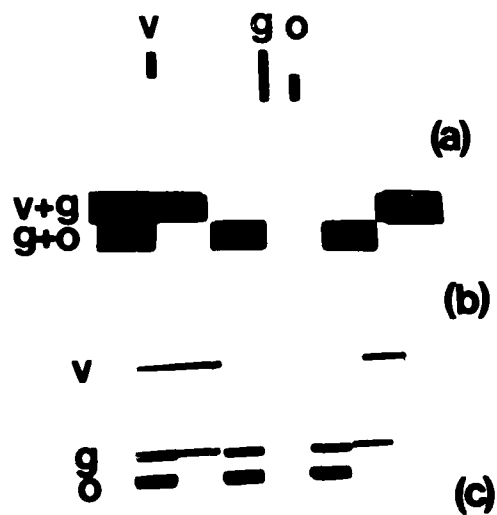


Fig. 4.9 Color multiplexed complex vector-matrix multiplication.
(a) input, (b) mask output, (c) system output. (Printed
in black and white.  V = violet, G = green, O = orange).

demonstrate in Phase 2 of this program.

## 4.8 SYSTEM CONSIDERATIONS

Either LEDs or laser diodes can be used as the light source. Laser diodes are preferable because of their smaller size, higher power output, variety of wavelengths available, and their large linear dynamic range of output light intensity with input current. Laser diodes require heat sinking to compensate for temperature effects, but often this can be performed directly on the chip. Pulse width source modulation appears to be necessary with LED sources because of their non-linear behavior at low current. This will decrease the system's speed but it is still more than adequate for the APAR application. A system cycle time of 1 $\mu$sec appears possible. However, multiplexed input and output electronics are preferable for reasons of cost and man hours. Even with pulse width modulation and input and output multiplexing, adequate system speeds for the APAR program are easily obtainable.

A major concern in such an iterative processor is its accuracy. The results of computer simulations have shown that cross talk and nonuniform illumination of the $P_2$ mask and detector nonuniformity are the major error sources. As suggested in Section 4.4, use of fiber optic connectors between $P_1$ and $P_2$ appears to solve the uniformity and cross talk problems. A fixed auxiliary mask in front of $P_2$ is planned to compensate for any nonuniformity that still remains. The optics between $P_2$ and $P_3$ will be removed in the next system by designing the front end so that the detector array can be mounted flush with the $P_2$ mask. LED nonlinearity will be decreased by use of pulse width input modulation. Any differences that remain between the saturation levels of the different LEDs and any sensitivity differences present between individual photodetectors will be compensated for electronically using a programmable read only memory in the electronic feedback circuitry.

This IOP system appears to be most promising and to merit further research with major attention given to its accuracy and to fabrication of the prototype system utilizing recent advances in LED, fiber optics, detector, and solid-state electronics and the extensive test, analysis and demonstration of the system fabricated.

REFERENCES

4.1 J. W. Goodman, et al., Opt. Letts., 2, 1 (1978).

4.2 D. Psaltis, et al., SPIE, 180 (1979).

4.3 D. Psaltis, et al., Opt. Letts. (Nov. 1979).

4.4 C. Burckhardt, Appl. Opt., 9, 1949 (1970).

4.5 J. W. Goodman and L. M. Woody, Appl. Opt., 16, 2611 (1977).

BIBLIOGRAPHY

1.  L. Cutrona, Optical and Electro-optical Information Processing, pp. 97-98, ed. J. Tippett, et al., (MIT Press, Cambridge, MA 1965).

2.  A. Edison and M. Nobel, Final Report, Contract AF19 (628-4199), General Electric (Nov. 1966).

3.  D. Mengert, et al., U.S. Patent 3,525,856, Filed 6 Oct. 1966.

4.  W. Schneider and W. Fink, Optica Acta, 22, 879 (1975).

5.  M. Monahan, Digest IOCC (Washington, D.C.), pp. 25-33, IEEE Cat. No. 75-CH09L11-5C (Apr. 1975).

CHAPTER 5

SUMMARY AND CONCLUSION

Three different and new optical signal processing techniques and system architectures for adaptive radar processing have been described, analyzed, initial experiments performed, component availability assessed and recommendations provided.

## 5.1 OPTICAL RESIDUE ARITHMETIC

The first technique considered utilized residue arithmetic. The two motivations for considering such an approach for adaptive radar processing were the high-speed and parallel nature of a residue arithmetic processor (specifically, no carries are necessary) and that high computational accuracy is possible with modest accuracy in each subcomputation. Application of residue arithmetic techniques to an optical processor is thus attractive because of the parallel nature of an optical system, which provides a vehicle with which to perform the many parallel computations necessary in a residue arithmetic system. It is also attractive because all individual computations need be performed to an accuracy equal to that of the basis rather than the full number. Thus, an optical residue arithmetic processor provides an attractive method to improve the accuracy of an analog processor.

We first developed a new correlation formulation of residue arithmetic processors. This allows such processors to be realized using correlators rather than conventional systems that perform additions, subtractions, etc. Since optical, CCD and other technologies perform correlations rather than the more conventional mathematical operations, such a formulation leads more directly to implementation of residue processor architectures in such technologies.

As the first two special components of an optical residue arithmetic processor, we considered the input and output problems, specifically converting digital and decimal data into residue form for input to a residue arithmetic processor and then techniques for converting residue data into digital and decimal form at the output

of the system. Optical decimal/residue and residue/decimal converters were
designed, and experimental laboratory system was assembled and experimental
demonstration of these two new systems were obtained. An optical residue
arithmetic adder and vector-matrix multiplier system were then designed.

The two major issues of concern in such a processor are how to input data
to such a system in the proper format and the availability of the necessary
component technology. The first issue requires more extensive study and
analysis as well as a reformulation of the adaptive radar problem. In all sys-
tems considered, the control system to provide input data of the proper form
and in the proper locations appears to require such extensive logic that the
parallel processing features of a residue arithmetic processor become less
attractive. Implementation with 2-D spatial light modulators, integrated optical
systems and other optical technologies appears to require such extensive device
and component development that implementation of such systems appears to be years
away. The most readily implementable residue arithmetic processing technique
appears to utilize fiber optics and thus capitalize on rapid advances in this
area for communication applications. Because the other two optical processors
we considered for adaptive radar applications can be realized with existing
components and appear to be capable of the necessary system performance, we
recommend that one keep abreast of developments in integrated optics, CCD devices,
Josephson junction technology and other candidate residue arithmetic system
components and that further research be performed on the COC and IOP systems
for adaptive phased array radar.

5.2 COC PROCESSOR

The second candidate optical system considered is the closest of any to
a conventional optical processor. The basic system is a hybrid processor con-
sisting of a frequency plane correlator modified to function as a multi-channel

system. The multi-channel output correlation plane pattern is then slit integrated using a specially shaped solid-state detector. A simple digital inverse DFT postprocessor can then compute the necessary adaptive weights from this output for many scenarios.

This COC processor operates on the heterodyned received signals at the antenna elements. It computes the correlation of the N received antenna signals with a reference signal from one antenna element in parallel. The multi-channel optically computed output correlation plane pattern is such that each noise source at a different angle produces a set of correlation peaks that align in one row at a given angle in the optical correlation plane proportional to the azimuth angle $\theta_m$ of the noise source. Thus, after integrating the multi-channel correlation output along different radial lines (using a special solid-state detector with angular shaped detector elements), the angular distribution of the noise field $N_m (\theta_m)$ is obtained.

For a single monofrequency noise source and a linear array with equally spaced elements, an inverse DFT postprocessor has been found to be sufficient to compute the weights from the N $(\theta)$ information. Initial experiments and computer simulations of this system produced outputs as expected. A statistical analysis of this system was conducted in which the accuracy of the estimate was related to the number of adaptive elements, signal bandwidth and observation time. Computation of the optimum weights from the N $(\theta)$ pattern were performed using maximization of the output SNR and minimization of the output noise as two goodness criteria. To obtain the optimum weights using SNR as the criteria required computation of the full covariance correlation matrix and its full inversion. Conversely, the second criteria required computation of only one column of the correlation matrix, as the COC system performs. Thus, we expect the weights computed from the hybrid optical/digital COC system to be optimum for minimizing the output noise rather than the output SNR.

Our major concern with the present COC system was the need for real-time
and reusable 2-D spatial light modulators and the need to process long time
bandwidth product signals to obtain adequate noise statistics. We thus advocate
use of the same basic correlation and system concept using instead a time
integrating acousto-optic correlator to achieve the long signal integration
time bandwidth products needed and to utilize more available real-time trans-
ducers.

## 5.3 IOP SYSTEM

The third optical system for adaptive phased array radar processing appears
to be the most attractive one that is both most directly analyzed and most readily
implemented. The basic system uses a linear input LED array, 2-D mask and linear
detector array to perform a vector-matrix multiplication. Addition of a vector
to this system's output and returning the output to the LED inputs results in
an iterative optical processor using feedback. This IOP system can then solve
the vector-matrix equation of adaptive radar for the output weights using an
iterative algorithm. The inputs to this non-coherent optical processor are the
covariance matrix M and the steering vector S.

Three techniques that enable this system to operate on complex data have
been developed and experimentally demonstrated. These include a new color
multiplexed technique.

The accuracy of this or any such feedback or iterative system was our primary
concern. Uniform illumination of each row of the mask, crosstalk between rows,
and non-linear LED responses were determined by analysis, experiment, and
simulation to be the major error sources of concern. The use of fiber optic
coupling from the LEDs to the mask (and a fixed mask in front of the variable
mask) overcomes the nonuniform illumination and crosstalk problems noted above.
The use of pulse width modulation of the LED source outputs or amplitude modulation

of laser diode sources overcomes the source nonlinearity problems noted. Differences in the saturation level of the LED sources and differences in the sensitivity of the output detector elements can be corrected in the electronic feedback system itself.

The system fabricated, initial tests performed on it, and the results of the simple adaptive phased array radar problems performed to demonstrate the use of the system were most encouraging. We thus recommend the fabrication of a prototype of such a system as described above with extensive component tests and attention to the accuracy and system performance obtainable together with extensive testing of the use of the system and diverse adaptive phased array radar problems.

APPENDIX

```
00100   C       THIS PROGRAM GIVES THE CORRELATION OF THE NOISE RECEIVED FOR
00200   C       EACH ELEMENT OF AN ANTENNA ARRAY WITH THE NOISE RECEIVED FOR
00300   C       THE ELEMENT IN THE MIDDLE OF THE ARRAY WHICH I WILL CALL
00400   C       REFERENCE ELEMENT, THE OUTPUT IS IN A PLOTTING FORM.
00500   C       TO EXECUTE IT THE FOLLOWING SEQUENCE HAS TO BE DONE:
00600   C       @ TAKE SYS:TEK6
00700   C       @ EXE @ANTENN.CMD,SYS:TEKT.REL
00800   C       IN WHICH ANTENN.CMD IS A COMAND FILE WITH ROB.FOR,SUB.FOR,
00900   C       IMAGE.FOR AND PLOT.FOR IN IT.
01000
01100
01200           REAL AIL(0:127),REF(0:127),ARRAY(0:127,0:38),UPPERX,UPPERN
01300           INTEGER  A,X,N
01400
01500           A       = 1
01600           UPPERX  = 127.0
01700           UPPERN  =  38.0
01800           FR1     =   0.1
01900           FR2     =   0.09
02000           ANGLE1  =   0.5
02100           ANGLE2  =   0.707
02200           MAX     =   0.0
02300           PI      =   4*ATAN(1.0)
02400
02500
02600
02700
02800
02900   C       IN THIS PROGRAM I GAVE TWO POSSIBLE INPUTS AS NOISE SOURCES
03000   C       AT FIRST THE NEXT DO LOOPS IN THE PROGRAM CAN BE USED TO
03100   C       EMULATE THE NOISE OF A SOURCE WHICH GIVE A WAVE AS COS(PHI)
03200   C       ONLY FOR PHI BETWEEN ZERO AND TWO PI, IT MEANS ONLY ONE PERIOD
03300   C       ITS A NON-PERIODICAL NOISE.
03400   C       THE OTHER POSSIBILITY IS A SECOND GROUP OF DO LOOPS FOR THE
03500   C       CASE WHEN THE NOISE IS PERIODICAL(COS(PHI)).
03600
03700   C       NON-PERIODICAL NOISE
03800           DO 100          X=0,UPPERX
03900             REF(X)=0.0
04000             HR1 = 2*PI*FR1*X - PI*ANGLE1*19
04100             HR2 = 2*PI*FR2*X - PI*ANGLE2*19
04200                 IF((HR1.GE.0.0).AND.(HR1.LE.(2*PI)))
04300        1           REF(X)=A*(COS((2*PI*FR1*X)+(PI*ANGLE1*19))+1)
04400   C             IF((HR2.GE.0.0).AND.(HR2.LE.(2*PI)))REF(X)=REF(X)+
04500   C    1           A*(COS((2*PI*FR2*X)+(PI*ANGLE2*19))+1)
04600   100     CONTINUE
04700           DO  200         N=0,UPPERN
04800               DO 150          X=0,UPPERX
04900                 ALL(X)=0.0
05000                 HA1= 2*PI*FR1*X - PI*ANGLE1*N
05100                 HA2= 2*PI*FR2*X - PI*ANGLE2*(UPPERN-N)
05200                     IF((HA1.GE.0.0).AND.(HA1.LE.(2*PI)))ALL(X)=
05300        1               A*(COS((2*PI*FR1*X)+(PI*ANGLE1*N))+1)
05400                     IF((HA2.GE.0.0).AND.(HA2.LE.(2*PI)))ALL(X)=
05500        1               ALL(X)+A*(COS((2*PI*FR2*X)+
05600        1               (PI*ANGLE2*UPPERN-N))+1)
05700   150     CONTINUE
05800
05900
06000
```

```
6100
6200    C           PERIODICAL NOISE
6300    C           DO 1000        X=0,UPPERX
6400    C                  REF(X)=A*(COS(2*PI*FR1*X + PI*ANGLE1*19) +
6500    C           1              COS(2*PI*FR2*X + PI*ANGLE2*19) + 2)
6600    C1000    CONTINUE
6700    C           DO 200         N=0,UPPERN
6800    C                  DO 1500        X=0,UPPERX
6900    C                     ALL(X)=A*(COS(2*PI*FR1*Y + PI*ANGLE1*N) +
7000    C           1              COS(2*PI*FR2*X + PI*ANGLE2*(UPPERN-N))+2)
7100    C1500    CONTINUE
7200
7300
7400            CALL CORREL(127,ALL,REF)
7500            DO 200         X=0,UPPERX
7600                  ARRAY(X,N)=ALL(X)
7700    200     CONTINUE
7800    C       CALL PLOTIN(127,39,ARRAY,'ROBERT.DAT',MAX)
7900    C       OPEN(UNIT=21)
8000    C       WRITE(21,250)ARRAY
8100    250     FORMAT( 9(1XG10.5))
8200    C       CLOSE(UNIT=21)
8300            CALL PLOT2D(127,38,ARRAY)
8400            PAUSE
8500            CALL NOISAN(UPPERX,UPPERN,ARRAY)
8600            STOP
8700            END
8800
8900            SUBROUTINE NOISAN(UPPERX,UPPERN,ARRAY)
9000            REAL   RAD,ATITA(180),ARRAY(0:127,0:38)
9100            INTEGER  X0,Y0,X,TITA,Y,Y1
9200
9300            PI= 4*ATAN(1.0)
9400            X0= UPPERX/2
9500            Y0=UPPERN/2+4
9600
9700            DO 300         TITA=1,180
9800            ATITA(TITA)=0.0
9900    300     CONTINUE
0000            DO 400         TITA=1,180
0100                  RAD=(TITA/180.0)*PI
0200                  IF (TITA.EQ.90) GOTO 400
0300                  DO   410       X=0,UPPERX
0400                     Y=(SIN(RAD)/COS(RAD))*(X-X0)+Y0+0.5
0500                     Y1=UPPERN-Y
0600                     IF((Y1.LT.0).OR.(Y.LT.0))  GOTO 410
0700                     ATITA(TITA)=ATITA(TITA)+ARRAY(X,Y)
0750    410     CONTINUE
0800    400     CONTINUE
0900            CALL PLOTID(180,ATITA,1.0,1.0)
1000            STOP
1100            END
```

This is another
of the coming noise

```
00100    C
00200    C
00300          SUBROUTINE CORREL(NU ,TX,TY)
00400    C     PREFORMS A CIRCULAR CORRELATION OF THE REAL
00500    C     ARRAYS TX(0:NUM) TY(0:NUM).   THE RESULT IS IN
00600    C     TY(0:NUM) AND IS SHIFTED SO THAT TX(0)=TX(NUM/2)
00700    C
00800          INTEGER I,NUM,N
00900          REAL TX(0:1023),TY(0:1023)
01000          COMPLEX X(0:1023),Y(0:1023)
01100          DO 400 I=0,NUM
01200    400      X(I)=CMPLX(TX(I),0.0)
01300          DO 500 I=0,NUM
01400    500      Y(I)=CMPLX(TY(I),0.0)
01500          CALL FFT(NUM,X,1)
01600          CALL FFT(NUM,Y,1)
01700          CALL CONJ(NUM,Y)
01800          DO 600 I=0,NUM
01900    600      Y(I)=Y(I)*Y(I)/(NUM**2)
02000          CALL FFT(NUM,X,-1)
02100          N=NUM/2
02200          DO 700 I=0,N
02300             TX(I)=ABS(Y(I+N+1))
02400    700      TX(I+N+1)=ABS(X(I))
02500          RETURN
02600          END
```

```
00100     C
00200     C
00300           SUBROUTINE FFT(NUM,X,INV)
00400     C     THIS SUBROUTINE DOES THE FFT OF THE ONE DIMENSIONAL
00500     C     COMPLEX VECTOR X(0:NUM),NUM=2**N-1.   THIS IS
00600     C     A DECIMATION-IN-TIME,RADIX 2,IN-PLACE FFT ROUTINE
00700     C     TO DO INVERSE FFT SET INV TO -1 OTHERWISE SET TO 1
00800     C
00900           INTEGER NUM,I,N,L,K,L2,L3,J,INV
01000           REAL PI
01100           COMPLEX X(0:1023),U,W,T
01200           N=INT(ALOG(NUM+1.0)/ALOG(2.0)+0.5)
01300           IF(ALOG(NUM+1.0)/ALOG(2.0)-N.GE.0.001) GO TO 3000
01400           J=0
01500           DO 300 I=0,NUM
01600               IF(I.GE.J) GO TO 100
01700               T=X(J)
01800               X(J)=X(I)
01900               X(I)=T
02000     100       K=(NUM+1)/2
02100     200       IF(J.LT.K.OR.I.EQ.NUM) GO TO 300
02200               J=J-K
02300               K=K/2
02400               GO TO 200
02500     300       J=J+K
02600           PI=3.1415926535
02700           DO 2000 I=1,N
02800               L=2**I
02900               L2=L/2
03000               L3=L2-1
03100               U=(1.0,0.0)
03200               W=CMPLX(COS(PI/L2),-SIN(PI/L2))
03300               IF(INV.EQ.-1) W=(1.0,0.0)/W
03400               DO 2000 J=0,L3
03500                   DO 1000 K=J,NUM,L
03600                       T=X(K+L2)*U
03700                       X(K+L2)=X(K)-T
03800     1000              X(K)=X(K)+T
03900     2000              U=U*W
04000           RETURN
04100     3000  WRITE (5,4000)
04200     4000 FORMAT(' THE NUMBER OF ELEMENTS IN THE INPUT',//,
04300          1         ' VECTOR IS NOT 2**N')
04400           RETURN
04500           END
```

```
00100    C        TO USE SUBROUTINES IN  THE LIBRARY PLOT.FOR
00200    C        IN A PROGRAM ON THE TEKTRONIX 4006 STORAGE
00300    C        SCOPE EXECUTE THE PROGRAM AS FOLLOWS
00400    C             @TAKE SYS:TEK6
00500    C
00600    C             @EXECUTE PLOT.FOR,PROGRAM.FOR,SYS:TEKT.REL
00700    C
00800    C
00900            SUBROUTINE PLOT2D(X,Y,P)
01000    C        THIS SUBROUTINE PLOTS THE VALUES IN THE POSITIVE
01100    C        REAL 2-D ARRAY P(0:X,0:Y).  THE PLOT IS MADE UP OF
01200    C        Y+1 HORIZONTAL LINES EACH CONTAINING X+1 POINTS.
01300    C        THE MAXIMUM NUMBER OF LINES AND POINTS IS 512.
01400    C
01500            INTEGER X,Y,I,J,MINX,MINY,N,M,H
01600            REAL P(0:X,0:Y),YMAX(0:511),XINC,YINC,PMAX,RATIO
01700            WRITE (5,50)
01800         50 FORMAT(' IF COPY IS WANTED TYPE 1 IF NOT TYPE 0',//,
01900          1        ' AFTER PLOT IS FINISHED',//,
02000          2        ' WHEN READY SPACE AND RETURN')
02100            READ (5,75) I
02200         75 FORMAT(I1)
02300            YINC=512.0/Y
02400            RATIO=FLOAT(X)/FLOAT(Y)
02500            XINC=512.0/Y
02600            PMAX=P(0,0)
02700            DO 100 I=0,X
02800                 DO 100 J=0,Y
02900    100              IF(PMAX.LT.P(I,J)) PMAX=P(I,J)
03000            DO 200 I=0,X
03100    200          YMAX(I)=0.0
03200            CALL INITT(480)
03300            CALL DWINDO(0.0,FLOAT(Y),0.0,PMAX)
03400            DO 600 J=0,Y
03500                 MINX=512-XINC*J
03600                 MINY=YINC*J
03700                 CALL SWINDO(MINX,511,MINY,511)
03800                 CALL MOVEA(0.0,0.0)
03900                 DO 400 I=0,X
04000                     IF(P(I,J).LT.YMAX(I)) GO TO 300
04100                     CALL DRAWA(FLOAT(I),P(I,J))
04200                     YMAX(I)=P(I,J)
04300                     GO TO 400
04400    300              CALL MOVEA(FLOAT(I),P(I,J))
04500    400              CONTINUE
04600                 M=INT(RATIO*FLOAT(J+1))-INT(RATIO*FLOAT(J))
04700                 N=Y-M
04800                 DO 500 I=0,N
04900    500              YMAX(Y-I)=YMAX(X-I-M)-PMAX/Y
05000                 M=M-1
05100                 DO 600 I=0,M
05200    600              YMAX(I)=P(I,J+1)
05300            CALL MOVABS(0,512)
05400            CALL DRWABS(512,0)
05500            CALL DRWABS(1023,0)
05600            CALL MOVABS(0,767)
05700            CALL ANMODE
05800            READ (5,*) H
05900            IF(H.EQ.1) CALL HCCOPY
06000            RETURN
```

```
06100          END
06200      C
06300      C
06400          SUBROUTINE PLOT1D(NUM,P,YMIN,YMAX)
06500      C   PLOTS THE REAL ARRAY P(0:NUM).
06600      C   NUM MAX IS 1023.
06700      C   YMIN AND YMAX ARE THE MINIMUM AND MAXIMUM
06800      C   VALUES OF THE ARRAY P.   THEY ARE FOR SCALING.
06900      C   IF TWO PLOTS ARE TO HAVE THE SAME SCALE
07000      C   THEN THEY MUST HAVE THE SAME VALUES OF YMAX
07100      C   AND YMIN. IF THE SUBROUTINE IS TO DO THE
07200      C   SCALING THEN SET YMAX EQUAL TO YMIN.
07300      C
07400          INTEGER I,NUM,H
07500          REAL P(0:NUM),YMIN,YMAX,XMIN,XMAX
07600          WRITE (5,250)
07700      250 FORMAT(" IF COPY IS WANTED TYPE 1 IF NOT TYPE 0",/,
07800         1          " AFTER PLOT IS FINISHED",/,
07900         2          " WHEN READY SPACE AND RETURN")
08000          READ (5,275) I
08100      275 FORMAT(I1)
08200          IF(YMIN.NE.YMAX) GO TO 350
08300          YMIN=P(0)
08400          YMAX=P(0)
08500          DO 300 I=0,NUM
08600              IF(P(I).LT.YMIN) YMIN=P(I)
08700      300     IF(P(I).GT.YMAX) YMAX=P(I)
08800      350 XMIN=0.0
08900          XMAX=FLOAT(NUM)
09000          CALL INITT(480)
09100          CALL DWINDO(XMIN,XMAX,YMIN,YMAX)
09200          CALL MOVEA(0.0,P(0))
09300          DO 400 I=1,NUM
09400      400     CALL DRAWA(FLOAT(I),P(I))
09500          CALL MOVABS(0,767)
09600          CALL ANMODE
09700          READ (5,*) H
09800          RETURN
09900          END
```

# MISSION
## of
## Rome Air Development Center

*RADC plans and executes research, development, test and selected acquisition programs in support of Command, Control Communications and Intelligence ($C^3I$) activities. Technical and engineering support within areas of technical competence is provided to ESD Program Offices (POs) and other ESD elements. The principal technical mission areas are communications, electromagnetic guidance and control, surveillance of ground and aerospace objects, intelligence data collection and handling, information system technology, ionospheric propagation, solid state sciences, microwave physics and electronic reliability, maintainability and compatibility.*

**F**

**g**